THE CATALYTIC REMOVAL OF AMMONIA AND NITROGEN OXIDES FROM SPACECABIN ATMOSPHERES

by A. J. Gully, R. R. Graham, J. E. Halligan, and P. C. Bentsen

Prepared by
INSTITUTE OF SCIENCE AND ENGINEERING
TEXAS TECH UNIVERSITY
Lubbock, Texas
for Langley Research Center

1. Report No. NASA CR-2132	2. Government Accession No.	3. Recipient's Catalog No.
4. Title and Subtitle THE CATALYTIC REMOVAL OF AMMONIA AND NITROGEN OXIDES FROM SPACECABIN ATMOSPHERES		5. Report Date February 1973
		6. Performing Organization Code
7. Author(s) A. J. Gully, R. R. Graham, J. E. Halligan and P. C. Bentsen		8. Performing Organization Report No. None
		10. Work Unit No.
9. Performing Organization Name and Address Institute of Science and Engineering Texas Tech University Lubbock, Texas		11. Contract or Grant No. NAS 1-9506
		13. Type of Report and Period Covered Contractor Report
12. Sponsoring Agency Name and Address National Aeronautics and Space Administration Washington, D. C. 20546		14. Sponsoring Agency Code

15. Supplementary Notes

16. Abstract

Investigations were made on methods for the removal of ammonia and to a lesser extent nitrogen oxides in low concentrations from air. The catalytic oxidation of ammonia was studied over a temperature range of 250°F to 600°F and a concentration range from 20 ppm to 500 ppm. Of the catalysts studied, 0.5% ruthenium supported on alumina was found to be superior. This material is active at temperatures as low as 250°F and was found to produce much less nitrous oxide than the other two active catalysts, platinum on alumina and Hopcalite.

A quantitative design model was developed which will permit the performance of an oxidizer to be calculated. The ruthenium was found to be relatively insensitive to low concentrations of water and to oxygen concentration between 21% and 100%. Hydrogen sulfide was found to be a poison when injected in relatively large quantities. The ruthenium catalyst was found to have a very stable activity under normal operating conditions with one charge having been used for several weeks without a loss in activity.

The adsorption of ammonia by copper sulfate treated silica gel was investigated at temperatures of 72°F and 100°F. Ammonia feed concentrations investigated ranged from 80 ppm to slightly over 500 ppm. A quantitative model was developed for predicting adsorption bed behavior. Limited investigation indicated that the treated silica gel could be thermally desorbed with little loss of capacity.

17. Key Words (Suggested by Author(s)) Ammonia oxidation Ammonia adsorption Catalytic oxidation of ammonia Kinetics of ammonia removal	18. Distribution Statement Unclassified - Unlimited	
19. Security Classif. (of this report) Unclassified	20. Security Classif. (of this page) Unclassified	21. No. of Pages 162	22. Price* $3.00

TABLE OF CONTENTS

LIST OF TABLES

vi

LIST OF FIGURES

THE CATALYTIC REMOVAL OF AMMONIA AND NITROGEN

OXIDES FROM SPACECABIN ATMOSPHERES

By A. J. Gully, R. R. Graham, J. E. Halligan,
and P. C. Bentsen

Chemical Engineering Department
Texas Tech University

1.0 SUMMARY

Investigations were made on methods for the removal of ammonia and to a lesser extent nitrogen oxides in low concentrations from air. The catalytic oxidation of ammonia was studied over a temperature range of 250°F to 600°F and a concentration range from 20 ppm to 500 ppm. Of the catalysts studied, 0.5% ruthenium supported on alumina was found to be superior. This material is active at temperatures as low as 250°F and was found to produce much less nitrous oxide than the other two active catalysts, platinum on alumina and Hopcalite.

A quantitative design model was developed which will permit the performance of an oxidizer to be calculated. The ruthenium was found to be relatively insensitive to low concentrations of water and to oxygen concentration between 21% and 100%. Hydrogen sulfide was found to be a poison when injected in relatively large quantities. The ruthenium catalyst was found to have a very stable activity under normal operating conditions with one charge having been used for several weeks without a loss in activity.

The adsorption of ammonia by copper sulfate treated silica gel was investigated at temperatures of 72°F and 100°F. Ammonia feed concentrations investigated ranged from 80 ppm to slightly over 500 ppm. A quantitative model was developed for predicting adsorption bed behavior. Limited investigation indicated that the treated silica gel could be thermally desorbed with little loss of capacity.

2.0 INTRODUCTION

In a closed system such as a spacecabin, the volume of free atmosphere per inhabitant is extremely small resulting in large increases in concentration of contaminants with the addition of very small amounts of contaminant gases. If the contaminant is metabolically produced (as is ammonia) then very reliable systems for contaminant removal must be included in the contaminant control system. The release of nitrogen containing compounds into the atmosphere of spacecabins is an unavoidable occurrence even though considerable effort is made to control these compounds at the source of the release. Once the nitrogenous compounds are released into the atmosphere of the spacecabin, their concentration must be controlled by the trace contaminant removal system in order to maintain a life supporting environment. The contaminant of particular concern in this investigation is ammonia. Ammonia production rates are estimated to be as high as 1.2×10^{-4} lb/hr. within a 2000 cubic foot cabin volume.

Two different control methods were evaluated in this investigation. These methods were the catalytic oxidation of ammonia and the adsorption of ammonia on treated silica gel. The removal of ammonia by catalytic oxidation to yield nitrogen and water is theoretically a very attractive method of controlling this contaminant provided no undersirable reaction products are produced. Currently proposed trace contaminant control systems contain a catalytic burner through which the cabin air is circulated. The products of ammonia oxidation within the catalytic burner could include nitrogen dioxide (NO_2), nitrous oxide (N_2O), and/or nitric oxide (NO). The particular nitrogen oxides produced and their rates of production undoubtedly depend on the type of catalyst used and on the temperature at which the oxidation is carried out. For this reason the reaction rates and product distribution for the catalytic oxidation of ammonia were explored over a rather wide range of operating conditions and catalytic materials.

The second method of ammonia removal investigated, adsorption on copper sulfate treated silica gel, is also attractive provided the capacity of the solid for ammonia is sufficiently high and provided regeneration of the saturated bed can be made rapidly and without significant loss of capacity.

The oxides of nitrogen and ammonia are all undesirable contaminants in a life supporting atmosphere. The presence of nitrogen dioxide in particular must be minimized. The maximum allowable concentration levels measured at one atmosphere and 72°F for continuous exposure to these materials are reported (ref. 1) as follows:

NH_3 .... 5.0 ppm by volume
N_2O .... 26.0 ppm by volume
NO .... 26.0 ppm by volume
NO_2 .... 0.5 ppm by volume

2.1 Objectives

The objective of the work reported here was to investigate the removal of ammonia and its oxidation products from spacecabin or other closed system atmospheres. In order to pursue this objective, the following research and development program was followed:

1. Analytical techniques were perfected which would permit the convenient and accurate quantitative analysis of mixtures of ammonia, the nitrogen oxides and air.

2. Several noble metal and metal oxide catalysts were screened in order to determine their activity for ammonia decomposition.

3. The three most promising catalytic materials (ruthenium supported on alumina, platinum supported on alumina, and Hopcalite) were investigated for ammonia decomposition activity and product distribution over a wide range of conditions.

4. The ammonia oxidation data from Step 3 was correlated in order to permit prediction of reactor performance under conditions expected within the contaminant control system of a spacecabin.

5. The adsorption of ammonia on copper sulfate impregnated silica gel was investigated. A model was developed which would permit the prediction of adsorber performance.

2.2 Research Outline

The search for an effective ammonia removal technique was pursued along two fundamentally different routes; these were (a) catalytic oxidation at elevated temperature, and (b) adsorption at ambient temperature. These two efforts were carried out simultaneously and essentially independently.

From very early in the investigation it was known that the major problem which would have to be overcome in order to make catalytic ammonia oxidation a viable method for ammonia removal was to determine ways of minimizing the production of nitrogen oxides. The two major manipulatable variables available for controlling the nitrogen oxides production were catalyst type and oxidation temperature. The experimental program then was to determine the general characteristics of several potentially active catalysts and from these try to pick two or three for more detailed study. Historically the most active ammonia oxidation catalysts known were supported noble metal.

The optimization of reactor temperature is a crucial item. Higher reaction temperatures tend to produce proportionally more nitrogen oxides, particularly nitric oxide and nitrogen dioxide. Since nitric oxide is known to be easily oxidized to nitrogen dioxide at lower temperatures, these two oxides can be considered together. The other undersirable product, nitrous

oxide, is produced in most abundance at temperatures below those which yield nitrogen dioxide. Thus the essential problem was to determine the rates of ammonia removal and nitrogen oxides production over the temperature range potentially available for use in a catalytic removal device.

In the ammonia adsorption phase of the project, the experimental program was designed to provide a series of ammonia breakthrough curves at constant temperature and humidity level. From these curves an isotherm could be determined. Breakthrough curves would also supply the necessary information for development of quantitative relationships for the design of an ammonia adsorption system.

4

3.0 SYMBOLS

A_A = experimental constant in Langmuir equation (ft^3/lb)

A_c = external area of adsorbent, ft^2/lb

A_{NH_3} = pre-exponential term in ammonia rate expression

A_{N_2O} = pre-exponential term in N_2O rate expression

a = external area of catalyst per unit mass (cm^2/g cat)

B_B = experimental constant in Langmuir equation (ft^3/mol)

C = concentration of adsorbate in bulk gas phase (mols/ft^3)

C_{BET} = dimensionless constant in BET equation

C_p = concentration of adsorbate in pore (mols/ft^3)

C_S = adsorbate concentration in equilibrium with solid surface (mols/ft^3)

c = ammonia concentration in bulk phase (ppm)

c_{Ai} = inlet concentration of A (mols A/total mols)

c_{Ao} = outlet concentration of A (mols A/total mols)

c_{Bo} = outlet concentration of B (mols B/total mols)

c_{NO_2} = outlet NO_2 concentration (ppm)

c_{N_2O} = outlet N_2O concentration (ppm)

c_i = ammonia concentration at gas-solid interface (ppm)

c_j = concentration of component j

D = diffusivity (cm^2/sec)

D_K = Knudsen diffusivity (cm^2/sec)

d_p = catalyst particle diameter (cm)

E' = constant in Arrhenius equation, activation energy (Btu/mol)

E_f = effectiveness factor

E_{NH_3} = activation energy for ammonia reaction (Btu/lb mol/°R)

E_{N_2O} = activation energy for N_2O formation (Btu/lb mol/°R)

F_i = inlet flow rate (g mol/hr)

G_M = superficial velocity (mol/hr/cm^2)

h = Thiele modulus, dimensionless

K_g = bulk gas phase mass transfer coefficient (ft/hr)

k = reaction rate constant

k_f' = mass transfer coefficient (g mol/hr/atm/cm^2)

k_1 = true first order rate constant

$(k_1)_{obs}$ = ammonia reaction rate constant

k_{N_2O} = N_2O formation rate constant (g mol N_2O/hr/g cat/(ppm NH_3)$^{0.62}$)

k_0 = experimental rate constant

M = molecular weight of diffusing species

N = rate of mass transfer (g mol/hr/g cat)

N_{Re} = Reynolds number, dimensionless

n = empirically determined reaction order

P = partial pressure

P_T = total pressure (atm)

P_g = partial pressure in bulk phase (atm)

P_i = partial pressure at gas solid interface (atm)

P_o = vapor pressure of adsorbate, in. Hg

R = bed radius, ft

$\hat{R}$ = adsorption rate (mols gas/ft^3 solid - hr)

R_p = pore radius (cm)

R_g = universal gas constant (Btu/mol °R)

r = reaction rate

r_{N_2} = N_2 formation rate (g mol/hr/g cat)

r_{NH_3} = ammonia reaction rate (g mol/hr/g cat)

r_{N_2O} = N_2O formation rate (g mol/hr/g cat)

r_{NO_2} = NO_2 formation rate (g mol/hr/g cat)

r_{eff} = reaction rate in a porous catalyst when there is no internal diffusion resistance (g mol/hr/g cat)

S_X = external area of a single catalyst particle (cm^2)

T = time (hr)

T, T' = absolute temperature (°R)

V = gas phase superficial velocity (ft/hr)

V_P = total volume of a single catalyst particle (cm^3)

V_g = pore volume per unit mass of catalyst (cm^3/g cat)

W = catalyst weight (g)

W = adsorbate loading on solid (mols adsorbate/lb adsorbent)

W_E = equilibrium surface concentration (mols/lb)

W_M = monomolecular coverage of adsorbent by gas (mols/lb)

YK = adsorption rate constant for surface adsorption rate controlling the adsorption (lb/ft^3 hr)

Z = bed length (ft)

α = empirically determined ammonia reaction order, dimensionless

β = empirically determined N_2O formation order, dimensionless

ϵ_B = adsorbent void fraction, diemnsionless

ϵ_P = internal void fraction, dimensionless

Γ =   pore diffusivity, ft^2/hr
μ =   viscosity (g/cm/sec)
ρ =   density (g/cm^3)
ρ_B =   apparent adsorbent density, lbs/ft^3

4.0 PERFORMANCE OF AN AMMONIA OXIDIZER

A major objective of the present study was to develop the data and techniques necessary to design and predict the operating performance of a catalytic oxidizer for ammonia. It was realized early in the project that the variables of primary concern were catalyst type and operating temperature. The activity of catalytic materials for ammonia oxidation varies greatly from material to material. The activity and product distribution of a catalyst are strong functions of reaction temperature. In the following sections the experimental behavior of ammonia over several catalysts is presented.

4.1 Literature Survey

A considerable amount of information regarding the high temperature oxidation of ammonia (above 450°C) is available due to the commercial significance of this reaction in the manufacture of nitric acid (ref. 2). At a temperature of 800°C ammonia can be oxidized almost exclusively to NO using a platinum catalyst.

Much less information is available on the oxidation of ammonia at temperatures below 450°C. Griffiths et al. (ref. 3) performed an infrared study of the adsorption and oxidation of ammonia on silica-supported platinum at temperatures up to 300°C. The authors operated with a 12:1 molar ratio of oxygen to ammonia (total pressure 10 torr) which they state is the optimum condition for a maximum N_2O yield. Up to 178°C they observed the same spectra for ammonia and oxygen as they did for ammonia alone. At 178°C and 191°C they observed a doublet corresponding to gaseous N_2O. The appearance of NO or NO_2 was not reported. The appearance of N_2 was not reported and it is not known whether N_2 would have been detectable with their apparatus.

Amano and Taylor (ref. 4) studied the decomposition of ammonia admixed with N_2 and H_2 only over ruthenium, palladium, and rhodium catalysts supported on alumina. Their temperatures ranged from 340°C and 400°C and the maximum ammonia decomposition observed was 10%. Hydrogen was found to inhibit the reaction over palladium and ruthenium while N_2 was found to be without influence. An observed activation energy of 30 kcal/mol was reported.

Schriber and Parravano (ref. 5) investigated the kinetics of ammonia oxidation over a 0.5% ruthenium catalyst supported on aluminum oxide using a fixed bed recirculation reactor. Their investigation was conducted at six temperatures in the range of 246°C-345°C and at total pressures ranging to 4 atm. The feed composition ranged from 5.3 to 16.5 mol percent ammonia with approximately 10 mol percent O_2, 3 mol percent H_2O, and helium as the diluent. The authors found that the oxidation products were N_2, H_2O, and N_2O. The production of NO_2 was not reported and it is questionable whether it could have been detected.

8

Schriber and Parravano state that the relationship between N_2, N_2O and ammonia can be described by the following reaction scheme:

$$\begin{array}{ccc}
& \xrightarrow{k_1} & N_2O + H_2O \\
NH_3 & & \Big\downarrow k_3 \\
+ & & \\
O_2 & \xrightarrow{k_2} & N_2 \; + H_2O
\end{array}$$
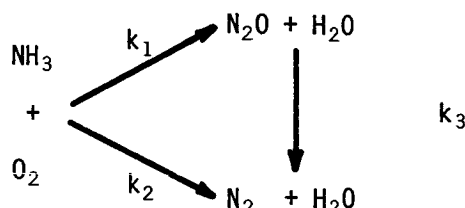
Under the experimental conditions described the authors found that k_3 was much less than k_2 and that the oxidation could thus be represented by two parallel reactions occurring on the ruthenium surface. External mass transfer was not found to be a controlling factor in the kinetics of the reaction, and the authors reasoned that pore diffusion could not be important since the ruthenium metal was deposited on the exterior of the catalyst pellet. The following empirical rate equations were derived from the experimental data:

$$r_{N_2} = (k_0)_{N_2} \; P_{NH_3} \; P_{O_2}^{0.46} \; P_{H_2O}^{-0.40} \tag{4.1}$$

$$r_{N_2O} = (k_0)_{N_2O} \; P_{NH_3}^{1.35} \; P_{O_2}^{0.46} \; P_{H_2O}^{-0.40} \tag{4.2}$$

where k_0 = experimental rate constant
P = partial pressure
r = reaction rate

The apparent activation energies for the formation of N_2 and N_2O were found experimentally to be 12,600 and 35,000 cal/mol respectively. The authors were able to reconcile their experimental k_0 values with theoretical values calculated from absolute rate theory. To make this calculation they assumed that the reaction involved imide (NH) and nitroxyl (HNO) surface intermediates. These two surface compounds had been hypothesized in earlier work (ref. 2).

The catalytic oxidation of NH_3 by air over a promoted nickel oxide catalyst was investigated by N. Giordano, et al. (ref. 6). In the temperature range between 300° and 450°C, the reaction was reported to proceed mainly to N_2 and N_2O. As more sodium or lithium promotor was added both activity and yield of nitrous oxide increased. Doping with trivalent ions tended to depress both activity and yield of nitrous oxide.

The minimum N_2O yield reported at 352°C was approximately 12% and was obtained using NiO doped with 2% Fe_2O_3. However the reaction rate was also

relatively low as only 4% conversion of a 0.3 gmole/hr feed stream was obtained using 0.85 g of catalyst. At 441°C the minimum N_2O yield was approximately 17% using the same catalyst and flow conditions. The sodium and lithium doped catalysts gave 50% to 95% yields of N_2O.

4.2 Modelling Techniques

Generally speaking, the two most common methods of correlating catalytic reaction rate data are the overall fractional order rate expressions and the Langmuir-Hinshelwood rate expressions. The Langmuir-Hinshelwood method attempts to describe the overall reaction in terms of the elementary processes that occur at or near the catalyst surface. The overall rate expressions, on the other hand, neglect the elementary steps and rely instead on a simple rate expression which contains empirical constants having little physical significance. An often used overall rate expression is of the form

$$r = kc_j^n \tag{4.3}$$

where r   = reaction rate
       c_j = concentration of component j
       k,n = empirically determined constants.

In order to reflect the influence of temperature on the reaction rate, the Arrhenius equation is used for the forward rate constant.

$$k = Ae^{-E/RT} \tag{4.4}$$

Kinetic data over a relatively wide range of temperature can usually be represented by the use of this relationship.

A primary advantage of a rate expression of the form

$$r = Ae^{-E/RT} c^n \tag{4.5}$$

is that the effect of the two most important variables is correlated with a minimum number of experimentally determined parameters. This fact is important since the amount of kinetic data generally available is not sufficient to confidently fit a complicated multi-parameter model.

All fluid solid catalytic reactions can be broken down into the following series of steps which occur either in series or in parallel near the catalyst surface:

1. Transport of reactants from the bulk fluid phase to the fluid-solid interface

10

2. Transport of reactants into the catalyst pores

3. Adsorption of reactants on the catalyst surface

4. Surface reaction

5. Desorption of products from the catalyst surface

6. Diffusion of products out of the catalyst pores

7. Transport of products back into the bulk fluid phase.

All of the above listed steps except 2 and 3 occur in series. Steps 2 and 3 occur in parallel because adsorption and reaction occur continually as the reactants pass through the catalyst pores. Steps 1 and 2 are of special significance to this study and will be discussed in more detail. Steps 3 through 5 will be correlated by use of the previously discussed fractional order rate expression.

4.2.1 External Diffusion. - In any catalysis study it is important to ascertain whether or not the reaction rate is strongly influenced by the rate of reactant diffusion to the catalyst surface. When reactant diffusion to the catalyst surface is a rate limiting step then the true nature of the catalytic reaction, including the reaction product distribution, can be masked if the effects of mass transport are not properly accounted for.

Fluid passing over the surface of a catalyst develops a boundary layer external to the catalyst pellet in which the fluid velocity parallel to the surface varies from zero, at the surface, to the bulk stream velocity over a short distance. In the bulk stream, mixing is primarily by turbulent transport, whereas in the boundary layer region transport is by molecular diffusion. Mathematically, the rate of mass transfer from the bulk phase to the catalyst surface can be described by the expression

$$N = k_f' \, a(P_g - P_i).$$ (4.6)

For reactions which are occurring at steady state the rate of mass transfer is also equal to the rate of reaction; therefore

$$r = k_f' \, a(P_g - P_i)$$ (4.7)

where N = rate of mass transfer
k_f' = mass transfer coefficient
a = external area of catalyst particle per unit mass
P_g = partial pressure in bulk phase
P_i = partial pressure at gas-solid interface.

11

The mass transfer coefficient is a function of the physical properties of the compound which is diffusing, as well as the nature of the flow around the catalyst surface. Hougen and Wilkie (ref. 7) developed the following correlations of these variables for packed beds:

$$j_D = \frac{k_f' \, P_T}{G_M} \left(\frac{\mu}{\rho D}\right)^{2/3} = 0.989 \, (N_{Re})^{-0.41} \tag{4.8}$$

and

$$j_D = \frac{k_f' \, P_T}{G_M} \left(\frac{\mu}{\rho D}\right)^{2/3} = 1.82 \, (N_{Re})^{-0.51} \tag{4.9}$$

where $N_{Re} = \dfrac{d_p \, G_M}{\mu}$

d_p = diameter of catalyst particle

G_M = superficial molar velocity

μ = viscosity of mixture

M_m = mean molecular weight

ρ = density of reaction mixture

D = diffusivity

j_D = dimensionless mass transfer number.

Equation (4.8) is valid for Reynolds numbers greater than 350, while Equation (4.9) is valid for lower values.

Using Equations (4.8) and (4.9) it is possible to estimate the value of k_f'. Once k_f' is determined and experimental rate data are available it is possible to estimate the concentration gradient external to the catalyst surface through the use of Equation (4.7). If the value of $P_g - P_i$ in Equation (4.7) is a small fraction of P_g then the resistance of the boundary layer can be neglected. However if not, then the reactant partial pressure at the gas-solid interface must be used in Equation (4.5).

4.2.2 Internal Diffusion. - For a given concentration driving force the rate of surface adsorption in heterogeneous catalysis may be high in comparison with the rate of diffusion, resulting in concentration gradients down the catalyst pores. For this reason the interior of a catalyst pellet may be less effective than the exterior.

Diffusion in catalyst pores may occur by ordinary diffusion, Knudsen diffusion, or surface diffusion. Ordinary diffusion occurs if the size of the pore is large with respect to the mean free path of the molecules. If the size of the pore is small in comparison to the mean free path, then collisions with the pore walls become important. Most catalysts of industrial significance have pore sizes such that Knudsen diffusion predominates (ref. 8). The Knudsen diffusivity can be calculated from the expression

$$D_K = 9.7 \times 10^3 \; R_p \sqrt{T/M} \qquad (4.10)$$

where D_K = Knudsen diffusivity

R_p = pore radius

T = absolute temperature

M = molecular weight of diffusing species.

Surface diffusion occurs as a result of the limited mobility which adsorbed molecules have. Considerably less is known about surface diffusion than Knudsen and ordinary diffusion. Satterfield (ref. 9) states that surface diffusion cannot be important unless very weak surface adsorption bonds are formed.

The effect of pore diffusion on the apparent activation energy can be important, especially at high temperatures. This is because the surface processes (adsorption and surface reaction) increase in rate exponentially with temperature while diffusion rates are not affected as greatly. Thus rate measurements at high temperatures reflect diffusional resistances much more than do low temperature measurements. Satterfield (ref. 9) states that the effect of temperature on diffusion rates is equivalent to an activation energy of 1 to 3 kcal/mol, and that the apparent activation energy when pore diffusion is important will be approximately one-half that of the true activa-

Designating r_{eff} as the reaction rate in a porous catalyst when there is no internal diffusion resistance, an effectiveness factor, E_f, can be defined as

$$E_f = \frac{r}{r_{eff}} \; . \qquad (4.11)$$

It can be seen from Equation (4.11) that the effectiveness factor is the ratio of the observed reaction rate to the reaction rate which would be observed if all the active catalyst surface were on the periphery of the catalyst particle. The effectiveness factor can also be related to the Thiele modulus (ref. 10)

$$E_f = \frac{\tanh (h)}{h} \qquad (4.12)$$

13

where the Thiele modulus, h, is defined as

$$h = 2 \frac{V_p}{S_\chi} \sqrt{\frac{k_1}{2V_g D_k}} \qquad (4.13)$$

where V_p = total volume of a single catalyst particle

S_χ = external area of a single catalyst particle

k_1 = true first order reaction rate constant

V_g = pore volume per unit mass of catalyst.

Using the above equations along with experimentally determined rates, a simple trial and error procedure can be used to obtain E_f.

1. A value of E_f is assumed, and h is calculated from Equation (4.12)

2. Knowing V_p, S_χ, and D_k, k_1 is calculated from Equation (4.13)

3. A new E_f is calculated from

$$E_f = \frac{(k_1)_{obs}}{k_1}$$

where $(k_1)_{obs}$ - observed first order rate constant.

4. If the E_f calculated agrees with the E_f assumed, then the correct value of E_f has been found. If it does not, Step 1 is repeated.

4.2.3 Limitations on Fractional Order Models. - Fractional order rate expressions (as with all empirical expressions) must be used with extreme caution outside of the range of the independent variables used in determining the activation energy and concentration dependency. At higher reagent concentrations the value of n in Equation (4.3) is generally less than one. Since most reactions approach a dependency of one as reagent concentration goes to zero, it is recommended that the value of n be made one for extrapolations of reaction rate at concentrations much below those used in experimentally determining n. This will almost surely result in predicted reaction rates which are slower than physically occur and thus an over designed reactor. However due to the uncertainty involved this conservative approach is warranted.

14

4.3 Preliminary Screening of Catalyst

During the first half of the project, ammonia oxidation data was
obtained using thirteen different catalyst materials. Shown in Table 4.1
are the catalysts which were included in this preliminary screen matrix.
All of the materials tested showed some activity for the removal of am-
monia; however, platinum, ruthenium and Hopcalite seemed most promising
and were selected for further detailed study. Each of these materials
will be separately discussed later.

Both the fixed-bed reactor and the stirred-tank reactor were used
in the preliminary catalyst screening tests. In order to make a relative-
ly easily interpretable comparison of the low temperature ammonia oxida-
tion activity of these catalysts, a first order reaction rate approximation
was used and the resulting rate constant was plotted versus reciprocal tem-
perature.

Although this procedure may not fully compensate for concentration
effects, the procedure does permit the ranking of catalyst in terms of
their activity. Shown in Figure 4.1 are the results of the preliminary
screen tests. These tests were made using air with less than 500 ppm
water. A high first order rate constant at a low temperature is of
course the most desirable situation. As previously mentioned ruthenium,
Hopcalite, and platinum appear to be the most active catalyst. The two
cobalt containing catalysts (Co 0901 and Ni 1601) were both relatively
active, however they both tend to produce a relatively large fraction of
highly undesirable nitrogen dioxide product. "Gatalyst", copper oxide, and
nickel oxide all were considerably less active than the better materials.
The iron oxide, silver and manganese dioxide were not effective showing
only a small amount of reaction at the highest temperatures used.

4.4 Experimental Data - Ruthenium Catalyst

4.4.1 Ammonia Removal Kinetics. - Using the backmix reactor system
it was possible to collect data from which the overall ammonia reaction
rate, N_2O formation rate, and NO_2 formation rate could easily be calculated.
Table 4.2 presents the raw data for reactor inlet and outlet compositions
at five temperatures from 240°F to 442°F. The ammonia concentration in the
reactor outlet varied between 13 and 16 ppm while the ammonia removal rate
varied from 16 X 10^{-6} to 197 X 10^{-6} gmole NH_3/hr/g catalyst between 242°F
and 442°F. The N_2O formation rate was found to be approximately one order
of magnitude lower than the total ammonia removal rate while the NO_2 forma-
tion rate was in most cases less than half the N_2O rate.

Figures 4.2 and 4.3 show the total ammonia reaction rate versus bulk
concentration at five temperature levels. The curved lines through the
data on the figures were obtained by a linear least squares fit to the
three parameter equation

$$\ln r_{NH_3} = \ln A_{NH_3} + \alpha \ln c_i - \frac{E_{NH_3}}{RT} \qquad (4.14)$$

15

TABLE 4.1

CATALYSTS INCLUDED IN SCREENING TESTS

CATALYST MATERIAL	COMPANY DESIGNATION	SURFACE AREA m^2/g
2% MnO_2 supported on silica	Harshaw Mn-0501	258
0.3% Pd supported on high activity alumina	Harshaw Pd-0501	186
0.5% Pt supported on alumina	Englehard 0.5% Pt supported on alumina	93
0.5% Ru supported on alumina	Englehard 0.5% Pt supported on alumina	74
4% nickel oxide, 4% cobalt oxide, 4% iron oxide supported on activated alumina	Harshaw Ni-1601	78
14% nickel oxide supported on high activity alumina	Harshaw Ni-0707	140
10% CuO supported on high activity alumina	Harshaw Cu-0803	137
19% MnO_2 supported on activated alumina	Harshaw Mn-0201	69
20% Fe_2O_3 supported on activated alumina	Harshaw Fe-0301	41
3.5% Ag supported on inert alumina	Harshaw Ag-0101	1
5% Cobalt oxide, 5% copper oxide supported on activated alumina	Harshaw Co-0901	59
Not reported	General American Transportation "Gatalyst"	Not reported
Mixed oxides of Manganese and copper	Mine Safety Appliance "Hopcalite"	156

16
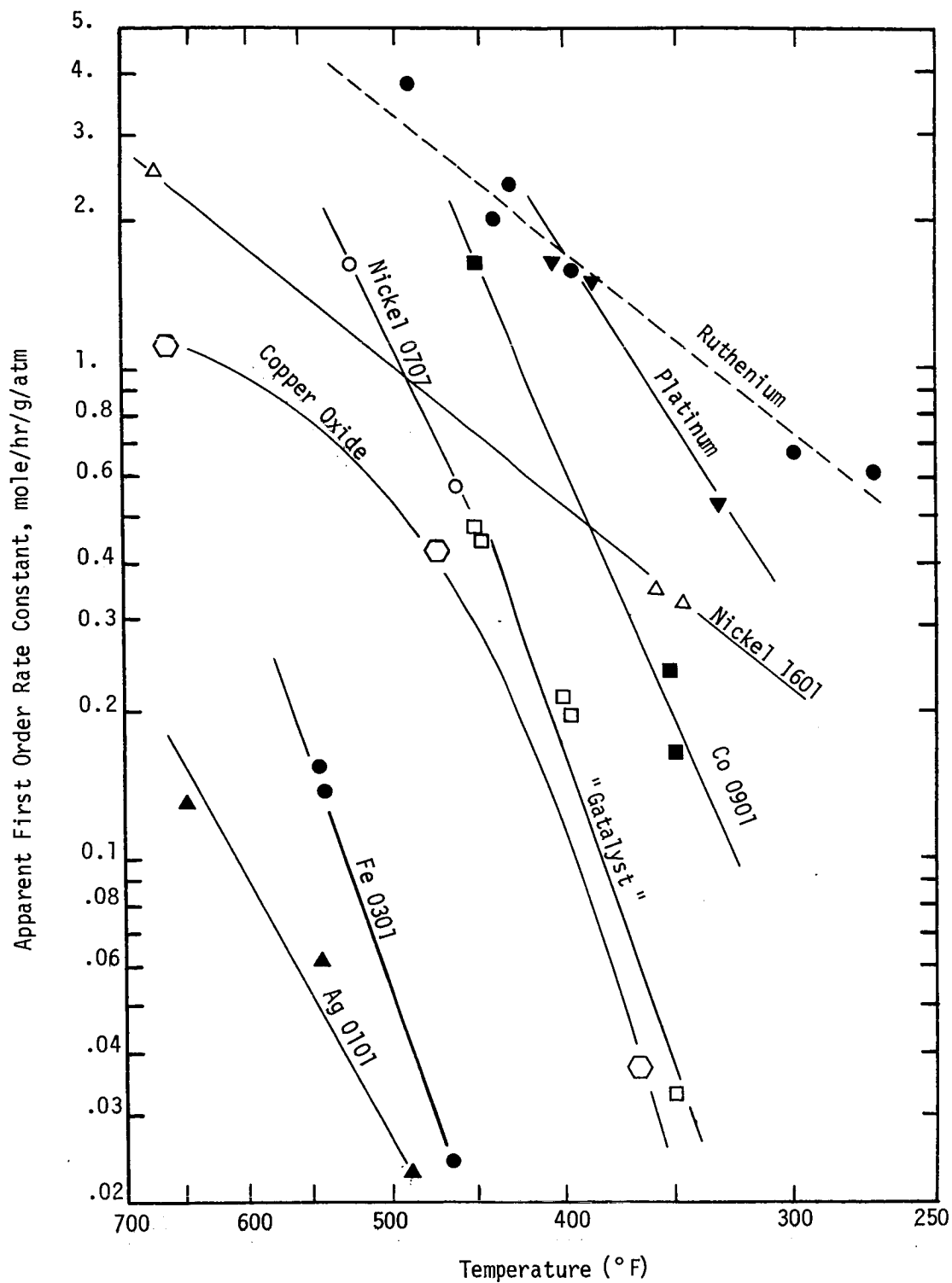
Figure 4.1 - Comparison of Catalytic

Activity for Ammonia

Oxidation

17

TABLE 4.2

BACKMIX REACTOR DATA FOR RUTHENIUM CATALYST*

Run No.	Catalyst Wt., g	Temp. °F	Air Flow g mol/hr	ppm NH_3 in	ppm NH_3 out	ppm NO_2 out	ppm N_2O out
2/ 8/71-2	6.903	240	2.425	232	109	1	2
2/ 5/71-1	6.903	242	2.425	74	28	1	2
2/ 5/71-2	6.903	242	2.425	105	42	NM**	2
2/ 5/71-3	6.903	242	2.425	195	92	NM	1
1/26/71-1	7.136	300	2.425	209	70	1	13
2/ 2/71-1	7.136	305	2.425	165	47	1	10
2/ 3/71-1	6.903	302	2.425	98	34	1	6
2/ 3/71-2	6.903	302	2.425	50	16	1	3
2/ 3/71-3	6.903	302	2.425	255	86	1	9
2/ 6/71-1	6.903	300	3.175	250	90	2	12
2/ 6/71-2	6.903	300	3.175	368	166	1	15
1/26/71-2	7.136	300	2.425	221	80	2	10
11/10/70-1	8.431	345	2.425	88	19	5	11
11/10/70-2	8.431	345	1.675	130	22	6	17
11/11/70-1	8.431	340	3.175	78	20	2	7
11/11/70-2	8.431	350	3.175	262	68	4	23
11/12/70-1	8.431	350	3.175	182	52	4	14
2/15/71-1	6.903	350	2.425	376	100	1	32
2/ 4/71-1	6.903	400	3.960	246	86	5	19
2/ 4/71-2	6.903	400	3.175	313	97	6	26
2/ 1/71-1	7.136	400	2.425	185	29	17	NM
2/ 1/71-2	7.136	400	2.425	284	41	11	NM
2/ 1/71-3	7.136	400	2.425	150	16	16	NM
1/21/71-1	7.136	402	2.425	167	28	33	17
1/21/71-2	7.136	400	2.425	181	18	NM	17
1/29/71-1	7.136	400	2.425	390	84	9	NM
1/29/71-2	7.136	400	3.175	265	69	9	NM
1/29/71-3	7.136	400	2.425	89	13	17	NM
2/12/71-2	6.903	400	2.425	302	57	6	27

TABLE 4.2 .....continued

Run No.	Catalyst Wt., g	Temp. °F	Air Flow g mol/hr	ppm NH₃ in	ppm NH₃ out	ppm NO₂ out	ppm N₂O out
3/26/71-1****	6.903	400	3.900	343	114	15	31
3/19/71-1****	6.903	400	2.425	189	23	15	19
3/22/71-1****	6.903	398	2.425	330	49	12	37
3/22/71-2****	6.903	398	2.425	147	24	15	15
3/13/71-1***	6.903	400	2.425	261	35	NM	28
3/15/71-1***	6.903	400	2.425	356	67	NM	NM
3/15/71-2***	6.903	400	2.425	317	66	NM	NM
3/24/71-1***	6.903	400	2.425	157	25	12	13
9/ 3/70-1	2.730	440	1.675	412	91	NM	NM
9/ 3/70-2	2.730	440	1.675	88	20	NM	NM
9/ 4/70-1	2.730	435	1.675	72	14	NM	NM
1/19/71-1	14.311	450	3.175	365	35	NM	NM
12/ 2/70-1	14.311	435	3.175	262	18	NM	29
12/ 2/70-2	14.311	435	3.175	262	30	NM	31
4/16/71-1	6.903	444	2.425	309	29	NM	24
4/16/71-2	6.903	444	2.425	470	67	NM	52

*   all runs made at atmospheric pressure
**   not measured
***   humidified run
**** pure O₂ run
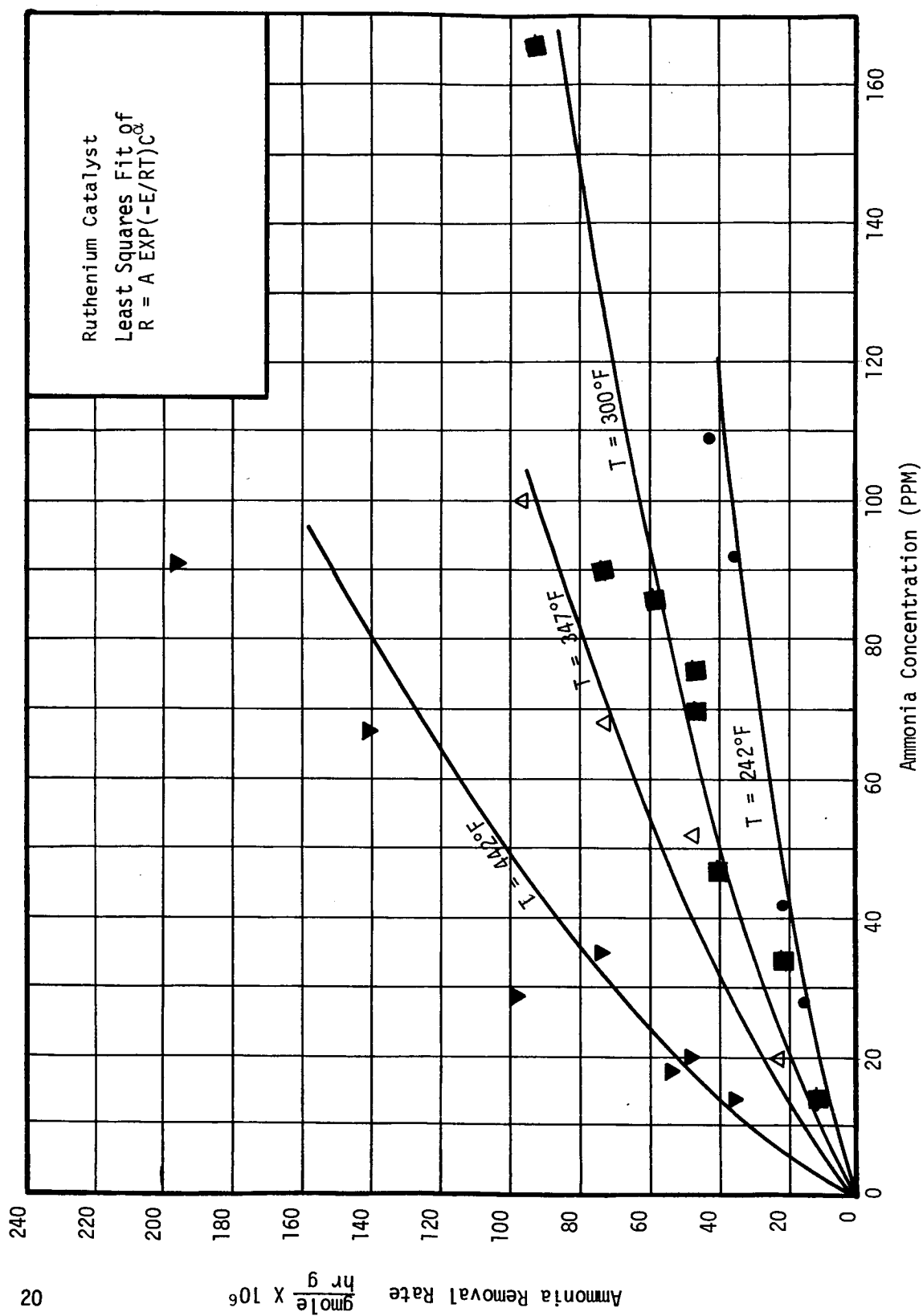
Figure 4.2 – Differential Data Showing Ammonia
Removal Rate Versus Concentration
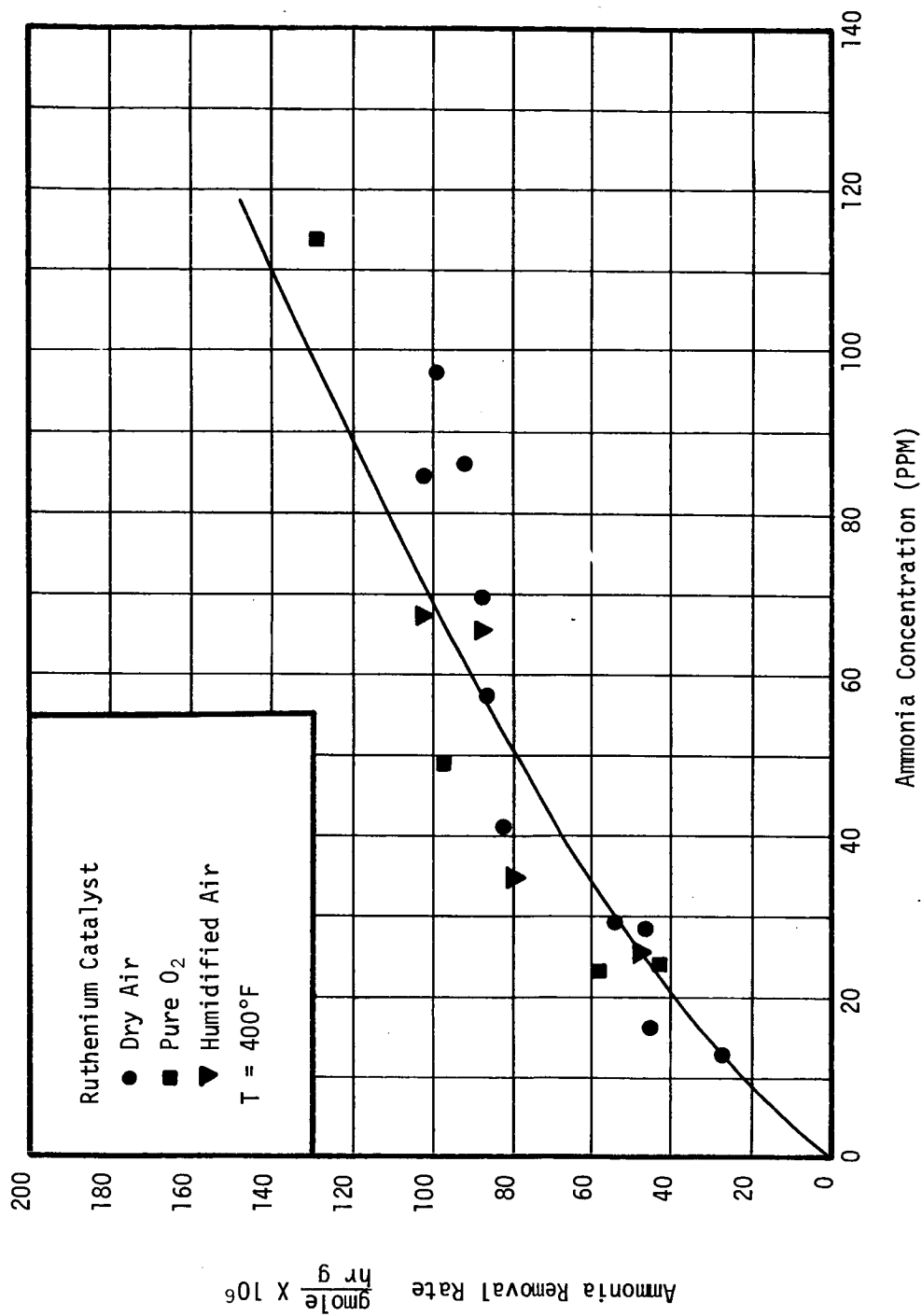
Figure 4.3 - Differential Data Showing Ammonia Removal

Rate at 400°F

where r_{NH_3} = ammonia reaction rate

A_{NH_3} = pre-exponential term in Arrhenius expression

E_{NH_3} = activation energy for ammonia reaction

R = universal gas constant

T = absolute temperature

c_i = ammonia concentration at gas-solid interface

α = reaction order.

The equation form used results in curves passing through the origin (as would be expected theoretically); however, caution should be used in extrapolation to concentrations outside of the data set. (See also Section 4.2.2). Although the concentration on the absicissas of Figure 4.2 and 4.3 refer to bulk ammonia concentration, interfacial values were used in determining the constants A_{NH_3}, E_{NH_3}, and α. The best values of A_{NH_3}, E_{NH_3}, and α were found by the least squares procedure to be

$$A_{NH_3} = 2.204 \times 10^{-3} \ \frac{(\text{gmole NH}_3)}{(\text{hr})(\text{g cat})(\text{ppm NH}_3)^{0.69}}$$

$$E_{NH_3} = 10,100 \ \frac{\text{Btu}}{\text{lb mol}}$$

$$\alpha = 0.69 \quad .$$

The average deviation between the predicted and experimental points of Figures 4.2 and 4.3 was found to be 14.5%. Inherent in using an equation such as (4.14) is the assumption that the order of the reaction does not change over the temperature range of interest. This is believed to be a reasonable assumption in view of the relatively low temperatures and short temperature range involved in this investigation.

The rate expression and experimentally determined kinetic parameters discussed above were used to predict the ammonia removal for an integral reactor. The fixed bed reactor was then operated to provide experimental integral reactor data to compare with the predicted ammonia removal. In order to make the integral reactor calculations a numerical integration program was utilized which included the effects of external diffusion as discussed in Section 4.2.1.

22

The comparison of experimental and calculated ammonia removal is shown in Figures 4.4 and 4.5 for reaction temperatures of 300°F and 400°F. The agreement shown in these tests indicates that the performance of an integral reactor using ruthenium on alumina catalyst can be predicted with confidence from the kinetic constants given above.

4.4.2 Nitrous Oxide Production Kinetics. - Figures 4.6 through 4.9 show the rates of formation of N_2O as a function of the bulk ammonia concentration at five temperatures. The curved lines shown were obtained by a linear least squares fit to the equation

$$r_{N_2O} = A_{N_2O} \exp\left(-\frac{E_{N_2O}}{RT}\right) c_i^{\beta} \qquad (4.15)$$

where r_{N_2O} = N_2O formation rate

A_{N_2O} = pre-exponential term in Arrhenius expression

E_{N_2O} = activation energy for N_2O formation

β = reaction order.

The best values of A_{N_2O}, E_{N_2O}, and β were found to be

$$A_{N_2O} = 0.126 \ \frac{(gmole \ N_2O)}{(hr)(g \ cat)(ppm \ NH_3)^{0\ 70}}$$

$$E_{N_2O} = 20,640 \ \frac{Btu}{lb \ mol}$$

$$\beta = .70 \ .$$

The average deviation between the predicted and experimental points for N_2O formation was found to be 30%. The low temperature point contributed the largest amount to the average deviation due to the very small reaction rates involved.

23
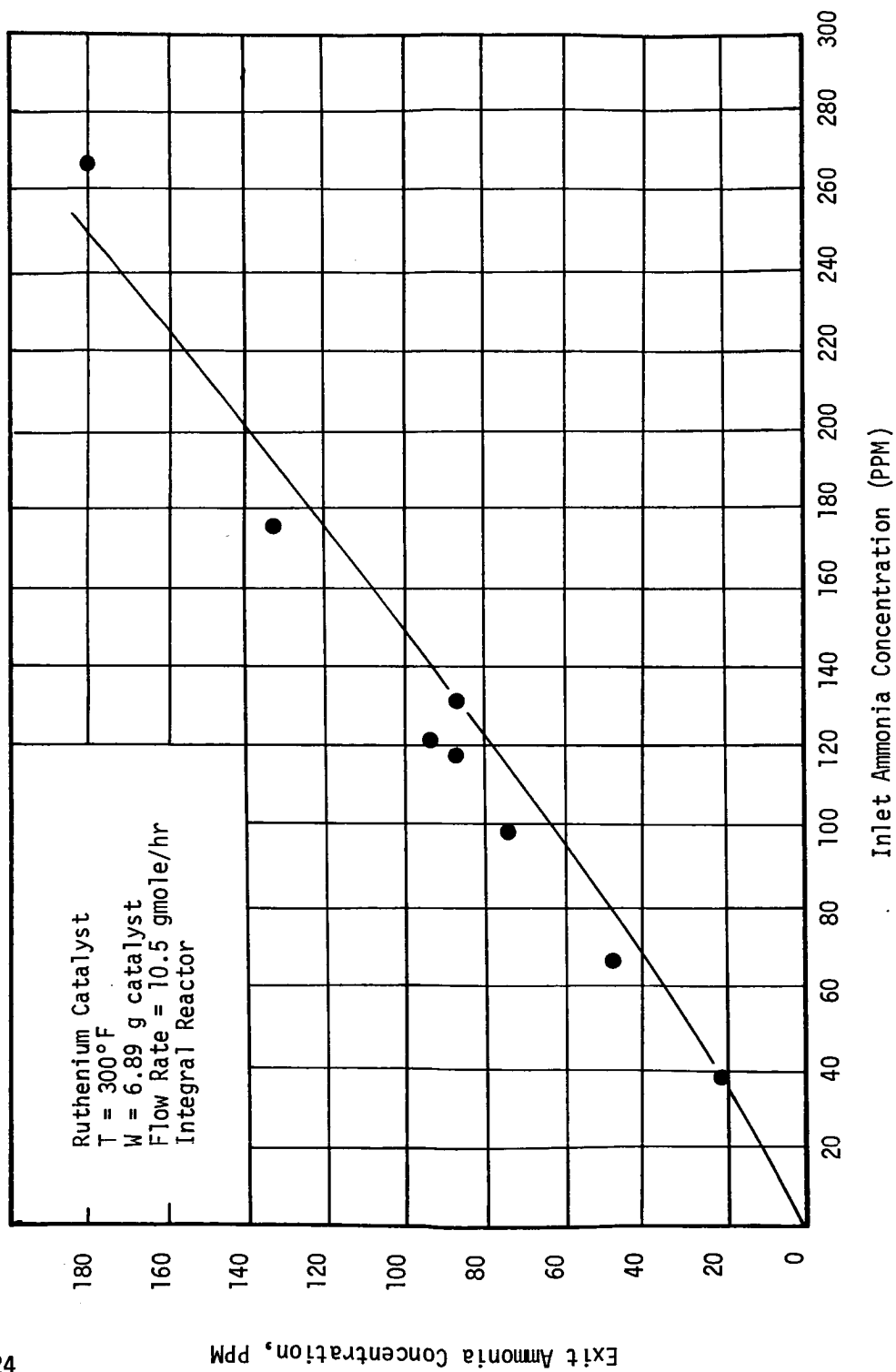
Figure 4.4 - Comparison of Calculated and Experimental

Ammonia Conversion for Fixed Bed Reactor

at 300°F

24
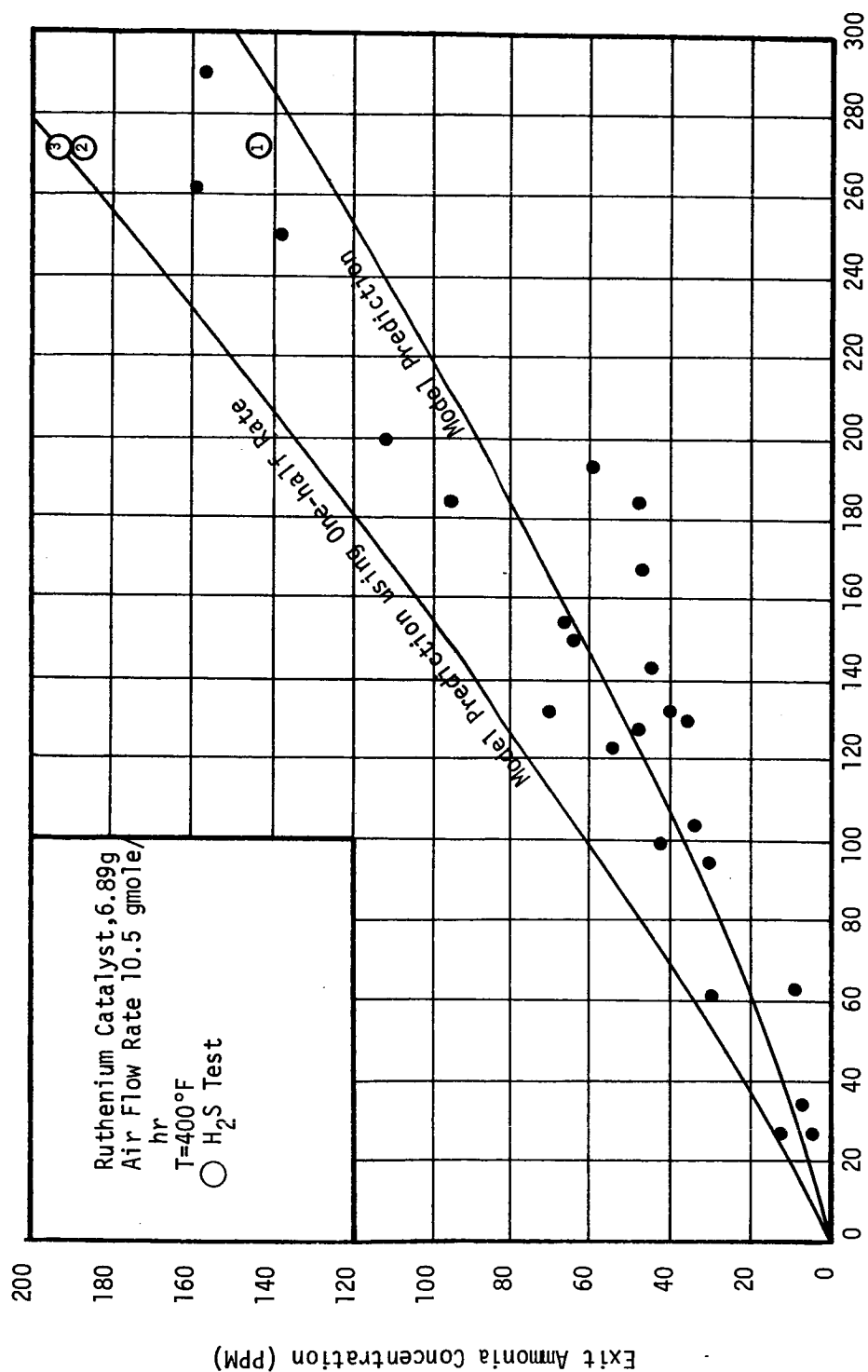
Figure 4.5 - Comparison of Calculated and Experimental Ammonia Conversion for Fixed Bed Reactor at 400°F

25
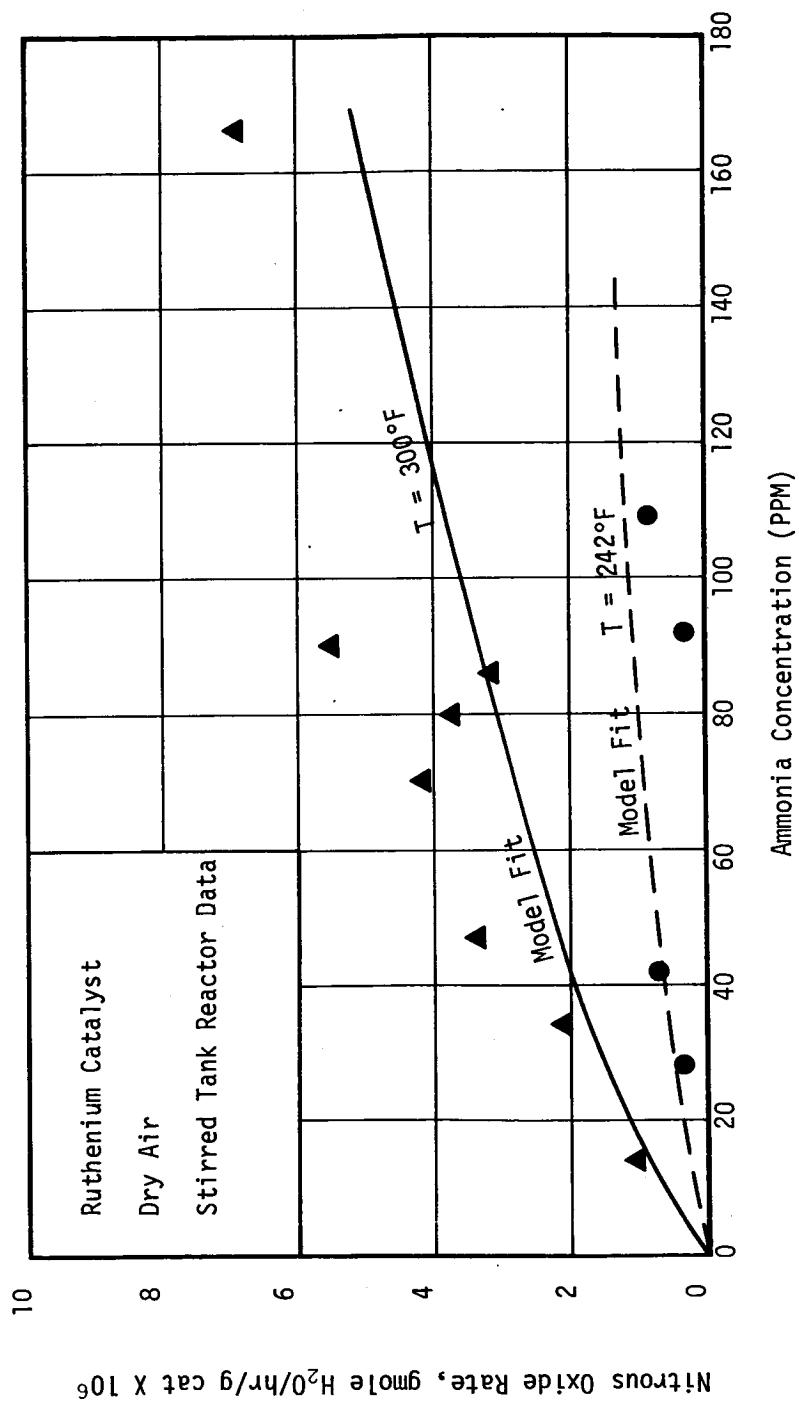
Figure 4.6 – Nitrous Oxide Production Rate Over Ruthenium at 242°F and 300°F
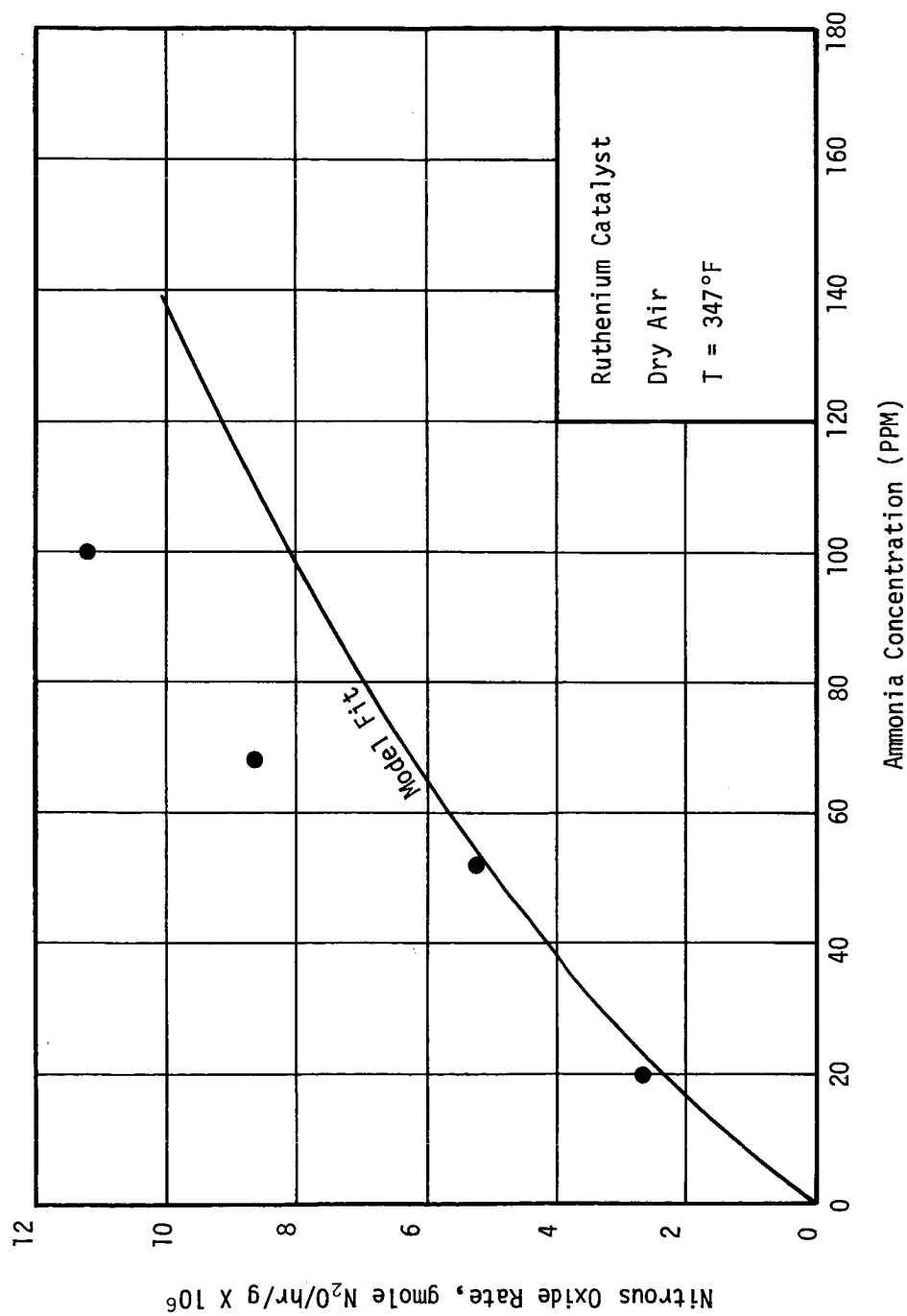
Figure 4.7 - Nitrous Oxide Production Rate
at 347°F

Ammonia Concentration (PPM)

Nitrous Oxide Rate, gmole N_2O/hr/g X 10^6

Ruthenium Catalyst

Dry Air

T = 347°F

Model Fit
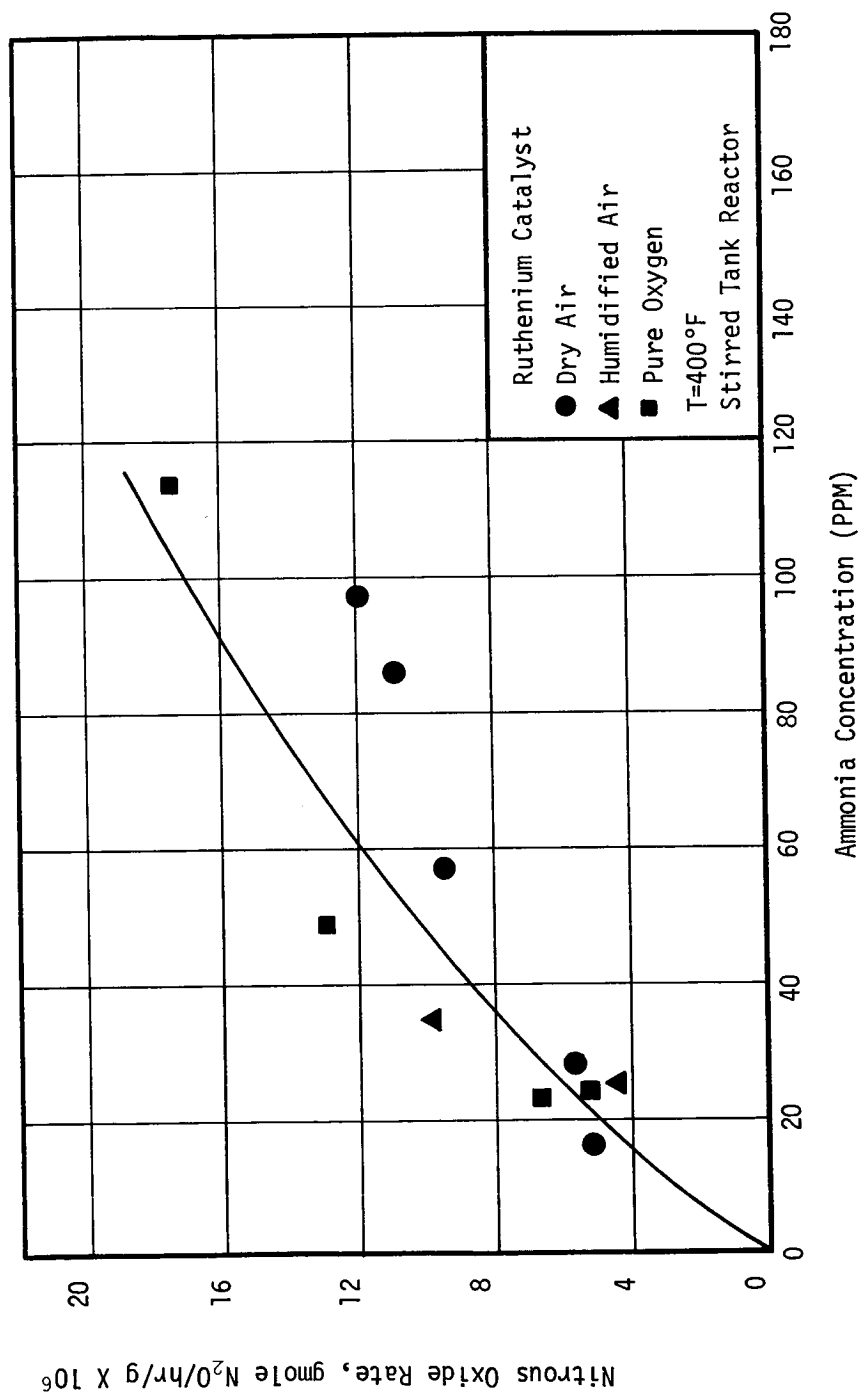
Figure 4.8 - Nitrous Oxide Production Rate at 400°F

Ammonia Concentration (PPM)

Nitrous Oxide Rate, gmole $N_2O/hr/g$ X 10^6

Ruthenium Catalyst
● Dry Air
▲ Humidified Air
■ Pure Oxygen
T=400°F
Stirred Tank Reactor

28
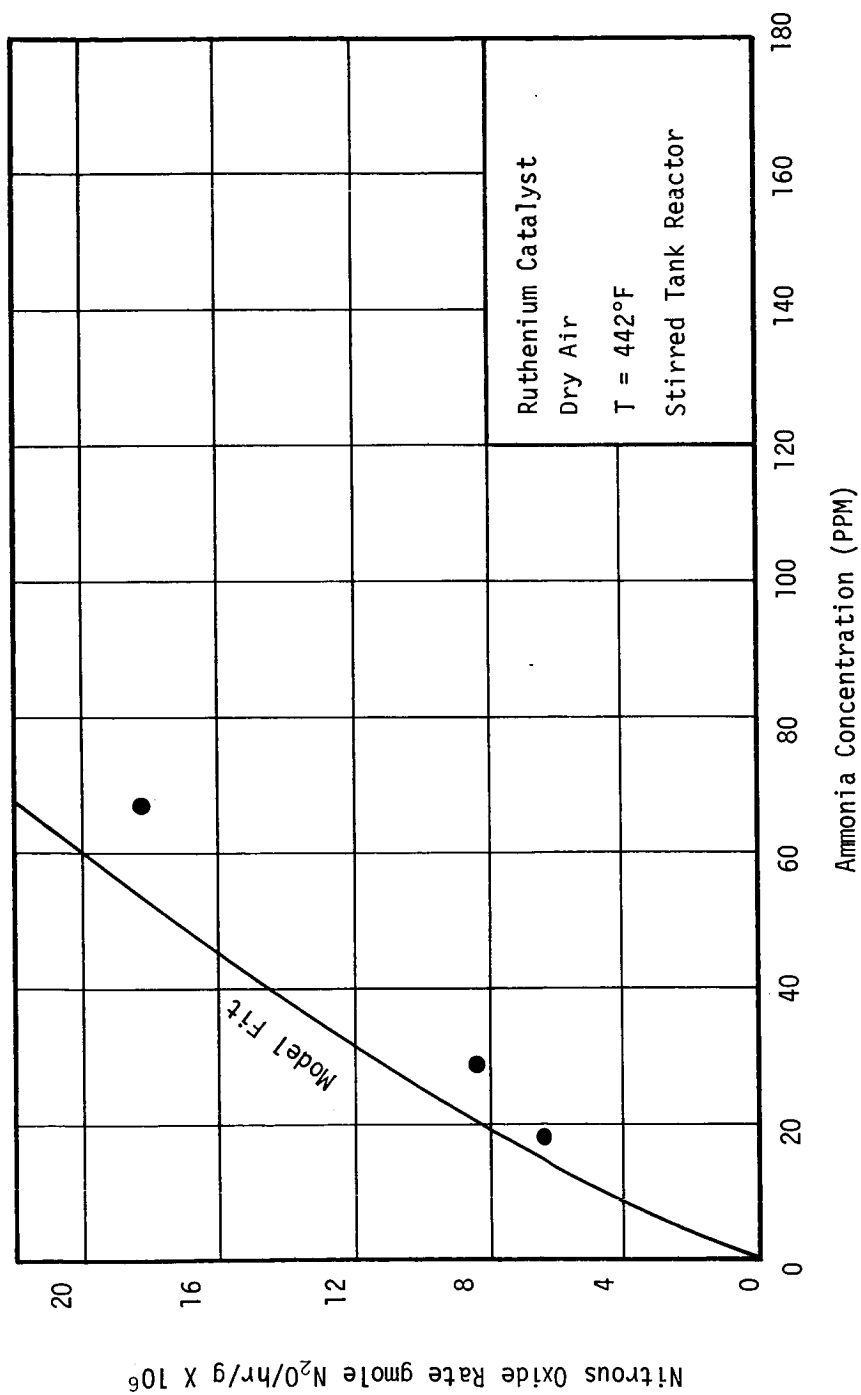
Figure 4.9 - Nitrous Oxide Production Rate

at 442°F

Ruthenium Catalyst
Dry Air
T = 442°F
Stirred Tank Reactor

Ammonia Concentration (PPM)

Nitrous Oxide Rate gmole N_2O/hr/g X 10^6

Model Fit

Just as with the ammonia removal data, the nitrous oxide production for an integral reactor was predicted based on the above kinetic constants. The fixed bed reactor was used to generate experimental nitrous oxide production data for comparison with the prediction. Shown in Figure 4.10 are the predicted and experimental nitrous oxide production for temperatures of 300°F and 400°F. The experimental nitrous oxide yield was less at both temperatures than the model prediction. Thus the model may be expected to predict more nitrous oxide than will be actually experienced.

Since the ammonia concentration dependency (or reaction order) of both the ammonia removal and nitrous oxide production are approximately the same, the percentage conversion to N_2O would not be dependent on ammonia concentration. However since the activation energy for nitrous oxide production is approximately twice that for ammonia removal, the percentage yield of nitrous oxide rises rapidly with increased temperature.

4.4.3 Nitrogen Dioxide Production Kinetics. - Nitrogen dioxide production rates were found to be a strong function of reaction temperature with an activation energy of approximately 28,000 Btu/mole. At all temperatures below 400°F the conversion to nitrogen dioxide was very small. At 400°F less than 2% of the reacted ammonia was converted to nitrogen dioxide and at temperatures of 300°F and below less than 1% conversion of ammonia to nitrogen dioxide was found.

4.4.4 Effect of Water. - The triangular data points on the 400°F data of Figures 4.3 and 4.8 represent runs in which the inlet air stream to the reactor was humidified to 0.7 mol percent H_2O (23% relative humidity at 72°F) and fed to the reactor. As can be seen from the positions of the data points in Figure 4.3, the overall NH_3 removal rate is not significantly depressed by the presence of H_2O at this concentration. Referral to Figure, 4.8 shows that H_2O also exhibits no inhibitory effect on N_2O formation. These facts are not in agreement with the findings of Schriber (ref. 5) who found H_2O to be a strong inhibitor as evidenced by his proposed rate equations

$$r_{N_2} = (k_o)_{N_2} \; P_{NH_3} \; P_{O_2}^{0.46} \; P_{H_2O}^{-0.40}$$

and

$$r_{N_2O} = (k_o)_{N_2O} \; P_{NH_3}^{1.35} \; P_{O_2}^{0.46} \; P_{N_2O}^{-0.40} \quad .$$

4.4.5 Effect of Oxygen. - The square data points of Figures 4.3 and 4.8 represent data taken with pure O_2 substituted for air in the reactor inlet. As can be seen from Figure 4.3, the additional O_2 does not seem to have an

30
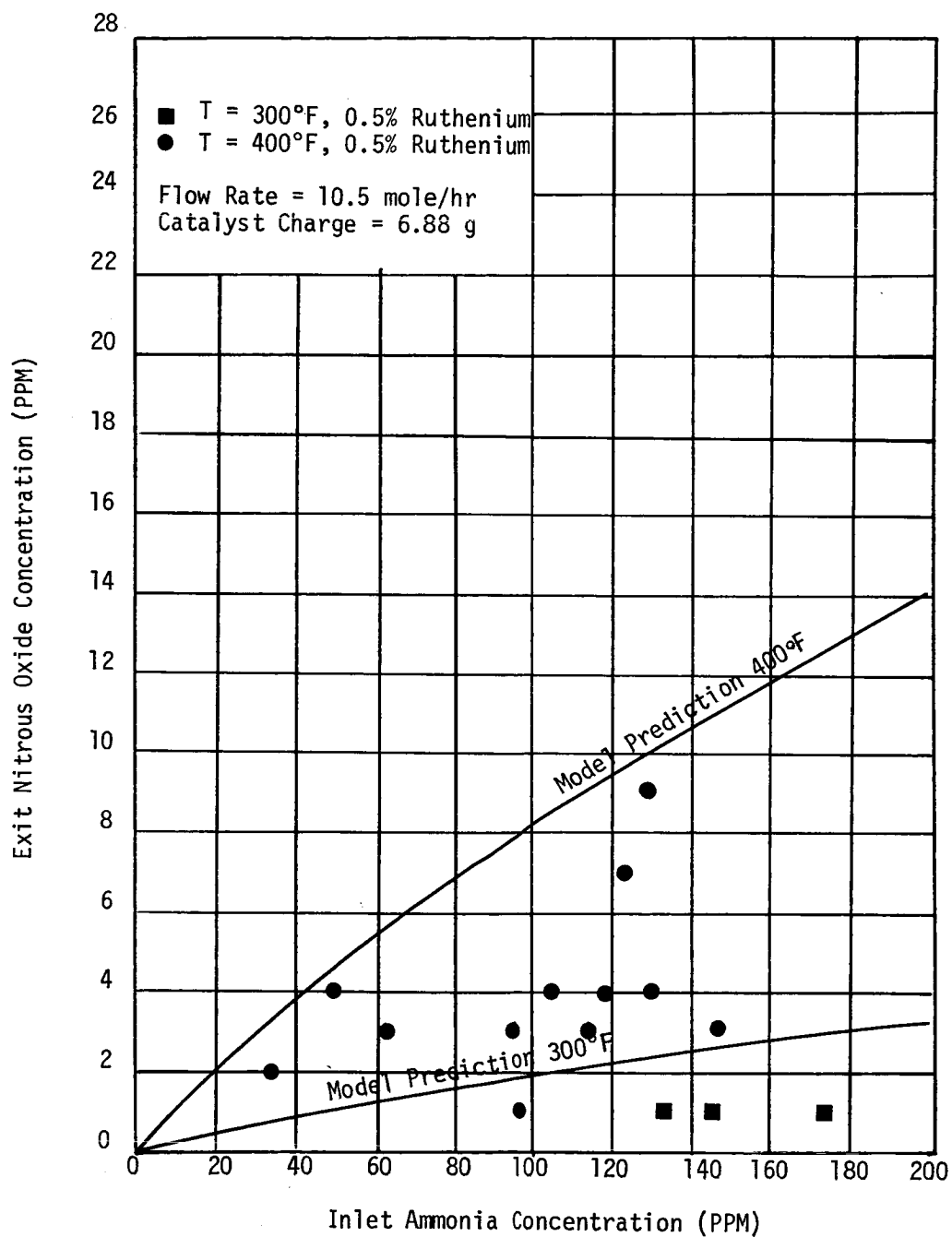
Figure 4.10 - Nitrous Oxide Production Using Integral

Reactor and Ruthenium Catalyst

effect on the overall ammonia removal rate. Referral to Figure 4.8 shows that the rate of formation of N_2O appears to be slightly increased due to the added O_2. If the rate of N_2 and NO_2 formation are unaffected, however, the additional N_2O formation would not be sufficient to cause a noticeable increase in the overall ammonia removal rate.

4.4.6 Internal Diffusion Effects. - In order to ascertain whether or not pore diffusion was a significant resistance, an effectiveness factor was calculated using the simplified scheme presented by Smith (ref. 8) and explained in section 4.2.2. Using an approximate first order rate constant of 5 gmole/hr/g cat. for the 400°F data and the catalyst properties supplied by the manufacturer (Appendix A), an effectiveness factor of 83.5% was calculated meaning that no significant concentration gradients would occur within catalyst pellets.

Examination of a catalyst pellet that had been sliced in two (see Figure 4.11) revealed a dark thin outer crust surrounding the inner alumina support (white). It is believed that this thin outer layer contained all of the ruthenium metal, thus lending support to the high calculated effectiveness factor.

4.4.7 Effect of Hydrogen Sulfide. - Noble metal catalyst for many reactions are notoriously susceptible to poisoning by sulfur containing materials particularily hydrogen sulfide. The ruthenium catalyst under study in this project was exposed to relatively large concentrations of H_2S for short periods of time and then the ammonia oxidation activity of the catalyst was determined.

In order to obtain a basis for comparison, the unpoisoned catalyst was tested in the integral reactor at 400°F with an inlet ammonia concentration of 271 ppm and flow rate of 10.5 gmole air/hr. Using a 6.89 g sample of catalyst the outlet ammonia concentration was 144 ppm. This point is shown in Figure 4.5 by the symbol ① . As can be seen from the figure, the conversion is in good agreement with the model predicted rate at this condition. A 50 cc sample of reagent grade H_2S was then injected into the feed stream to the reactor over a three minute time interval. Since H_2S is known to be oxidized in the presence of many metals, an unknown amount of the material could have been oxidized to sulfur or sulfur dioxide before reaching the catalyst. The relatively high concentration of H_2S was used in order to cause at least some unoxidized material to reach the catalyst. Based on the inlet flow rate the average inlet H_2S concentration was about 350 ppm. The reactor exit was sampled following the injection and the ammonia conversion was found to have fallen from 46.9% for unpoisoned catalyst to 30.2%. This point is indicated by the symbol ② on Figure 4.5. A second 50 cc injection further reduced the conversion to 28.4%. This point is indicated by the symbol ③ on Figure 4.5. The two injections together caused a reduction in reaction rate of approximately 50%.

Although exposure to hydrogen sulfide does significantly reduce oxidation activity it does not entirely deactivate the catalyst even in relatively large concentrations.

32
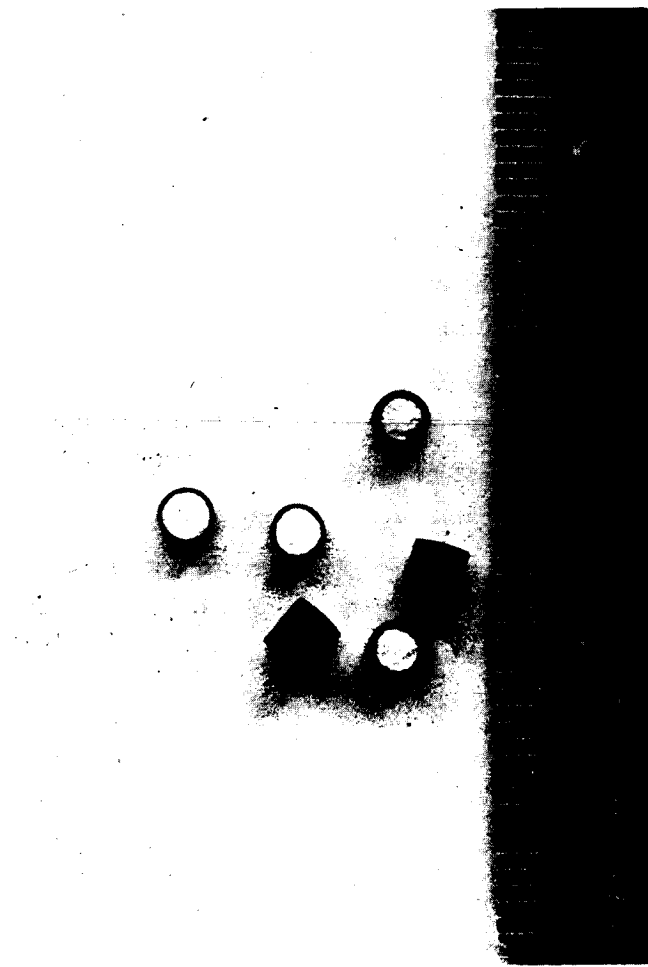
Figure 4.11 — Ruthenium Catalyst Pellets

4.4.8 Effect of External Mass Transfer. - In any catalytic reaction study it is important to ascertain whether or not there are significant concentration gradients between the bulk fluid and the catalyst surface. If mass transfer to the catalyst surface is a major resistance, the apparent activation energy which is measured will be lower than the intrinsic activation energy when surface adsorption and reaction are the controlling resistances.

Well established techniques are available for evaluating the importance of external mass transfer in fixed beds as was discussed previously in section 4.2.1. These methods were used directly in calculations involving the integral reactor.

In the case of the stirred-tank reactor, the data were obtained at a rotor speed of 550 r.p.m. This can be converted to a catalyst basket linear velocity of 242 cm/sec. Because the gas inside the reactor could be swirling at an unknown rate in the direction of travel of the catalyst basket, the difference in velocity between the gas and the catalyst baskets is unknown. It is this velocity difference, which shall be designated the slip velocity, which is important in estimating mass transfer coefficients for use in predicting external concentration gradients.

If a slip velocity is assumed, and it is assumed that this slip velocity is analogous to the true gas velocity in the interstices of a packed bed containing 30% voids, then the packed bed correlations can be used to estimate external concentration gradients in the backmix reactor. The following equation was used in the calculation:

$$\frac{k_f' \ P_T}{G_M} \ (\frac{\mu}{\rho D})^{2/3} = 1.82 \ (N_{Re})^{-0.51} \tag{4.16}$$

where

$$N_{Re} = \frac{d_P \ G_M}{\mu} \quad .$$

By assuming a slip velocity, G_M can be calculated thus making it possible to calculate k_f', the mass transfer coefficient. Since at steady state the rate of mass transfer through the external boundary layer is equal to the rate of reaction, the following equation can be used to calculate the concentration gradient:

$$r = k_f' \ a(P_g - P_i) = k_f' \ a \ P_T(c_g - c_i) \tag{4.17}$$

34

where P_T = total pressure

   c_g = bulk concentration

   c_i = concentration at gas-solid interface.

Knowing the bulk concentration enables one to calculate the interfacial concentration. Knowing the interfacial concentrations and the experimentally determined reaction rates, it is possible to obtain kinetic correlations which exclude bulk transport effects. This is what was done in the development of Equations (4.14) and (4.15). In obtaining these equations the slip velocity was taken to be equal to the basket velocity (242 cm/sec), thus allowing values of c_i to be calculated. Values of c_i, r_{N_2O}, and r_{NH_3} were then fit by the least squares procedure to Equations (4.14) and (4.15). Table 4.3 shows some typical results of the external mass transfer calculations which were made using the 242 cm/sec velocity. As can be seen from this table the external concentration gradient is negligible at 242°F but increases to a moderate level at 400 and 442°F. The slip factor has very little influence on the calculated value of either the activation energy or the reaction order. The calculated pre-exponential factor decreases with a decreased slip factor. These observations indicate that the activation energy for the lumped ammonia adsorption and reaction step is truly low (5610 cal/gmole), and is not seriously affected by the temperature dependency of the bulk transport step should the slip factor in actuality be less than one. If the slip factor is in actuality lower than the assumed value of 1.0, then the implication is that the proposed Equations (4.14) and (4.15) would predict rates which are low. Thus, a reactor which was operated with absolutely no external mass transfer resistance would show ammonia reaction rates and N_2O formation rates higher than those predicted by Equations (4.14) and (4.15).

The equations developed using the above mentioned procedure were verified with the results from the integral reactor. The Reynolds number in the integral reactor were typically about 35 which results in ammonia mass transfer coefficients of 1.15 to 1.20 gmole/hr/cm^2/atm.

Low intrinsic activation energies for other oxidation reactions have been reported in the literature. Johns (ref. 11) in an article on the oxidation of trace amounts of CH_4 at 500 to 600°F presents data from which an activation energy of 7,250 cal/gmole can be calculated. Satterfield (ref. 9) cites research on the oxidation of benzene in which an activation energy of 2,000 cal/gmole was obtained. In view of these facts, the activation energy reported in this work is not unreasonable.

TABLE 4.3

TYPICAL RESULTS OF EXTERNAL
MASS TRANSFER CALCULATION

Temp. °F	Experimental NH_3 Reaction Rate gmole/hr/g cat X 10^6	c ppm NH_3	N_{Re}	k'_f gmole/hr/cm²/atm	c_i ppm NH_3	$\frac{c-c_i}{c}$ X 100, %
242	21.7	42	104	1.61	41	2.4
300	39.7	47	93	1.58	44	6.4
347	49.1	52	85	1.56	48	7.7
400	82.0	41	77	1.53	35	14.6
442	73.1	35	72	1.52	30	14.3

4.5 Experimental Data - Platinum Catalyst

During the early screening of catalyst, supported platinum was found to be relatively active for ammonia oxidation (see Figure 4.1). The catalyst used and some of its properties are shown in Table 4.1 and Appendix A. In order to compare the ammonia oxidation characteristics of this 0.5% platinum to the previously studied ruthenium catalyst, 25 experimental runs were made using the fixed bed integral reactor. The results of these runs are shown in Figure 4.12 along with the calculated results using the ruthenium model. As may be seen the ammonia oxidation rate at 400°F is essentially the same with platinum as with ruthenium. Humidifying the air to 23% relative humidity at 72°F may have resulted in some small <u>increase</u> in the reaction rate.

The product distribution from platinum is definitely different than from ruthenium. Shown in Figure 4.13 is the exit nitrous oxide concentration versus inlet ammonia concentration for the integral reactor runs. For comparison the ruthenium model predicted nitrous oxide concentration is shown. The rate of nitrous oxide production using the platinum catalyst is two to three times greater than for ruthenium (see Figure 4.10 for a comparison).

These results indicate that although platinum may be more tolerant of humidity, its tendency to produce excessive nitrous oxide makes it a inferior catalyst to ruthenium for spacecabin applications.

4.6 Experimental Data - Hopcalite Catalyst

Of the catalyst investigated Hopcalite (see Appendix A and Table 4.1) was the only non-noble metal catalyst that showed promise. This catalyst is reported by the manufacturer to consist of mixed oxides of maganese and copper. Considerable oxidation data has been obtained for the Hopcalite catalyst at temperatures between 121 and 352°C with the air flow rate varying between 6.3 and 12.6 moles/hr. A summary of the data collected is given in Tables 4.4 and 4.5.

4.6.1 <u>Theoretical Development</u>. - During preliminary evaluation of the Hopcalite catalyst isothermal plots of ammonia removal rates as a function of average ammonia concentration appeared linear which suggested that the reaction is first order with respect to ammonia concentration.

To determine the validity of this assumption an Arrhenius plot was constructed from the data given in Table 4.4. The assumption of first order kinetics leads to the rate equation

$$r = Kc_{ave} = \frac{F}{W} (c_1 - c_2) \qquad (4.18)$$
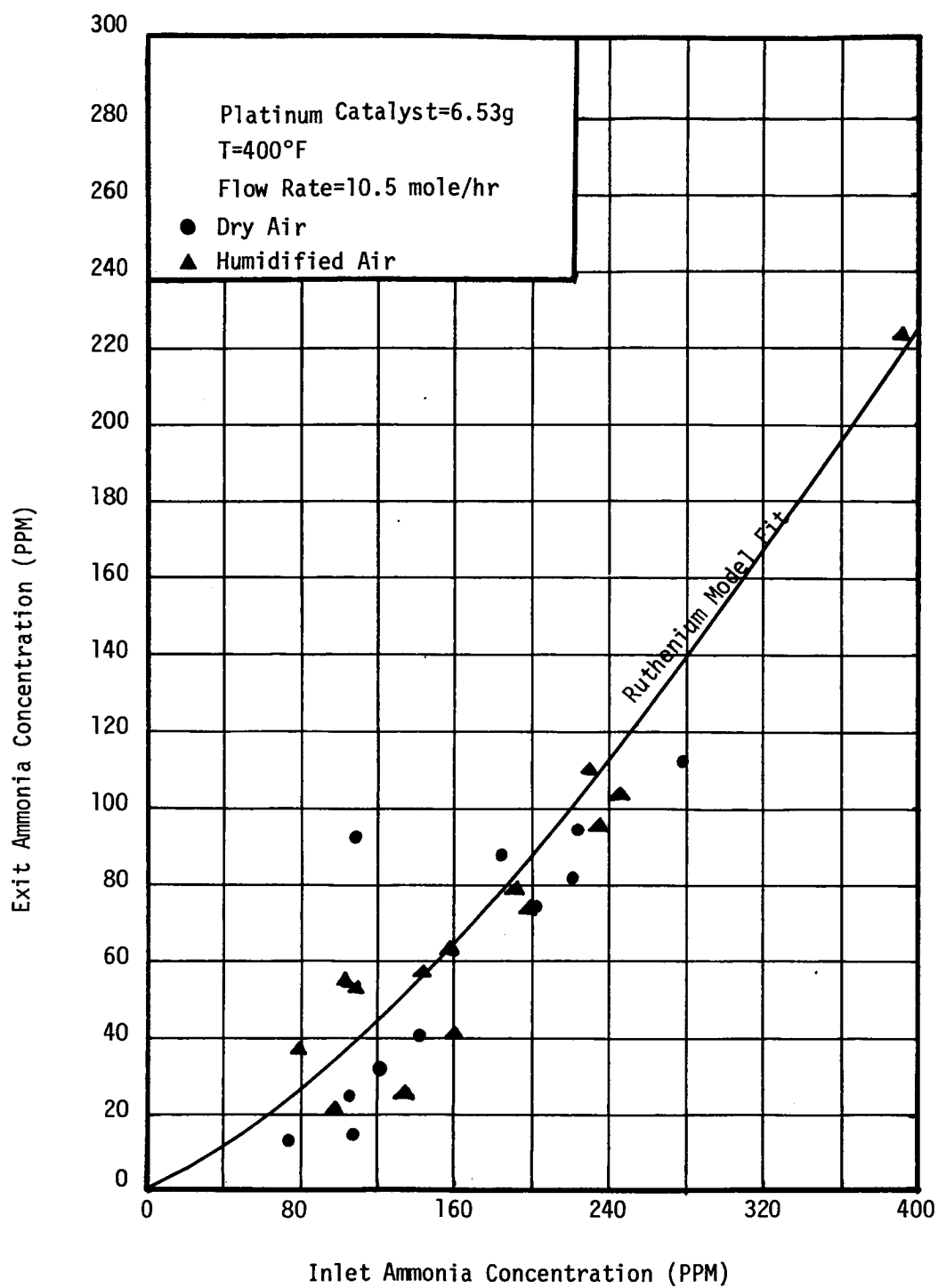
Figure 4.12 - Results of Integral Reactor

Oxidation Runs Using Platinum

Catalyst

38
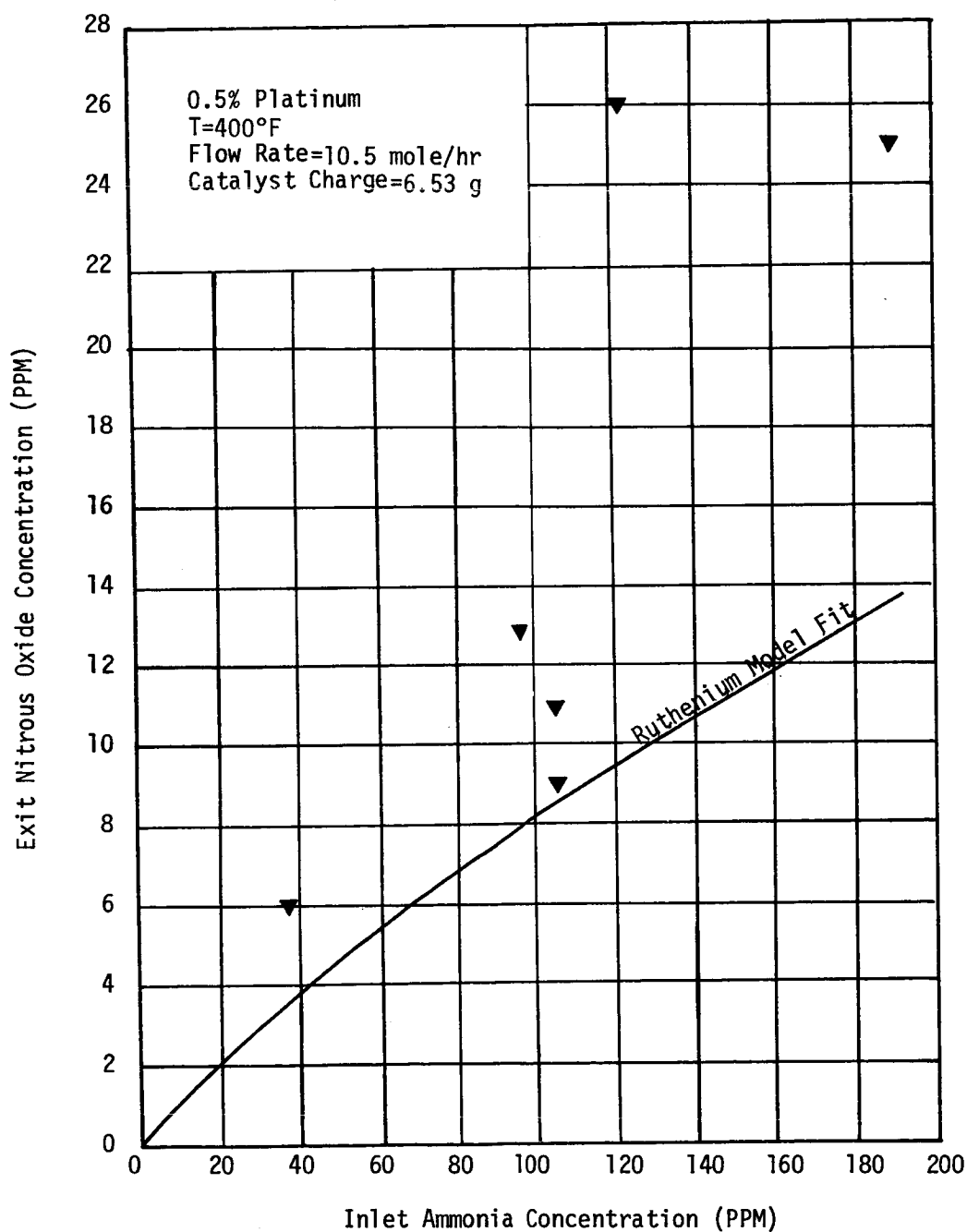
Figure 4.13 - Nitrous Oxide Production Using Integral
Reactor and Platinum Catalyst

TABLE 4.4

EXPERIMENTAL DATA HOPCALITE

RUN # HOPCALITE	AIR FLOW G-MOLE/HR	TEMP °F	PPM NH_3 IN	OUT	PPM NO_2 OUT	PPM N_2O OUT
12/22/70-1	12.1	287	62	38	0.2	20.2
12/22/70-2	7.7	292	168	77	0.2	11.3
12/28/70-1	7.6	291	184	92	0.2	12.3
12/28/70-2	12.3	290	118	79	0.2	4.9
12/29/70-1	12.6	292	94	70	0.2	2.8
9/ 1/70-3	7.4	300	252	126	0.5	NA
9/ 1/70-4	7.4	300	168	93	NA	NA
9/ 2/70-1	6.8	300	173	100	NA	14.0
2/26/71-1	10.4	305	151	88	0.0	NA
3/ 1/71-1	10.5	305	152	90	0.0	9.2
3/ 8/71-1	10.5	305	176	117	0.0	NA
3/12/71-1	10.5	305	164	101	0.0	6.3
3/17/71-1	10.4	305	159	98	0.0	6.5
3/19/71-1	10.4	305	179	112	0.0	8.5
3/22/71-1	10.4	303	189	104	0.0	7.9
3/23/71-1	10.4	305	140	93	0.0	7.3
3/24/71-1	10.4	300	138	94	0.0	7.6
3/26/71-1	10.4	305	152	97	0.2	7.3
3/29/71-1	10.5	302	149	94	0.0	NA
3/29/71-2	10.5	305	194	120	0.0	NA
3/31/71-1	10.4	302	112	70	0.0	NA
3/31/71-2	10.4	302	91	55	0.0	NA
4/ 7/71-1	10.4	304	156	98	0.0	NA
4/ 9/71-1	10.4	304	151	88	NA	NA
10/13/70-1	10.5	310	110	76	NA	1.0
12/31/70-1	10.4	322	146	79	NA	NA
1/ 4/71-1	10.4	320	142	80	0.0	NA
1/ 7/71-1	10.7	323	141	84	0.4	7.1
1/ 7/71-2	10.7	325	94	59	0.5	5.2
1/ 8/71-1	10.7	324	90	56	0.2	4.3
1/ 8/71-2	10.9	325	58	28	0.1	3.4
1/11/70-1	9.5	327	121	68	0.0	6.0
1/11/70-2	9.3	325	170	97	0.2	10.2
9/ 2/70-2	6.8	350	171	49	NA	27.0
9/ 1/70-1	10.3	380	245	112	0.4	NA
9/ 1/70-2	10.3	380	118	54	NA	NA
10/21/70-1	10.7	371	114	49	NA	10.0
10/22/70-1	10.7	371	61	40	NA	8.0
10/22/70-2	10.7	371	116	71	NA	NA
9/ 3/70-1	6.4	393	104	25	0.0	35.0
10/23/70-1	10.5	405	136	99	NA	20.0
10/28/70-1	10.7	400	88	26	NA	NA

40

TABLE 4.4 .....continued

RUN # HOPCALITE	AIR FLOW G-MOL/HR	TEMP °F	PPM NH_3 IN	PPM NH_3 OUT	PPM NO_2 OUT	PPM N_2O OUT
10/28/70-2	10.7	425	144	39	NA	NA
10/29/70-1	10.7	430	130	66	NA	NA
11/ 4/70-1	10.7	445	114	36	0.0	25.0
9/ 3/70-3	6.5	450	305	33	0.0	109.0
9/ 3/70-4	6.5	450	169	19	NA	54.0
8/31/70-1	6.3	460	273	8	1.5	NA
9/ 3/70-2	6.7	461	259	18	1.8	80.5
11/ 7/70-1	10.5	475	139	69	0.2	33.0
9/ 3/70-5	6.4	500	218	21	5.0	NA
11/10/70-1	10.4	502	118	17	4.0	34.9
11/11/70-1	10.2	520	111	17	6.2	33.0
11/11/70-2	7.4	520	166	4	10.0	49.2
11/13/70-1	7.3	523	152	6	9.6	51.0
11/13/70-2	7.3	523	166	19	9.6	51.0
11/14/70-1	13.1	520	95	14	4.8	NA
11/18/70-1	9.0	515	229	42	4.3	NA
11/20/70-1	7.6	524	262	21	7.8	89.9
9/29/70-1	12.0	665	118	5	31.2	11.0
4/14/71-1*	9.4	300	58	50	NA	1.0
4/19/71-1*	9.0	305	137	106	NA	3.0

TABLE 4.5

EXPERIMENTAL DATA TIME DEPENDENCY OF HOPCALITE REACTION RATE

RUN # HOPCALITE	AIR FLOW G-MOL/HR	TEMP °F	PPM NH_3 IN	PPM NH_3 OUT	PPM NO_2 OUT	PPM N_2O OUT
2/17/71-1	10.5	303	179	6	0.0	20.3
2/17/71-2	10.3	306	157	49	0.1	11.4
2/19/71-1	10.5	306	135	48	0.0	11.3
2/20/71-1	10.5	303	171	75	0.0	11.3
2/22/71-1	10.6	303	175	88	0.4	10.1
2/24/71-1	10.5	304	160	69	0.0	NA
2/26/71-1	10.4	305	151	88	0.0	NA
3/ 1/71-1	10.5	305	152	90	0.0	9.2
3/ 8/71-1	10.5	305	176	117	0.0	NA
3/12/71-1	10.5	305	164	101	0.0	6.3
3/17/71-1	10.4	305	159	98	0.0	6.5
3/19/71-1	10.4	305	179	112	0.0	8.5
3/22/71-1	10.4	303	189	104	0.0	7.9
3/23/71-1	10.4	305	140	93	0.0	7.3
3/24/71-1	10.4	300	138	94	0.0	7.6
3/26/71-1	10.4	305	152	97	0.2	7.3
3/29/71-1	10.5	302	149	94	0.0	NA
3/29/71-2	10.5	302	194	120	0.0	NA
3/31/71-1	10.4	302	112	70	0.0	NA
3/31/71-2	10.4	302	91	55	0.0	NA
4/ 7/71-1	10.4	304	156	98	0.0	NA
4/ 9/71-1	10.4	304	151	88	NA	NA

Catalyst Weight 6.604 grams
*NA not available

where   r = ammonia removal rate
        c_{ave} = average ammonia concentration
          K = reaction rate constant
          c_1 = ammonia inlet concentration, ppm
          c_2 = ammonia exit concentration, ppm
          F = air flow rate moles/hr
          W = catalyst weight, grams

If a material balance is made on a fixed bed plug flow reactor, the following equation is obtained

$$Fc_1 - Fc_2 = Kc \tag{4.19}$$

but the exit concentration can be expressed as a function of the inlet concentration

$$c_2 = c_1 + \frac{dc_1}{dW} \, . \tag{4.20}$$

If this is substituted into Equation (4.19) and simplified, equation (4.21) results

$$F \frac{dc}{dW} = Kc \quad . \tag{4.21}$$

This can be integrated through the bed from c_1 to c_2 obtaining:

$$\ln \frac{c_1}{c_2} = \frac{KW}{F} \quad . \tag{4.22}$$

This can now be equated to Equation (4.18) and the average concentration obtained as

$$c_{ave} = \frac{c_1 - c_2}{\ln c_1/c_2} \quad . \tag{4.23}$$

Substituting Equation (4.23) for c_{ave} in Equation (4.18) gives

$$\frac{WK}{F} = \ln c_1/c_2 \quad . \tag{4.24}$$

The reaction rate is proportional to the concentration of the reactant at the surface of the catalyst. This arises since the reaction takes place on the surface of the catalyst, but the surface concentration is controlled by the rate of mass transfer of the reactant to the particle surface

$$r = K_{act} \, c_S = kg \, A(c_B - c_S) \quad (4.25)$$

where K_{act} = intrinsic rate constant
kg = mass transfer coefficient
c_B = bulk ammonia concentration
c_S = ammonia concentration on the catalyst surface
A = catalyst surface area.

Equation (4.25) can be solved for the ammonia surface concentration

$$c_S = \frac{kg \, A \, c_B}{(K_{act} + kg \, A)} \quad \cdot \quad (4.26)$$

The design equation is

$$\frac{W}{F} = \int \frac{d \, c_B}{-r} = \int \frac{d \, c_B}{K_{act} \, c_S} \quad \cdot \quad (4.27)$$

Substitute for c_S

$$\frac{W}{F} = \int_{c_1}^{c_2} \frac{d \, c_B}{\left[\dfrac{kg \, A \, c_B}{K_{act} + kg \, A} \right]} = \left[\frac{K_{act} + kg \, A}{K_{act} \, kg \, A} \right] \ln \frac{c_1}{c_2} \quad (4.28)$$

Rearrangement gives

$$\ln \frac{c_1}{c_2} = \frac{W}{F} \frac{K_{act} \, kg \, A}{(K_{act} + kg \, A)} \quad (4.29)$$

44

Equation (4.22) provides an opportunity to calculate K or K_{obs} from the kinetic data. This value can be used to calculate the intrinsic rate constant, K_{act}, if Equations (4.29) and (4.22) are equated which results in

$$K_{obs} = \frac{K_{act} \text{ kg A}}{(K_{act} + \text{kg A})} \qquad . \qquad (4.30)$$

Equation (4.30) may be rearranged to

$$K_{act} = \left[\frac{\text{kg A } K_{obs}}{\text{kg A} - K_{obs}} \right] \qquad . \qquad (4.31)$$

By using (4.31) the intrinsic rate constant may be calculated from the mass transfer coefficient and the observed rate constant which is calculated from Equation (4.22). The results of these calculations are shown in Tables 4.6 and 4.7.

The Arrhenius equation relates the effect of temperature on the intrinsic rate constant and is given by

$$K_{act} = A \exp(-E/RT) \qquad (4.32)$$

where A = preexponential constant
       E = activation energy
       R = universal gas constant
       T = temperature $^\circ$K .

A plot of $\ln K_{act}$ vs $1/T$ will result in a straight line for first order kinetic reactions. The slope of this line is equal to $-E/R$. The Arrehenius plot for the data given in Table 4.4 is shown in Figure 4.14. The line indicated on the plot was obtained from a least squares fit of the data and represents an activation energy of 5900 cal/gmole. The value of the preexponential constant is 924.4. The first order rate equation can now be expressed as a function of both temperature and ammonia concentration

$$r = 924.4 \exp(-5900/RT) \ c_{NH_3} \qquad (4.33)$$
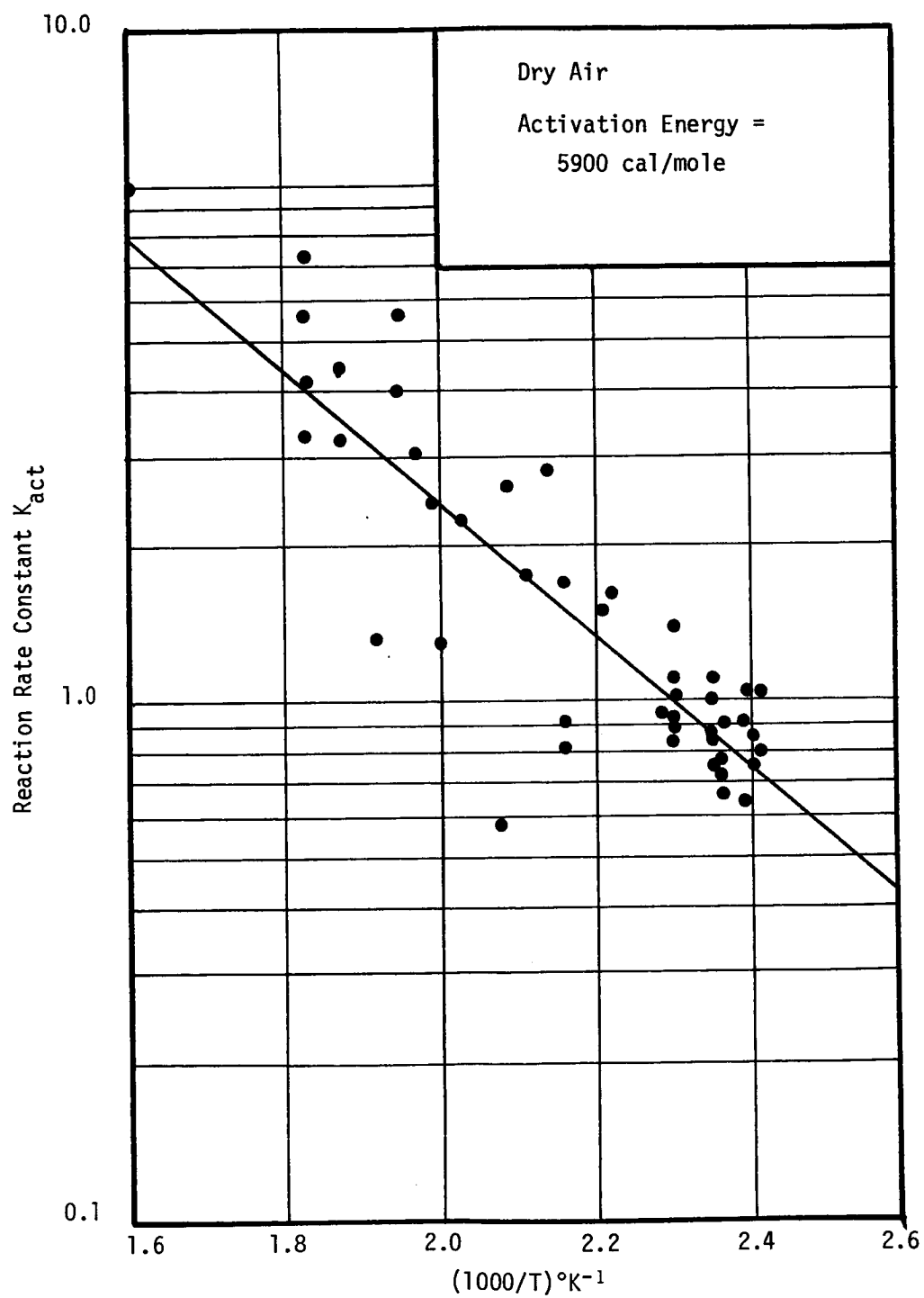
Figure 4.14 - Hopcalite Arrhenius Plot

The plot shows Reaction Rate Constant K_{act} (vertical axis, logarithmic from 0.1 to 10.0) versus $(1000/T)\,°K^{-1}$ (horizontal axis, from 1.6 to 2.6).

Dry Air

Activation Energy = 5900 cal/mole

46

4.6.2 The Effect of Time on Catalyst Activity. - It was frequently observed that immediately after replacement of the Hopcalite catalyst with a new charge, the catalyst activity appeared greater than normal. In order to investigate the phenomena a charge of 6.0039 grams of Hopcalite catalyst was allowed to operate continuously for 1222 hours at 151°C and 10.5 gmoles air/hr. The results of this test are given in Tables 4.5, 4.7, and 4.8. As suspected they show a significantly higher activity during the first 200 hours of the catalyst utilization. This fact is further depicted in Figure 4.15 where the observed rate constant is plotted as a function of time. In order to avoid this effect all data presented in Table 4.4 were obtained after at least 200 hours of operation.

4.6.3 Performance Data. - Hopcalite catalyst appears to be as effective as any of the ammonia oxidation catalyst tested. The rate of ammonia oxidation is comparable with both ruthenium and platinum. Figures 4.16, 4.17, 4.18, and 4.19 show the performance of the Hopcalite catalyst at 142°C, 151°C, 162°C, and 191°C, respectively. These figures indicate the exit ammonia concentration as a function of inlet concentration for a catalyst bed containing six grams of Hopcalite. Also shown is the predicted results for ammonia oxidation over ruthenium catalyst at identical conditions. Because of the linearity of the Hopcalite reaction (first order kinetics) the effectiveness of the Hopcalite catalyst is slightly better at concentrations greater than 80 ppm in the inlet stream. Unfortunately the product distribution for the Hopcalite is not as favorable as for the ruthenium. Figures 4.20 and 4.21 clearly indicate the greater N_2O production for the Hopcalite catalyst in comparison to the model prediction for the ruthenium catalyst operating at identical conditions.

The distribution of the nitrogen oxides as a function of temperature is shown in Figure 4.22. As indicated the conversion of ammonia to nitrogen dioxide increases with temperature. Conversely the conversion of ammonia to nitrous oxide maximizes at intermediate temperatures. This may lead to erroneous supposition that N_2O is a precursor of NO_2 in the reactors. Under the comparable conditions no nitrogen dioxide was formed when nitrous oxide was substituted for ammonia in the inlet to the reactor.

4.6.4 The Effect of Water Vapor on Hopcalite Activity. - To determine the effect of water vapor on the activity of Hopcalite catalyst, data was obtained at 300°F using humidified air. The air was humidified to 23% relative humidity at 72°F. The results of this work are presented in Figure 4.23. From the data collected on humidified operation it is apparent that water vapor depressed the ammonia removal rate by approximately 50% for Hopcalite catalyst at 300°F.

47

TABLE 4.6

REACTION RATE CONSTANTS-HOPCALITE

RUN # HOPCALITE	K_{obs}	K_{act}	1/T °K X 10^3
12/22/70-1	0.976	1.045	2.410
12/22/70-2	0.959	1.037	2.394
12/28/70-1	0.841	0.900	2.397
12/28/70-2	0.799	0.844	2.400
12/29/70-1	0.618	0.644	2.394
9/ 1/70-3	0.847	0.907	2.368
9/ 1/70-4	0.724	0.768	2.368
9/ 2/70-1	0.621	0.654	2.368
2/26/71-1	0.945	1.012	2.353
3/ 1/71-1	0.924	0.988	2.353
3/ 8/71-1	0.714	0.752	2.353
3/12/71-1	0.847	0.900	2.353
3/17/71-1	0.837	0.889	2.353
3/19/71-1	0.804	0.852	2.353
3/22/71-1	1.022	1.101	2.359
3/23/71-1	0.703	0.739	2.353
3/24/71-1	0.675	0.709	2.368
3/26/71-1	0.778	0.823	2.353
3/29/71-1	0.804	0.851	2.362
3/29/71-2	0.830	0.882	2.362
3/31/71-1	0.809	0.858	2.362
3/31/71-2	0.865	0.920	2.362
4/ 7/71-1	0.808	0.857	2.356
4/ 9/71-1	0.926	0.990	2.356
10/13/70-1	0.648	0.678	2.338
12/31/70-1	1.015	1.072	2.302
1/ 4/71-1	0.948	1.015	2.308
1/ 7/71-1	0.890	0.948	2.299
1/ 7/71-2	0.804	0.851	2.293
1/ 8/71-1	0.804	0.851	2.296
1/ 8/71-2	1.263	1.382	2.293
1/11/70-1	0.888	0.948	2.287
1/11/70-2	0.845	0.900	2.293
9/ 2/70-2	1.419	1.594	2.222
9/ 1/70-1	1.340	1.473	2.143
9/ 1/70-2	1.351	1.486	2.143
10/21/70-1	1.504	1.672	2.166
10/22/70-1	0.775	0.795	2.166
10/22/70-2	0.874	0.928	2.166
9/ 3/70-1	1.537	1.743	2.110
10/23/70-1	0.564	0.586	2.081
10/28/70-1	2.171	2.531	2.093

TABLE 4.6 .....continued

RUN # HOPCALITE	K_{obs}	K_{act}	$1/T \ ^\circ K \times 10^3$
10/28/70-2	1.925	2.200	2.034
10/29/70-1	1.207	1.308	2.022
11/ 4/70-1	2.063	2.377	1.989
9/ 3/70-3	2.410	2.933	1.978
9/ 3/70-4	2.349	2.843	1.978
8/31/70-1	3.764	5.222	1.957
9/ 3/70-2	2.985	3.816	1.954
11/ 7/70-1	1.210	1.310	1.925
9/ 3/70-5	2.514	3.072	1.875
11/10/70-1	3.333	4.215	1.871
11/11/70-1	3.237	4.060	1.837
11/11/70-2	4.652	6.855	1.837
11/13/70-1	3.878	5.298	1.831
11/13/70-2	2.619	3.198	1.831
11/14/70-1	4.227	5.587	1.837
11/18/70-1	2.563	3.079	1.846
11/20/70-1	3.227	4.140	1.829
9/29/70-1	6.296	9.701	1.600

TABLE 4.7

EXPERIMENTAL DATA TIME DEPENDENCY OF HOPCALITE REACTION RATE

RUN # HOPCALITE	K_{obs}	K_{act}	$1/T$ °K X 10^3
2/17/71-1	5.785	9.707	2.359
2/17/71-2	2.002	2.32	2.350
2/19/71-1	1.811	2.072	2.350
2/20/71-1	1.436	1.595	2.359
2/22/71-1	1.221	1. 34	2.359
2/24/71-1	1.462	1.628	2.356
2/26/71-1	0.945	1.012	2.353
3/ 1/71-1	0.924	0.988	2.353
3/ 8/71-1	0.714	0.752	2.353
3/12/71-1	0.847	0.900	2.353
3/17/71-1	0.837	0.889	2.353
3/19/71-1	0.804	0.852	2.353
3/22/71-1	1.022	1.101	2.359
3/23/71-1	0.703	0.739	2.353
3/24/71-1	0.675	0.709	2.368
3/26/71-1	0.778	0.823	2.353
3/29/71-1	0.804	0.851	2.362
3/29/71-2	0.830	0.882	2.362
3/31/71-1	0.809	0.858	2.362
3/31/71-2	0.865	0.920	2.362
4/ 7/71-1	0.808	0.857	2.356
4/ 9/71-1	0.926	0.990	2.356

50

TABLE 4.8

TIME DEPENDENCY OF HOPCALITE CATALYST ACTIVITY

RUN # HOPCALITE	ELAPSED TIME HOURS	NH_3 REMOVAL RATE* X 10^5	K_{obs}	K_{act}
2/17/71-1	0	30.16	5.78	9.71
2/17/71-2	8	18.54	2.00	2.33
2/19/71-1	48	15.26	1.81	2.07
2/20/71-1	67	16.75	1.44	1.60
2/22/71-1	119	15.45	1.22	1.33
2/24/71-1	166	15.87	1.46	1.63
2/26/71-1	214	11.02	0.946	1.01
3/ 1/71-1	286	10.94	0.925	0.99
3/ 8/71-1	455	10.32	0.715	0.75
3/12/71-1	551	10.98	0.847	0.90
3/17/71-1	672	10.55	0.837	0.89
3/19/71-1	720	11.49	0.804	0.85
3/22/71-1	788	14.57	1.02	1.1
3/23/71-1	814	8.09	0.704	0.74
3/24/71-1	839	7.72	0.676	0.71
3/26/71-1	886	9.56	0.779	0.82
3/29/71-1	958	9.62	0.804	0.85
3/29/71-2	960	12.81	0.831	0.88
3/31/71-1	1006	7.22	0.810	0.86
3/31/71-2	1008	6.20	0.865	0.92
4/ 7/71-1	1176	10.09	0.808	0.86
4/ 9/71-1	1222	10.08	0.926	0.99
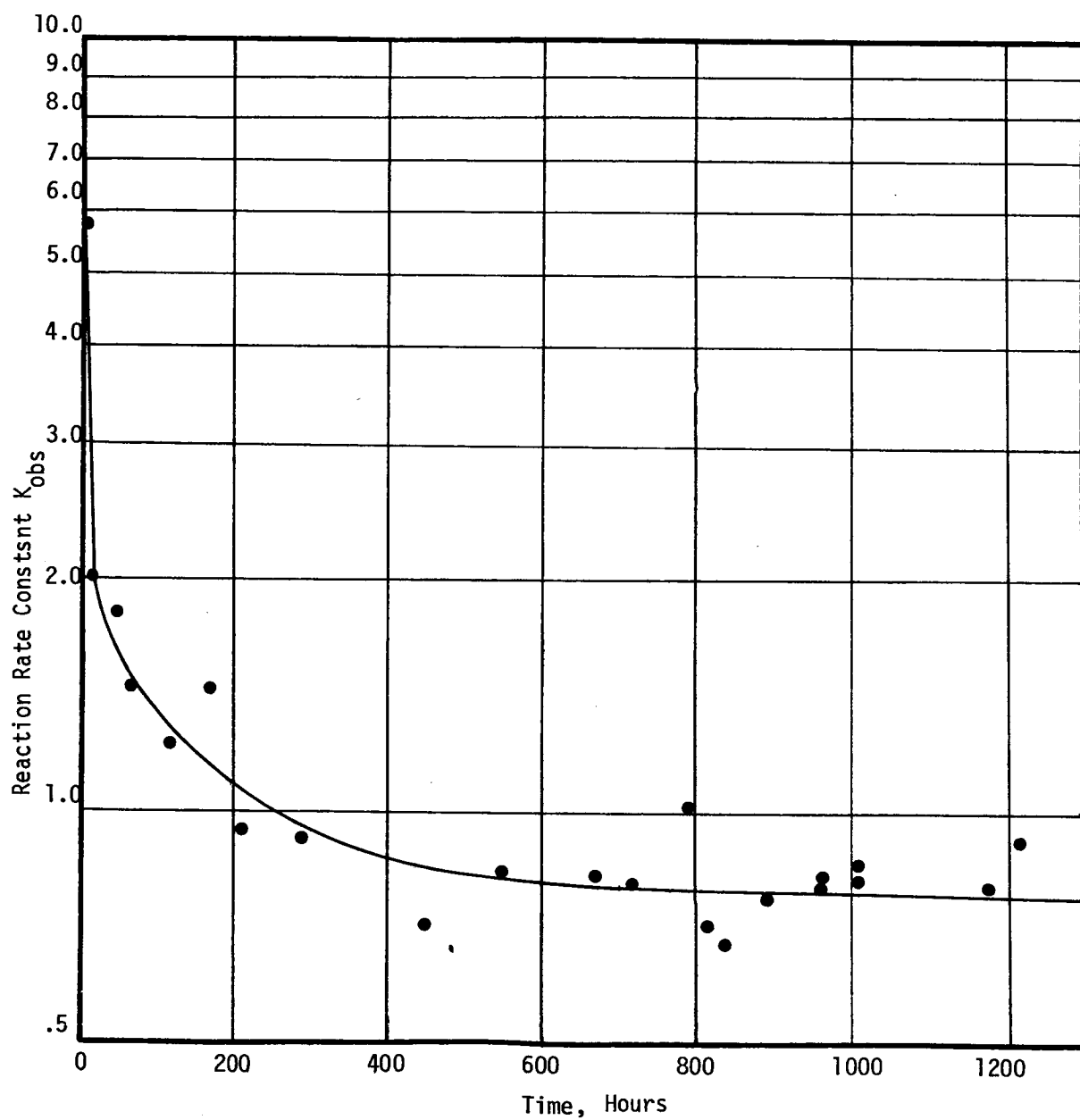
Figure 4.15 - Time Dependency of Hopcalite

Reaction Rate Constant

Figure 4.16 - Hopcalite Performance at 142°C

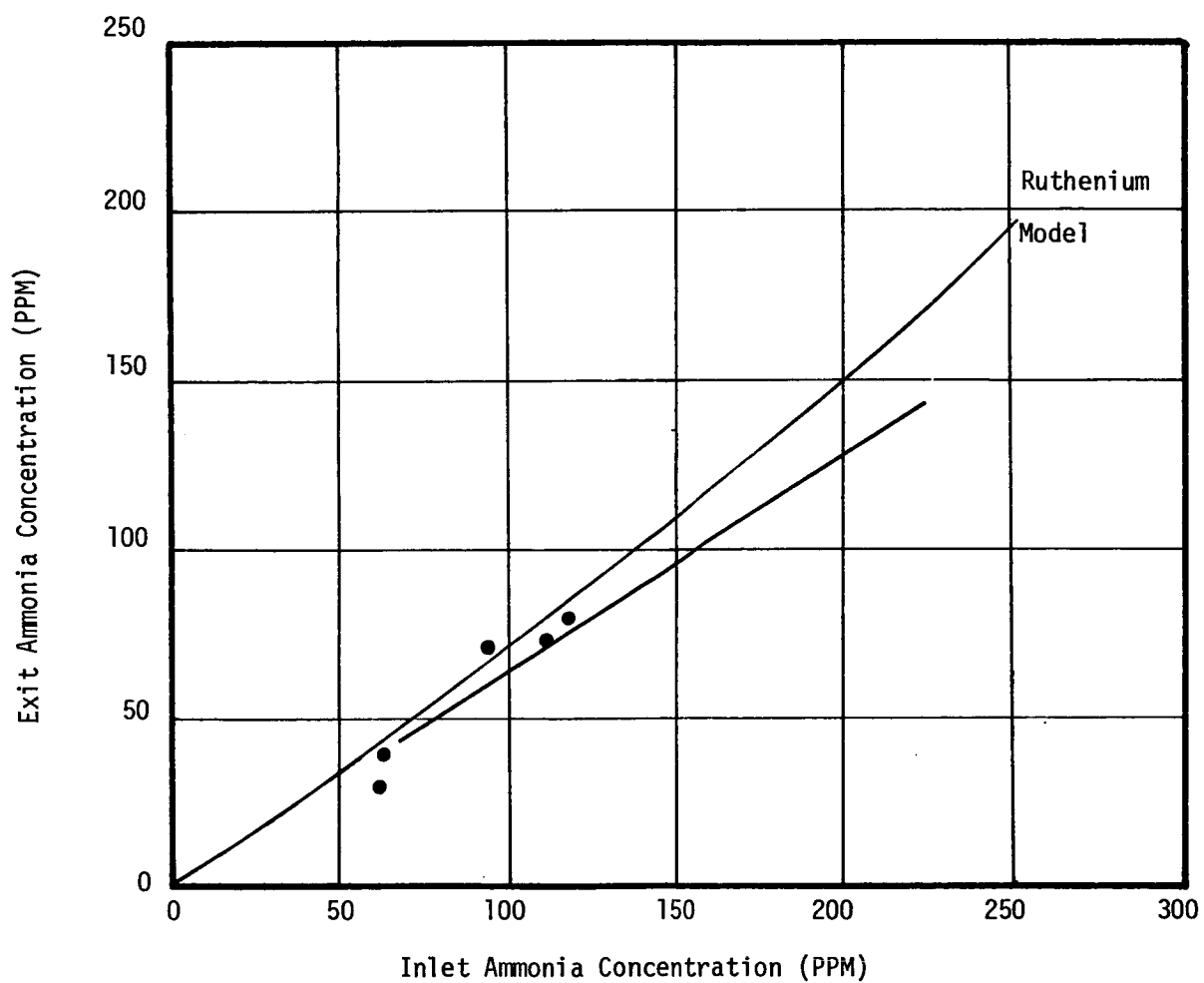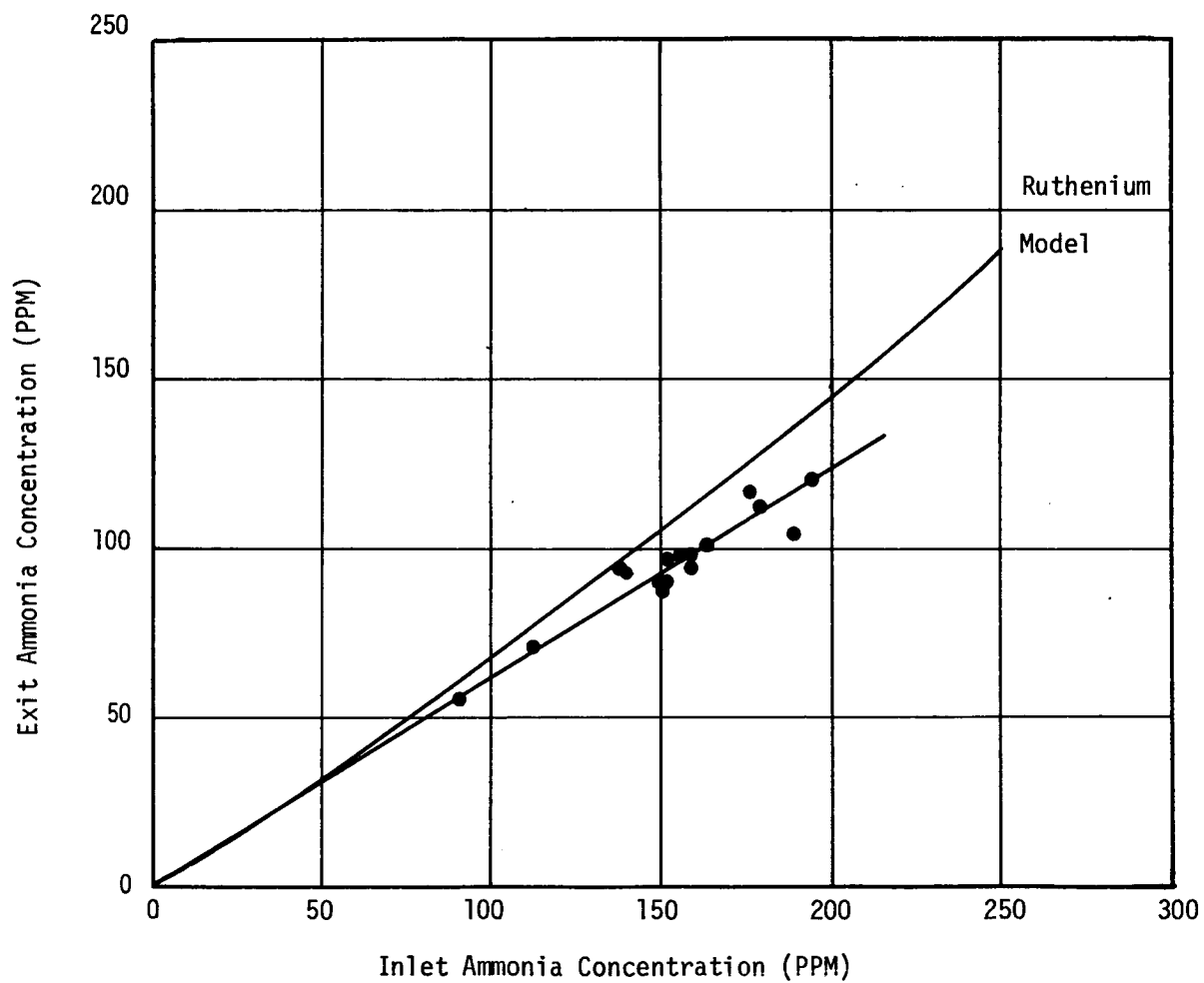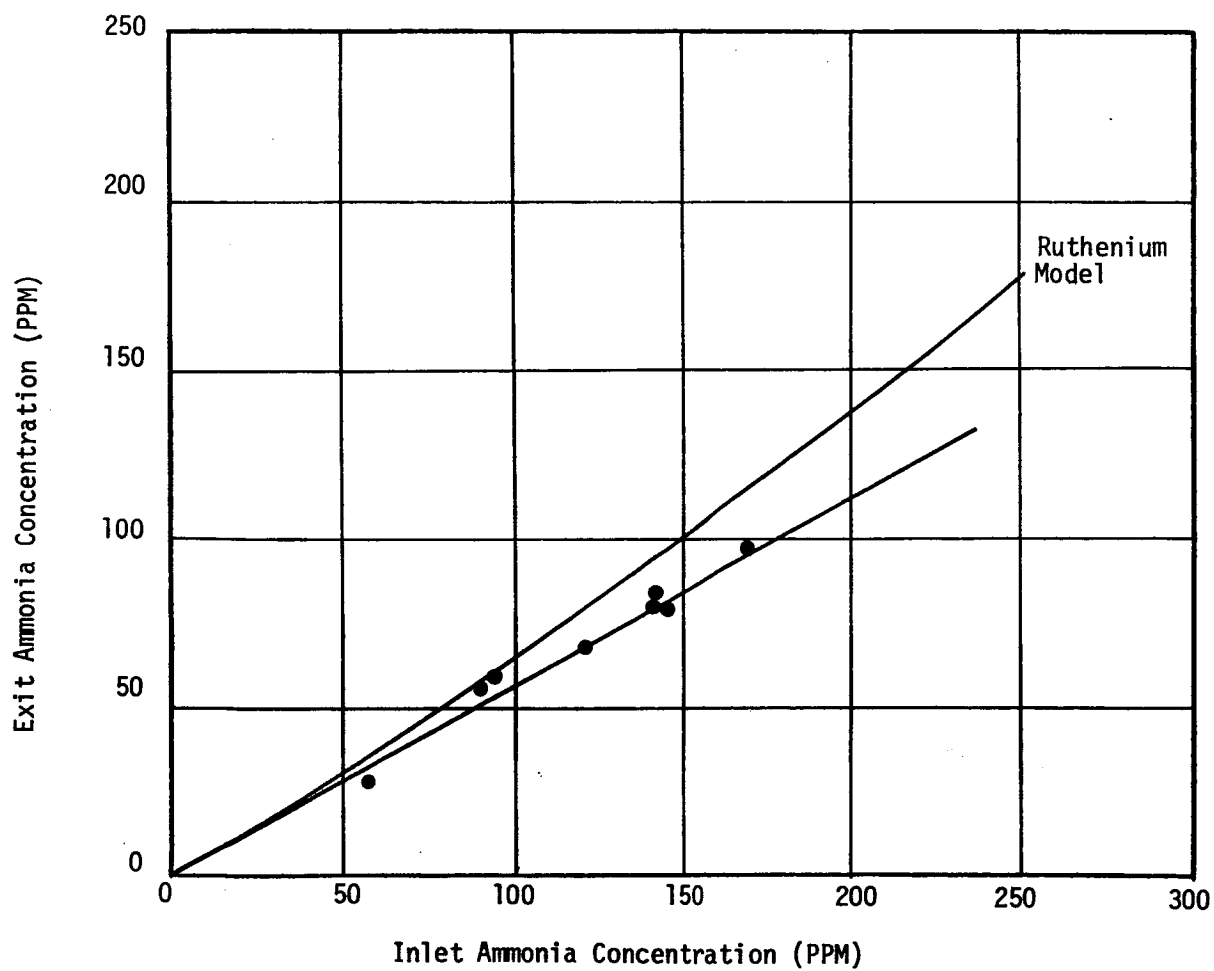Figure 4.17 - Hopcalite Performance at 151°C

54

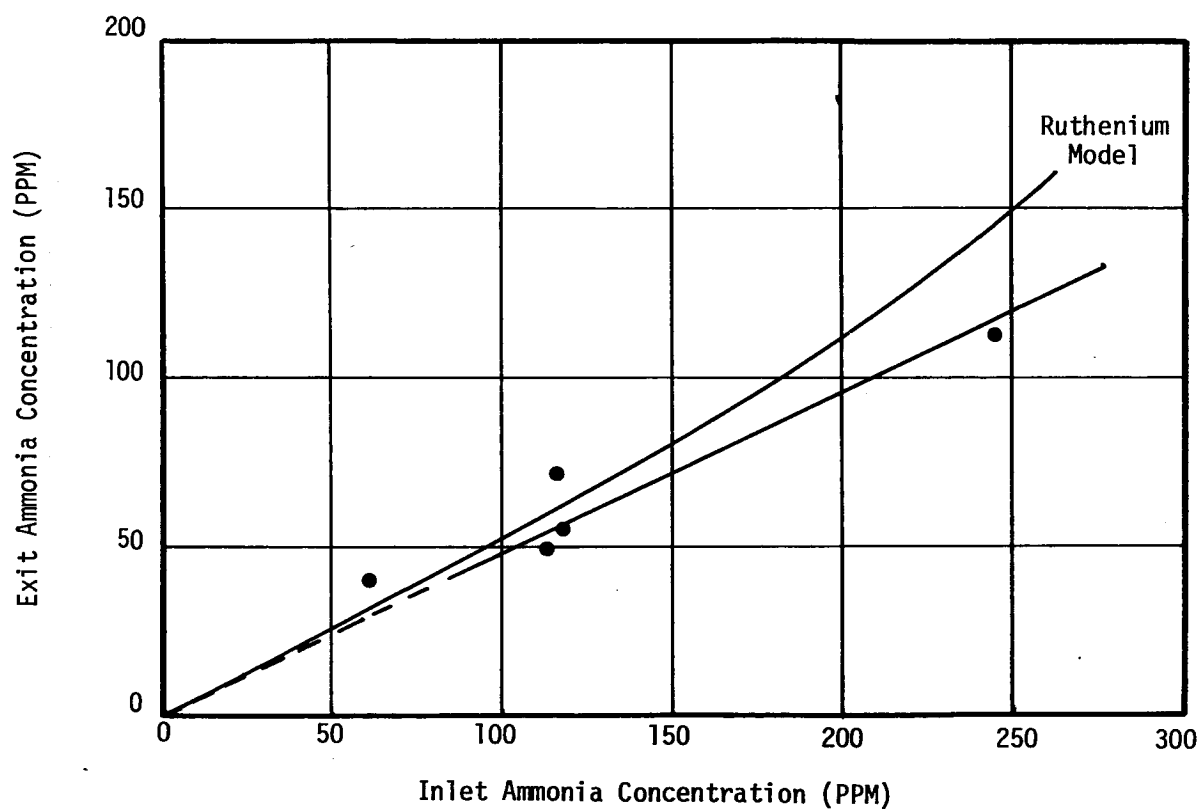Figure 4.18 - Hopcalite Performance at 162°C
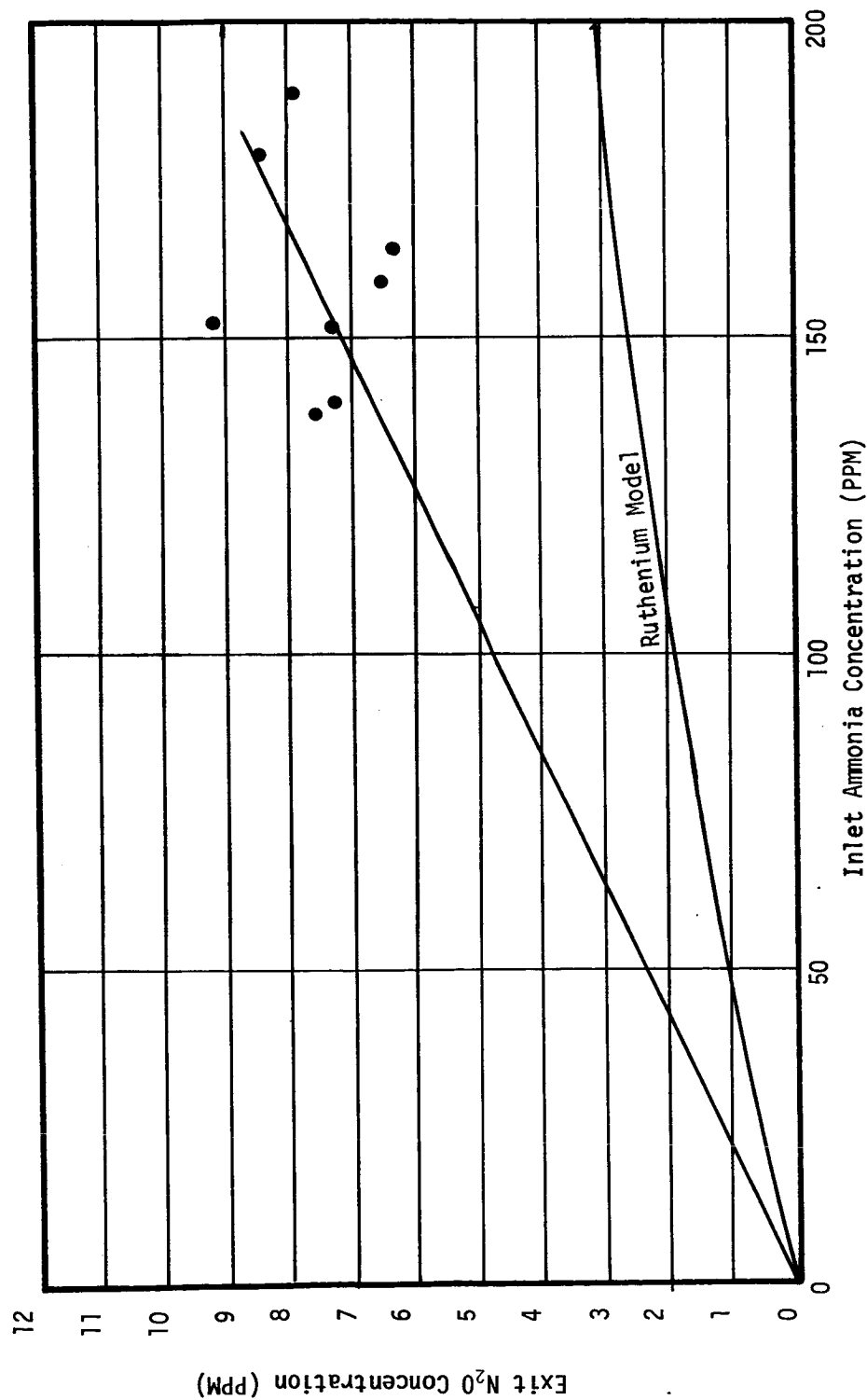
Figure 4.19 - Hopcalite Performance at 191°C

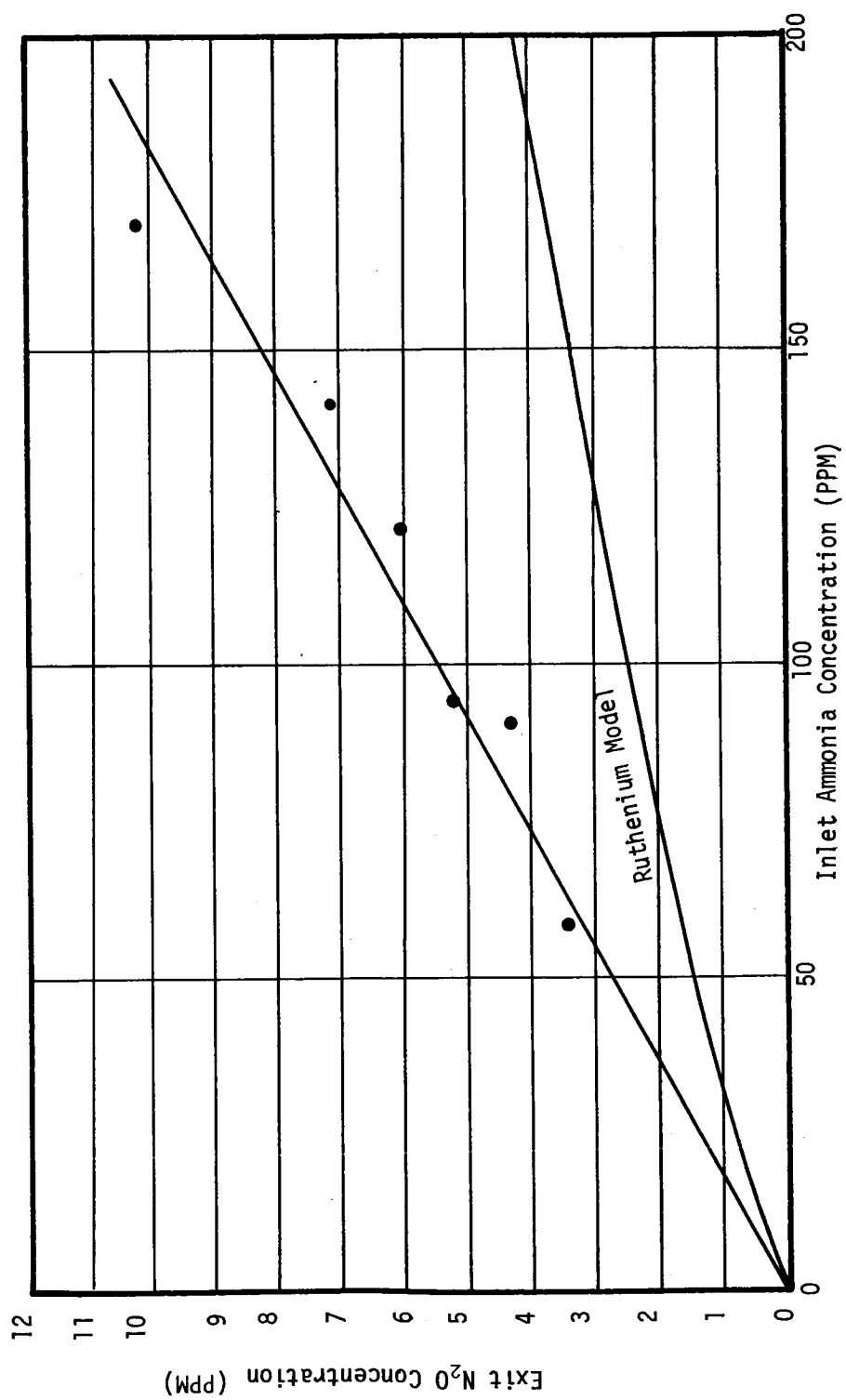Figure 4.20 – N_2O Production for Hopcalite Catalyst at 157°C

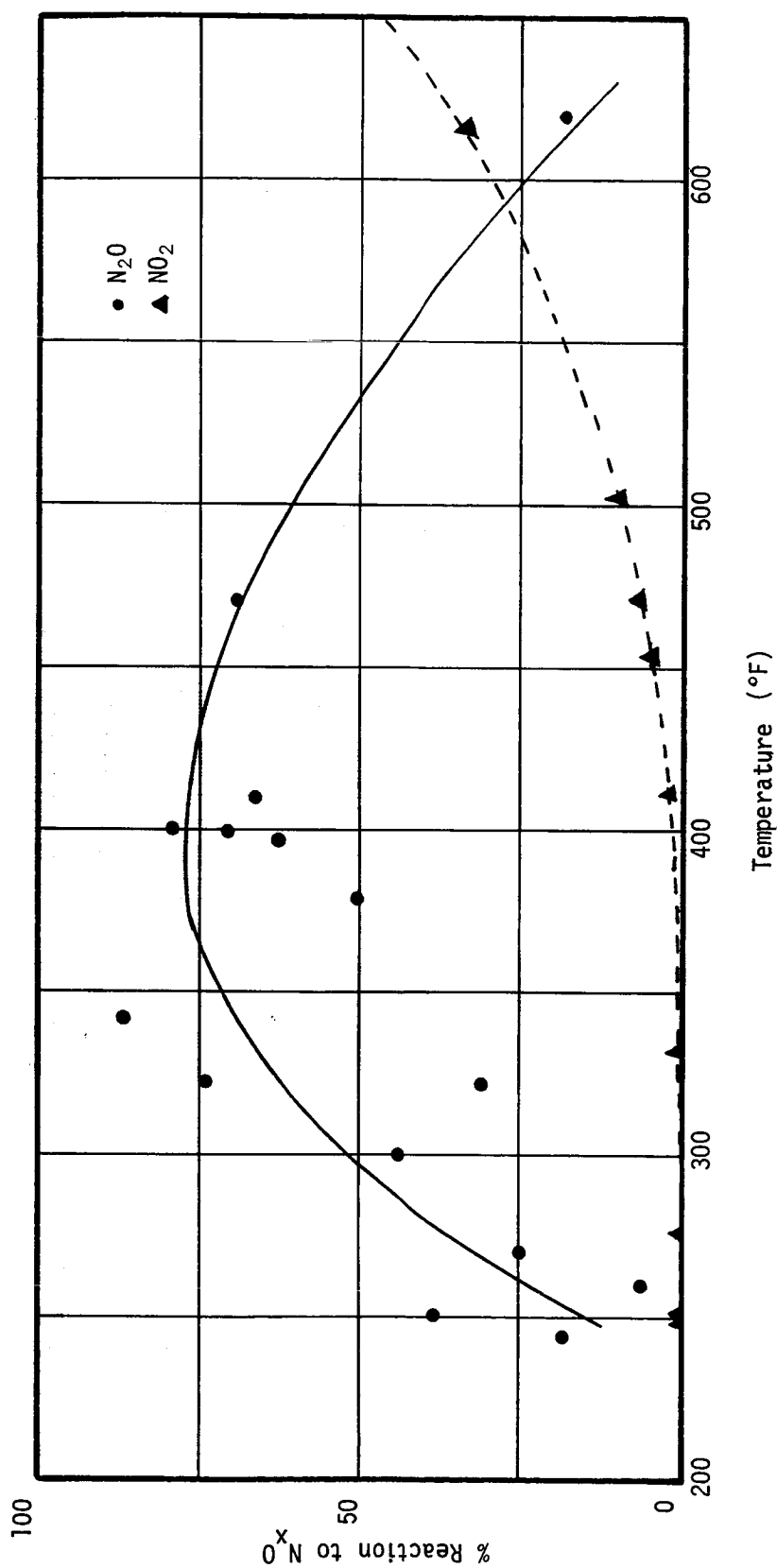Figure 4.21 - N_2O Production for Hopcalite Catalyst at 162°C

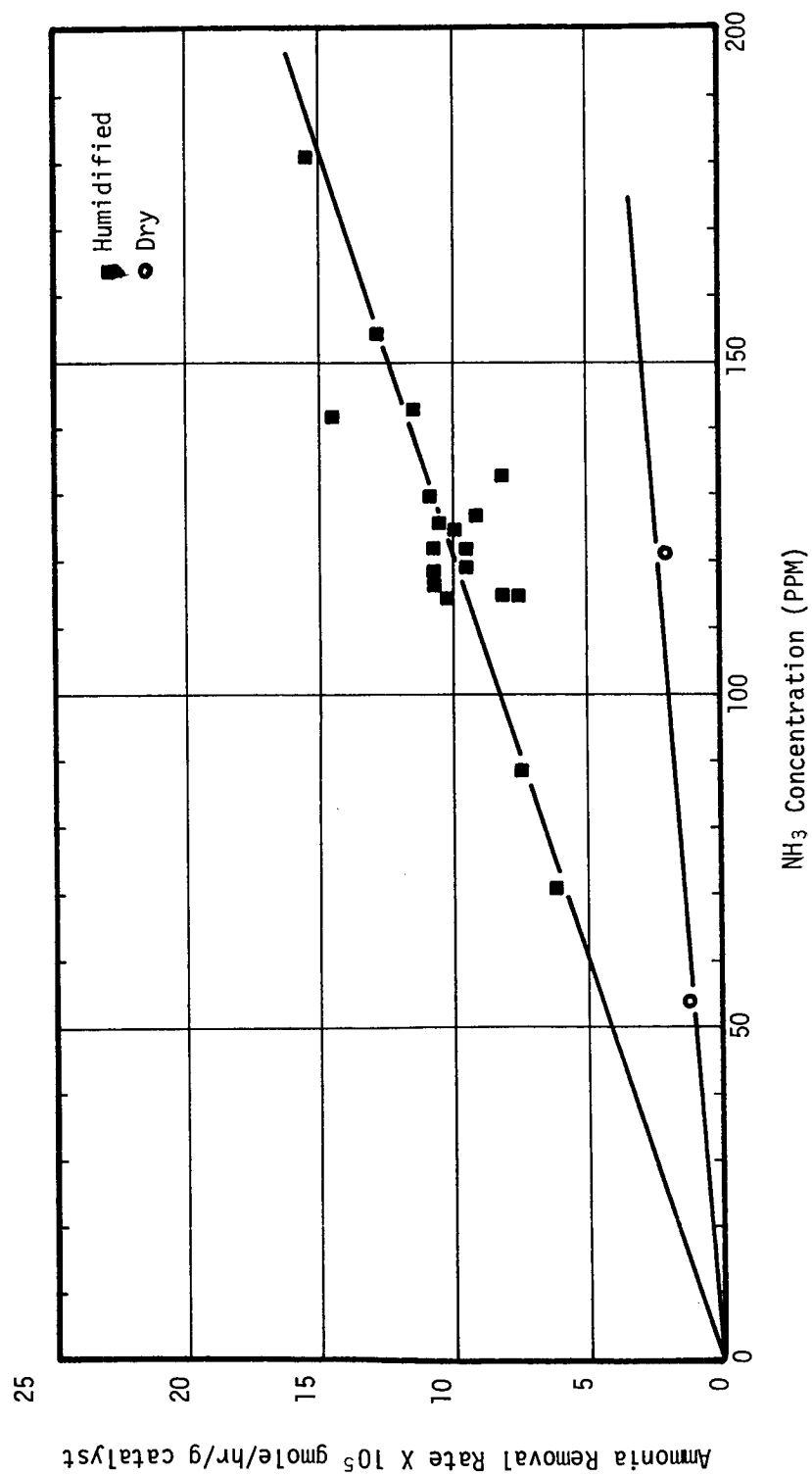Figure 4.22 – Product Distribution -vs- Temperature

for Hopcalite Catalyst

Figure 4.23 - Effect of Water on Ammonia Removal Rate

4.7 Estimated Performance of Catalytic Oxidation System

In this section information will be presented for estimating the performance of a fixed bed oxidizer using ruthenium catalyst. This catalyst has been shown to be the best one investigated with respect to low nitrogen oxides production.

The most critical variable in determining the performance of a given reactor is the temperature. In order to minimize the formation of nitrous oxide, the temperature in the reactor should be as low as is consistent with an acceptable ammonia removal rate. This temperature will probably be less than 300°F for normal operation.

The bed geometry does not influence the conversion so long as the Reynolds number is kept above about 35. Thus, pressure drop and mechanical considerations will determine the shape of the bed.

The amount of catalyst per mole of inlet air required will depend on the inlet ammonia concentration, the desired ammonia outlet concentration, the operating temperature, and the presence of poisons in the feed. Figure 4.24 has been prepared to show graphically the relationship between inlet and outlet concentration at various reactor temperatures. This figure can be used to calculate the catalyst required to treat any inlet ammonia concentration between about 10 ppm and 100 ppm. For example, at 250°F with an inlet ammonia concentration of 50 ppm 2.6 g of catalyst would be required per gmole air/hr of feed in order to reduce the outlet concentration to 10 ppm. At a temperature of 300°F 1.55 g of catalyst would be required to reduce a 50 ppm inlet to a 10 ppm exit at a flow rate of 1 gmole air/hr. For a larger flow rate, the catalyst charge would be multiplied by the flow rate in gmole per hour to get the required catalyst charge. (Note again that the particle Reynolds number should be above 35 to keep mass transfer resistances small).

The concentration of nitrous oxide in the reactor exit may be estimated by the use of Figure 4.25. The nitrous oxide concentration at the inlet ammonia concentration is subtracted from the nitrous oxide concentration at the exit ammonia concentration and the result is the exit concentration of nitrous oxide. For example, at 300°F if the inlet ammonia concentration is 50 ppm and the exit ammonia concentration is 10 ppm then the exit nitrous oxide concentration is 2.4 ppm.

In the contaminant control system it is very important that ammonia not be subjected to temperatures above about 400°F since large amounts of nitrous oxide and/or nitrogen dioxide can result. This means that the feed to a catalytic oxidizer used for methane oxidation and operating at 600°F to 650°F should be pretreated to remove the ammonia. This pretreatment could be a reactor operating at 250°F to 350°F and packed with ruthenium.
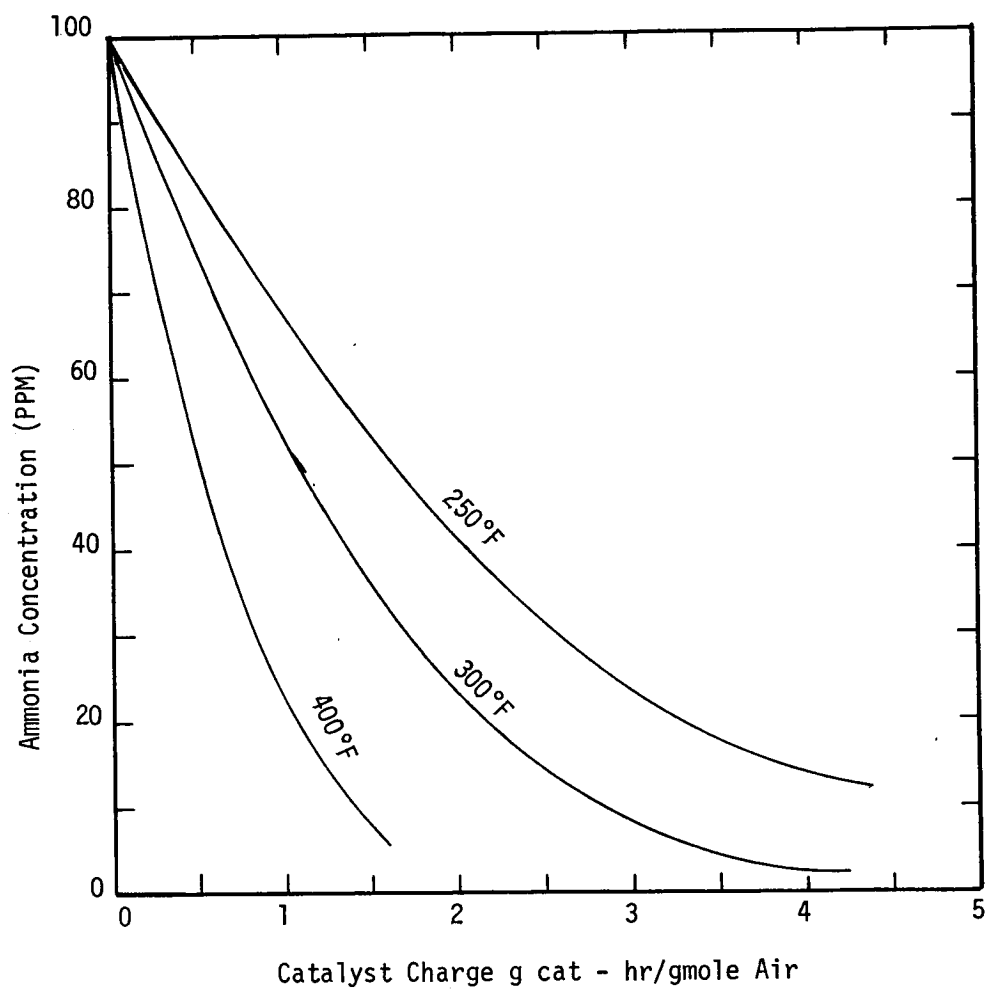
Figure 4.24 - Modelled Reactor Performance

The chart shows Ammonia Concentration (PPM) on the vertical axis ranging from 0 to 100, and Catalyst Charge g cat - hr/gmole Air on the horizontal axis ranging from 0 to 5. Three curves are labeled 250°F, 300°F, and 400°F.
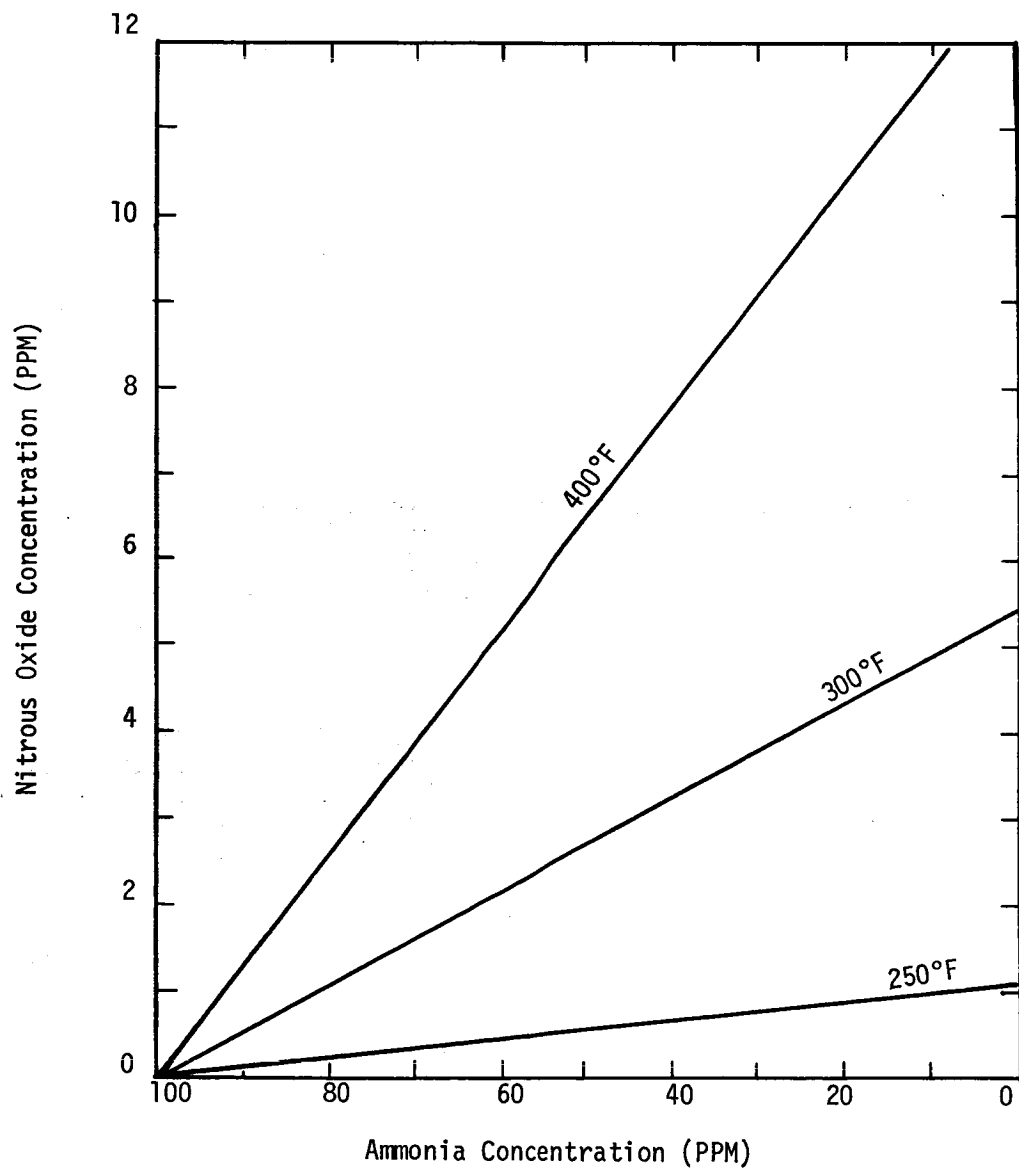
Figure 4.25 - Modelled Nitrous Oxide Yield

5.0 EXPERIMENTAL SYSTEMS FOR AMMONIA OXIDATION

In order to carry out the experimental portions of the ammonia oxidation studies two reaction systems were utilized. These systems, one a backmix (or stirred-tank) reactor and the other a fixed-bed reactor, are separately discussed below. The two different systems were selected in order to take advantage of the complementing features of having both differential and integral type reaction rate data available for analysis.

5.1 Backmix Reaction System

A schematic diagram of the backmix reactor system is shown in Figure 5.1. Air from a compressed air cylinder passes through a 1/4 in. stainless steel line and into a vertical glass tube containing $CaSO_4$ dessicant. From this point the air flows through a Hastings model LF 3K mass flowmeter transducer. The transducer is connected to a meter which provides a visual display of the air flow rate to the reactor. After passing through the Hastings meter the air passes through a 1/4 in. Whitey needle valve, mixes with a small stream of ammonia, and is fed into the reactor. Air flow out of the reactor occurs through leaks around the reactor end plates and around the agitator shaft.

Gaseous ammonia is fed to the reactor from a cylinder containing liquid ammonia. Ammonia vaporized from the cylinder passes through a pressure regulator and into a 1/4 in. stainless steel line which contains a 1/4 in. Whitey needle valve and connects to a high resistance tube. The resistance tube consists of a 3/8 in. O.D. glass tube packed with crushed glass to provide high resistance to flow.

A detailed schematic of the backmix reactor is shown in Figure 5.2. The reactor consists of a 4-1/2 in. diameter cylindrical shell, 15 in. in length with circular plates at each end. A shaft, which holds the catalyst baskets and agitator blades, extends through the centerline of the reactor. Thermowells and sample ports are located in both end plates. The reactor housing, end plates, agitator shaft, and agitator blades are all constructed of stainless steel. The outside of the reactor housing is wrapped with electrical resistance heaters which are connected to a variable voltage transformer. The outside of the reactor and both end plates are insulated to minimize heat losses. The temperature within the reactor is monitored with a bare iron-constantan thermocouple which is mounted in the end plate thermowell and connected to a Honeywell Electronik 15 recorder. With this arrangement the temperature can be monitored and controlled anywhere between ambient temperature and 900°F. The agitator shaft is driven by a variable speed Minarik model SL14 electric motor which is mounted on a wooden support which aligns the motor shaft and the agitator shaft.

The manner in which the catalyst pellets were stacked in the catalyst baskets was of concern. The catalyst pellets were cylindrical in shape with

64
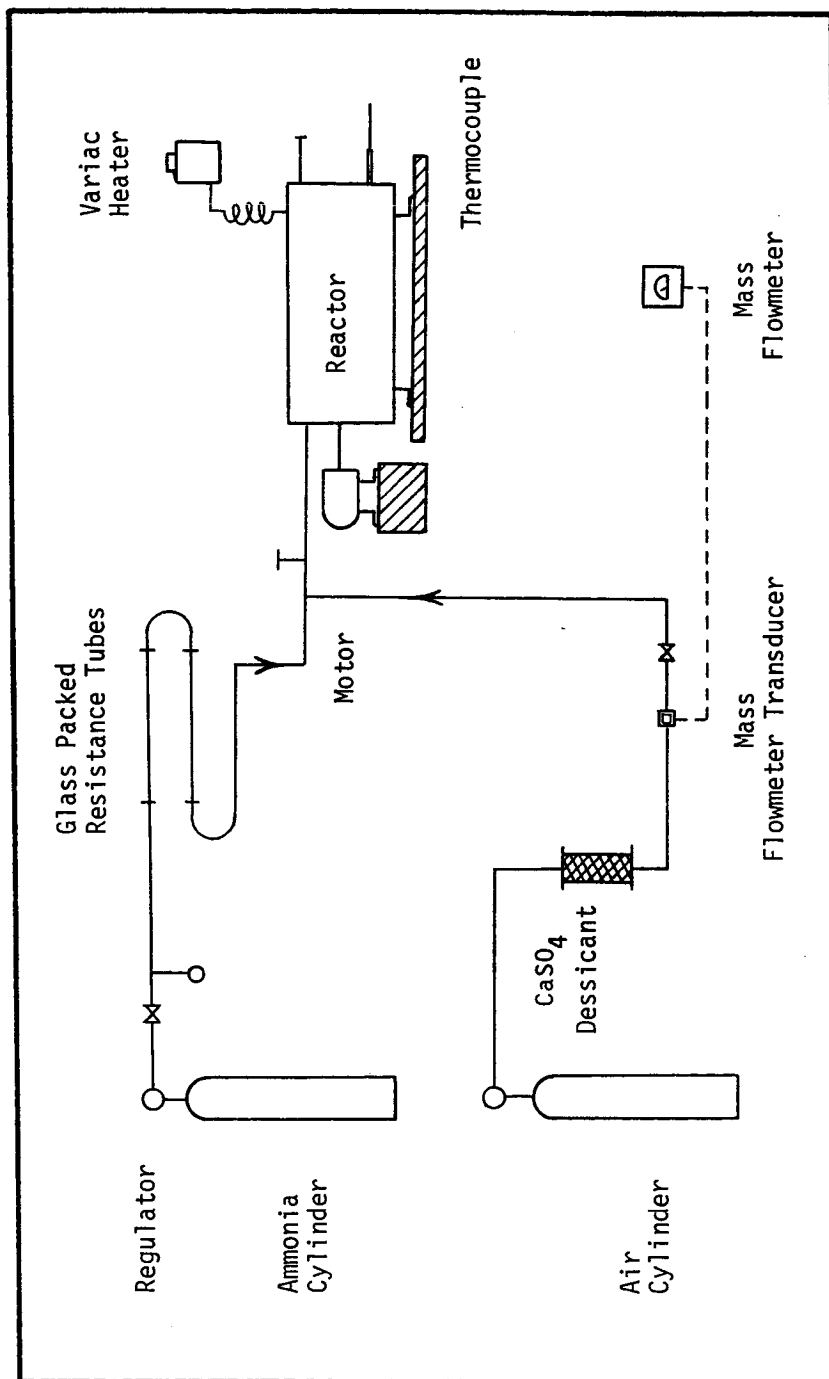
Figure 5.1 - Experimental Apparatus -
Backmix Reactor
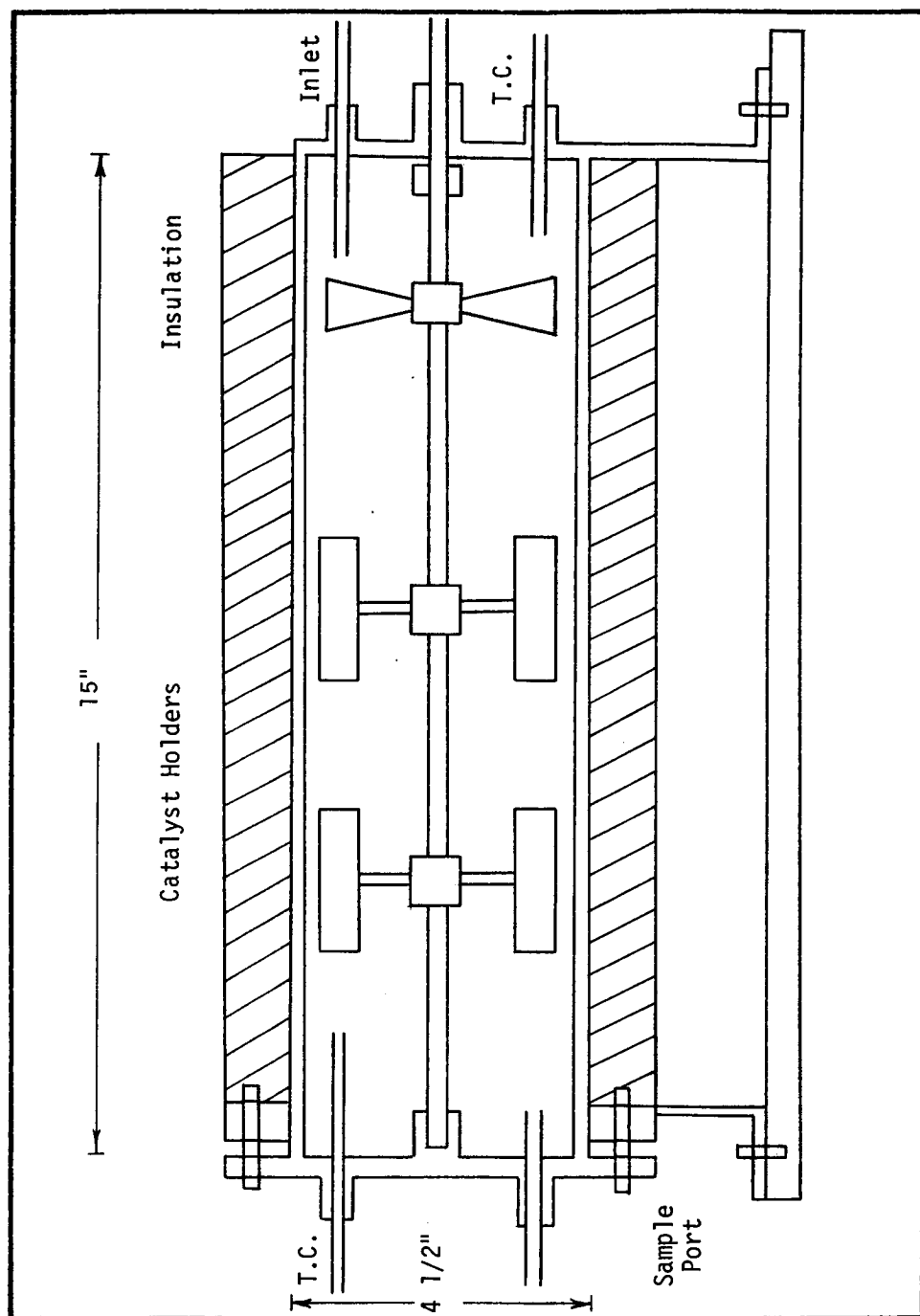
Figure 5.2 - Stirred Tank Reactor Detail

66
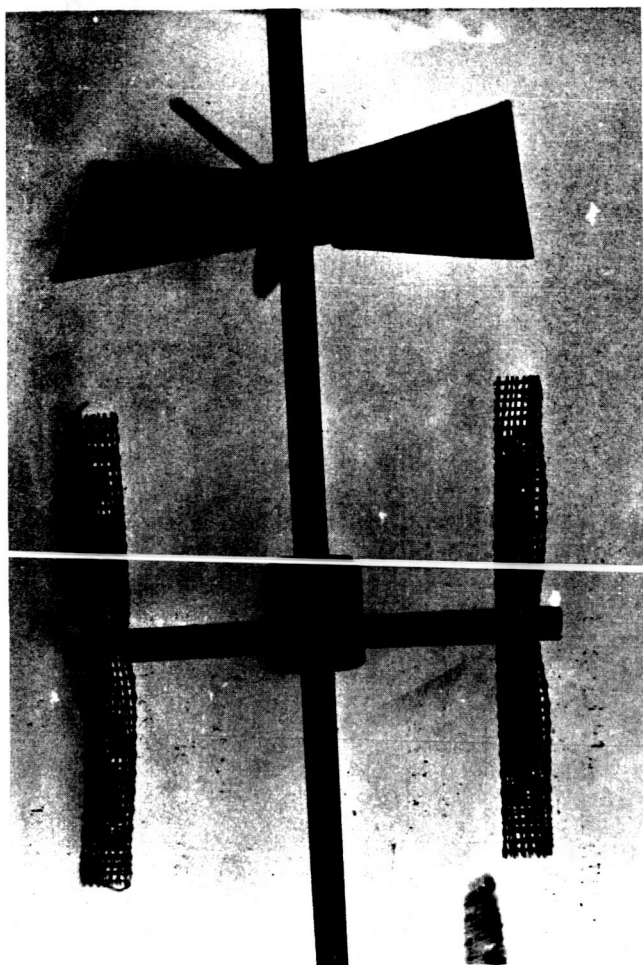
Figure 5.3 - Backmix Reactor Catalyst Baskets

a length and diameter of 1/8 in. The first baskets which were made had the catalyst stacked one behind the other approximately eight layers deep in the direction of rotation. It was suspected for this arrangement that the rear pellets were shielded from the gas by the front pellets thereby reducing the effectiveness of the catalyst charge. In order to have adequate exposure of all the catalyst pellets to the gas, it was necessary to have the catalyst spread out so that resistance to flow through the catalyst region was minimized. This was accomplished using the baskets pictured in Figure 5.3. The baskets were made from a flexible steel wire mesh.

Another area of concern was the degree of mixing within the reactor. In order for a backmix type reactor to provide meaningful data it is essential that there be no concentration gradients within the reactor. In order to check this, runs were made in which samples were taken from both ends of the reactor. Good agreement was obtained, at least within the accuracy of the analysis, indicating that the mixing was good. As another check on mixing, the temperature at both ends of the reactor was monitored. Here again good agreement was obtained.

The fact that the reactor itself was not catalyzing the reaction was established. With no catalyst in the reactor, samples were taken from the inlet feed line sample port and reactor end plate sample ports. Good agreement was obtained at temperatures as high as 450°F. At temperatures of 600°F and higher, however, some background oxidation of ammonia to nitrogen dioxide was noticed.

5.1.1 Operational Principle. - The backmix reactor is operated in a steady state manner in order to take advantage of its differential nature. The backmix (or stirred-tank) reactor has a significant experimental advantage over the more conventional gas-solid catalytic reactors such as the fixed bed reactor, in that reaction rates as a function of concentration are directly calculable. This can be seen by considering the continuous feed backmix reactor shown in Figure 5.4.
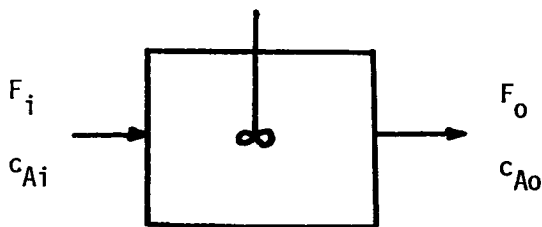
Figure 5.4 - Backmix Reactor Schematic

68

A steady state material balance on component A yields

$$F_i c_{Ai} - F_o c_{Ao} + r_A = 0 \qquad (5.1)$$

where F_i = total molar flow rate in

F_o = total molar flow rate out

c_{Ai} = inlet concentration of A

c_{Ao} = outlet concentration of A

r_A = reaction rate of A.

If the difference in inlet and outlet molar flow rates is zero or negligible, then Equation (5.1) can be rewritten

$$r_A = F_i(c_{Ao} - c_{Ai}) \cdot \qquad (5.2)$$

If a compound B is being produced by the reaction and no B is present in the inlet to the reactor, then the following holds:

$$r_B = F_i c_{Bo} \qquad (5.3)$$

where c_{Bo} = outlet concentration of B

r_B = production rate of B.

If the mixing in the reactor is good, it is apparent that the composition of the outlet, F_o, will be identical to that of the reactor contents. Thus the reaction occurs at the constant outlet concentrations c_{Ao} and c_{Bo}.

Relating Equations (5.2) and (5.3) to the specific case of ammonia oxidation and nitrogen oxides formation, the following can be written:

$$r_{NH_3} = F_i(c_{NH_{3_i}} - c_{NH_{3_o}}) \qquad (5.4)$$

$$r_{N_2O} = F_i c_{N_2O} \qquad (5.5)$$

$$r_{NO_2} = F_i c_{NO_2} \qquad (5.6)$$

where $c_{NH_{3_i}}$ = inlet ammonia concentration

$c_{NH_{3_o}}$ = outlet ammonia concentration

c_{N_2O} = outlet N_2O concentration

c_{NO_2} = outlet NO_2 concentration

r_{NH_3} = ammonia disappearance rate

r_{N_2O} = N_2O formation rate

r_{NO_2} = NO_2 formation rate.

5.1.2 Experimental Procedure

Prior to making each run the reactor temperature was adjusted to the desired level by manually adjusting the setting of the variable voltage transformer. The air flow to the reactor was set to the desired rate by adjusting the needle valve downstream of the mass flowmeter. The ammonia flow rate was set by adjusting the needle valve between the ammonia cylinder and the resistance tube and observing the pressure on the upstream side of the resistance tube. The purpose of this observation was to get a qualitative idea of what the ammonia concentration at the inlet to the reactor will be; for calculational purposes the inlet ammonia concentration was determined by colorimetric analysis. The agitator was set to the desired speed (550 r.p.m.) by adjusting the Minarik motor controller.

After the temperature and flow rates had been at their steady state values for approximately one hour, sampling was begun. The reactor contents were sampled first. The desired number of samples (usually three each) for ammonia, N_2O, and NO_2 analysis were taken via syringe at the sample port in the reactor end plate, being careful that the rate of sample withdrawal did not exceed the air flow rate into the reactor. This was important because a rapid sample withdrawal rate could result in room air leaking into the reactor thereby diluting its contents. After sampling of the reactor contents was completed, the air feed stream to the reactor is sampled for NH_3 via a septum in the air feed line downstream of the air-ammonia mixing point.

5.2 Fixed-Bed Reaction System

A fixed-bed reactor was constructed in order to provide a system for evaluation of ammonia oxidation catalyst. The equipment consists of an isothermal oven, a feed preparation system, and the reactor proper.

The oven was constructed of 18 gauge 314 stainless steel and insulated with one inch of glass fiber type insulating material. Oven temperature was manually controlled by adjustment of the applied voltage to a 500 watt electrical resistance. The oven temperature was monitored using three thermocouples placed inside of the oven. A long shafted 1/6 horsepower electric motor was used to provide air circulation inside of the oven and thus insured a uniform temperature distribution.

A schematic flow diagram of the fixed-bed apparatus is shown in Figure 5.5. The feed preparation system consisted of an ammonia supply tank connected through a high-resistance glass tube to the air feed line. This tube provided sufficient resistance to flow to allow very small amounts of ammonia to be continuously mixed with the air stream. The air feed was humidified prior to the ammonia connection by bubbling through a temperature controlled water bath. The humidified and ammonia containing stream then passed by a sample port and into the oven. The oven contained a 10 ft. by 1/4 in. stainless steel preheater coil which brought the feed up to reaction temperature. The stream then passed upward through the reaction section and out of the oven. An exit sample port was located on the gas stream following the reactor. The stream then passed through a wet test meter and was vented.

The reactor detail is shown in Figure 5.6. The reactor was constructed of a 1 in. outside diameter type 347 stainless steel tube approximately 6 in. long. The inside diameter of the tube was 0.765 in.
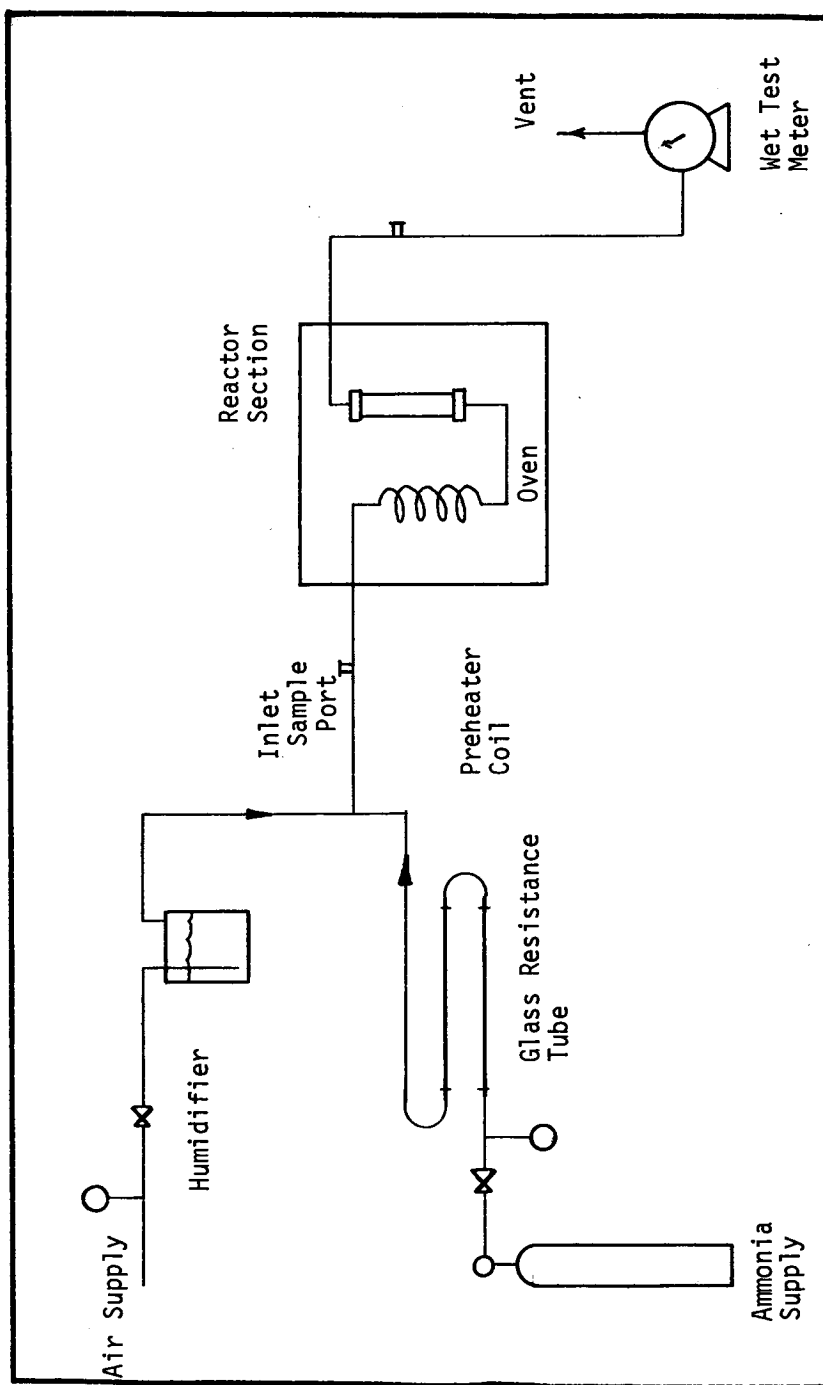
Figure 5.5 – Fixed-Bed Reactor System

EXIT

1/4" SS TUBING

1/4" SWAGELOK

1/4" PIPE TO 1/4" TUBING

1" SS SWAGELOK CAP

1" SS TUBING

CATALYST

ALUMINA PELLETS

FEED
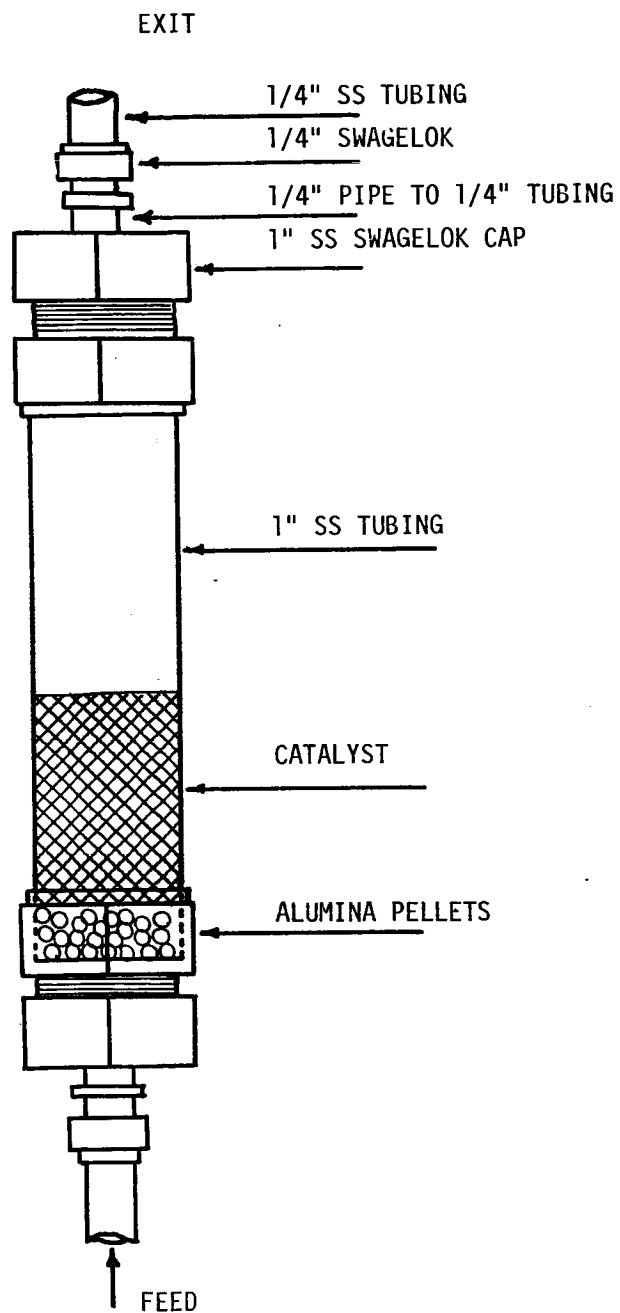
Figure 5.6 - Fixed-Bed Reactor Detail

6.0 PERFORMANCE OF AN AMMONIA ADSORBER

In order to investigate the performance of an ammonia adsorber it is desirable to have available at least the outlines of a mathematical model of the system. This assures that one has a reasonable grasp of the physical processes involved and it reduces the possibility of failure to measure a crucial parameter. In addition, these models are very useful in scaling up the system and in estimating its performance under conditions not too different from those used in testing the model.

6.1 Modelling Techniques

When a mathematical model is needed for an engineering system, the first approach frequently involves the application of the equations of change. For an isothermal ammonia adsorber this reduces to the description of the system using an unsteady-state mass balance. In addition to the mass balance it is essential to have available a model or relationship for the equilibrium behavior of the system. Since the nature of this behavior is at least as important as the differential mass balance, the form of this relationship will be discussed first.

6.1.1 Equilibrium. - What is needed for an ammonia adsorber is an equilibrium relationship between concentration or partial pressure of adsorbate in the gas phase, and the adsorbate loading on the solid surface. Such a relationship, when measured and expressed at constant temperature, is called an isotherm and a considerable amount of work in the past has been devoted to defining isotherms for various solid-gas systems. Plots of adsorbate bulk concentration (or partial pressure) versus equilibrium surface concentration at a particular temperature are also called isotherms.

These isotherms are particularly useful in design because they provide a means of estimating the minimum amount of material that would be required to adsorb a particular load. In addition, if the breakthrough occurs over a narrow time span, they can be used to estimate the time at which the adsorbent will break through the bed.

The Brunauer, Emmett, and Teller (or BET) equation (ref. 12) is, because of its easy use and accuracy, probably the most widely used isotherm equation. The BET equation can be written as:

$$\frac{P}{W_E(P_o-P)} = \frac{1}{W_M\,C_{BET}} + \frac{(C_{BET}-1)}{W_M\,C_{BET}}\frac{P}{P_o} \qquad (6.1)$$

where C_{BET} = dimensionless experimental constant

P = partial pressure of gas

P_o = vapor pressure of gas

74

W_E = equilibrium adsorbent loading

W_M = loading, corresponding to a monomolecular coverage of adsorbent by adsorbate.

The theory behind the BET equation has several deficiencies. The most obvious of these is that the BET model allows an adsorbate molecule to be adsorbed on top of an isolated adsorbed molecule. Also, the energy change upon adsorption is considered to be equal to that when the vapor is condensed to a liquid state in which each molecule has twelve nearest neighbors. Despite these shortcomings, results obtained with the equation have been quite good.

A simplification of the BET equation to the Langmuir equation is possible under certain conditions. If P is much smaller than P_o ($P < 10^{-3}$ atm and $P_o > 10$ atm), as is the case for the air-ammonia system, then:

$$P_o \doteq P_o - P \qquad (6.2)$$

so that

$$P = \cfrac{W_E}{\cfrac{W_M\ C_{BET}}{P_o} - \cfrac{W_E(C_{BET}-1)}{P_o}} \qquad (6.3$$

if

$$A' = \frac{W_M\ C_{BET}}{P_o} \qquad (6.4)$$

and

$$B' = \frac{C_{BET}-1}{P_o} \qquad (6.5)$$

then

$$P = \frac{W_E}{A' - B'W_E} \qquad (6.6)$$

which is identical in form to an equation proposed by Langmuir. Since P is proportional to C, equation 6.6 can be written as:

$$C = \frac{W_E}{A_A - W_E B_B} \qquad (6.7)$$

where A_A and B_B are experimentally determined constants.

For the copper sulfate treated sorbeads, as well as the wet and dry Hambeads data, an isotherm of this form was used to model the equilibrium data.

Once a suitable form has been determined for the equilibrium relationship, it may also be used to gain additional insight into the nature of the adsorption that is occurring through the calculation of isosteres.

6.1.2 Isosteres. - A plot of the natural logarithm of adsorbate partial pressure against inverse absolute temperature with the amount adsorbed held constant is called an isostere. Because of the difficulty in holding sorbent loading constant, isosteres are normally plotted from a fit of isotherm data and not directly from experimental results. The procedure for accomplishing this will be demonstrated in the results section.

Isosteric plots are generally straight lines. The slope of these straight lines is equal to the negative of the ratio of the latent heat of adsorption for the system to the gas constant. An isostere with a large negative slope represents a material with a higher heat of adsorption than an isostere with a smaller negative slope.

The Clausius-Clapeyron equation can be written:

$$\frac{d(\ln P_o)}{d(1/T')} = - \frac{q}{R_g} \qquad (6.8)$$

where   q = latent heat of a phase change, Btu/mol

R_g = gas constant, Btu/mol - °R

T' = absolute temperature, °R.

From equation 6.8, the slope of the natural log of vapor pressure plotted against inverse absolute temperature is the negative ratio of the latent heat of a phase change to the gas constant.

Therefore, from an isosteric plot, one can calculate the latent heat of adsorption for the adsorbate under study. One can also calculate the latent heat of condensation for the adsorbate (care should be taken here to calculate

76

the latent heat of condensation for temperatures at which the vapor pressure
is near the partial pressures used in the adsorption study). Once the latent
heat of adsorption and the latent heat of condensation are known, a comparison
of the two will show whether physical adsorption or chemisorption has occurred.
That is, if physical adsorption has occurred, the two latent heats will be
nearly the same. If both chemical adsorption and physical adsorption have
occurred, the latent heat of adsorption will be greater than the latent heat
of condensation.

Although the calculation of isosteres is an important use of the iso-
therm, the primary function of the adsorption isotherm in this study was in
conjunction with the differential mass balance and the adsorption rate ex-
pression. Since this combination is a set of relatively intractable equations,
a numerical procedure was used to calculate the predicted concentration history
in the bed effluent.

6.1.3 Gas Phase Material Balance. - The conservation equation can be
developed for an adsorber by writing an unsteady state gas phase material
balance for a differential element of the adsorbent bed. For this differen-
tial element one can write a general balance in the form:

$$\text{in - out + generation = accumulation}$$

Assuming the gas velocity is constant across the cross section of the bed,
one can write for a differential element:

$$\text{in} = (C \ V \ \pi \ R^2)_z$$

$$\text{out} = (C \ V \ \pi \ R^2)_{z+\Delta z}$$

$$\text{generation} = -\hat{R} \ \pi \ R^2 \ \Delta z$$

$$\text{accumulation} = \epsilon_B \ \pi \ R^2 \ \Delta z \ \frac{\Delta C}{\Delta T}$$

When these terms are substituted into the general balance:

$$(C \ V \ \pi \ R^2)_z - (C \ V \ \pi \ R^2)_{z+\Delta z} - \hat{R} \ \pi \ R^2 \ \Delta z = \epsilon_B \ \pi \ R^2 \ \Delta z \ \frac{\Delta C}{\Delta T} \ ,$$

rearranging,

$$\frac{(C \cdot V)_z - (C \cdot V)_{z+\Delta z}}{\Delta_z} = \hat{R} + \varepsilon_B \frac{\Delta C}{\Delta T} \quad .$$

If Δz and ΔT approach zero, the first and third terms of this equation become the definitions of the partial derivatives so that the material balance becomes:

$$-\frac{\partial VC}{\partial z}\bigg)_T = \hat{R} + \varepsilon_B \frac{\partial C}{\partial T}\bigg)_z \quad .$$

If the velocity is also assumed to be independent of axial position in the bed, this leads to:

$$-V \frac{\partial C}{\partial z}\bigg)_T = \hat{R} + \varepsilon_B \frac{\partial C}{\partial T}\bigg)_z \quad . \tag{6.9}$$

6.1.4 Rate of Adsorption. - The term $\hat{R}$ in equation 6.9 can be expressed in many forms depending on the adsorption model being proposed. However, the defining expression for the rate of adsorption is written in terms of the adsorbate loading on the solid. The form of the expression used in this work is:

$$\hat{R} = \rho_B \frac{\partial W}{\partial T}\bigg)_z \quad . \tag{6.10}$$

In order to be able to use the defining expression for the adsorption rate $\hat{R}$, it is necessary to determine which of several possible resistances are controlling. The first of these to be considered was the resistance to mass transfer from the bulk gas phase to the surface of the adsorbate. The applicable form of the general mass transfer equation relative to this situation is:

$$\frac{\hat{R}}{\rho_B} = K_g A_c (C-C_s) \tag{6.11}$$

The most difficult term to measure in this expression is the mass transfer coefficient, K_g. However, several good empirical correlations do exist which permit reasonable estimates to be made.

The second resistance which could be controlling concerns the transport within the adsorbent particles. If the movement of the ammonia into the pores of the adsorbate controls the rate of adsorption, then it would be necessary to consider pore diffusion.

Antonson and Dranoff (ref. 13), using the system ethane-air-molecular sieves, have divided the pore diffusion step into macropore and micropore diffusion (using approximately the same definitions of pore sizes as Dubinin (ref. 14), i.e. intermediate pore sizes from radius $15\overset{\circ}{A}$ to $2000\overset{\circ}{A}$ and macropores with radius over $2000\overset{\circ}{A}$). In their work, they concluded that micropore diffusion controlled the adsorption rate.

Descriptive equations of pore diffusion can be developed by writing a dynamic gas phase material balance for the pore region. This balance, or Fick's law as it is sometimes called, can be written as:

$$ \Gamma \left(\frac{\partial^2 C_p}{\partial r^2} + \frac{2}{r} \frac{\partial C_p}{\partial r} \right)_T = \epsilon_p \left(\frac{\partial C_p}{\partial T} \right)_r + \overset{\circ}{R} \quad . \tag{6.12} $$

Equation 6.12 is based on spherical particles and a constant pore size. While this is normally not the case, approximations made using these assumptions are usually acceptable. Note that here, as in the bulk diffusion case, the adsorption rate is a function of diffusivity (in equation 6.11, K_g is a function of diffusivity).

Equation 6.12 can be simplified by assuming a pseudo steady state, i.e. the term $\partial C_p / \partial T$ may be neglected. With this assumption, equation 6.12 becomes:

$$ \Gamma \left(\frac{\partial^2 C_p}{\partial r^2} + \frac{2}{r} \frac{\partial C_p}{\partial r} \right)_T = \overset{\circ}{R} \quad . \tag{6.13} $$

This equation, while not pursued further in this work, is another possible expression for the rate of adsorption when pore diffusion is the primary resistance.

If neither the movement from the bulk phase nor the diffusion into the pores is controlling, the main resistance may be due to surface effects. The rate of adsorption on the surface is generally considered in terms of the

79

fraction of the surface covered or in terms of adsorption spaces or sites. In either case, there is a maximum equilibrium amount of adsorbate (or maximum number of filled sites) that can be held on the surface (as a function of temperature and local gas phase concentration). It was this maximum surface concentration that was discussed by Bruauer, Emmett, and Teller (ref. 12) in their paper on equilibrium adsorption. This number of adsorption sites is directly related to the sorbent loading for a given adsorbent. It is reasonable then, to say that the driving force for surface adsorption is a function of the difference between equilibrium loading and instantaneous loading. In equation form this can be written as:

$$\hat{R} = YK \; (W_E - W) \tag{6.14}$$

When this equation was used in conjunction with the differential mass balance and a Langmuir expression for the equilibrium loading, the calculated concentration at the bed exit computed using a numerical algorithm compared favorably with the values observed experimentally.

6.2 Numerical Algorithms

In order to calculate the concentration of ammonia in the bed effluent, a numerical algorithm is needed.

If all three of the previously discussed resistances, (bulk phase mass transfer, pore diffusion, and surface adsorption), were significant in a particular process, the descriptive equations would be very complex. In order to achieve a manageable set, algorithms were developed which assumed that only one of these resistances was significant. Calculations made using the individual algorithms were then compared to experimental results to determine the value of the models as predictive tools.

6.2.1 Bulk Phase Mass Transfer Limiting Model. - If bulk phase mass transfer limits the adsorption rate, the following equations, which were developed previously are applicable:

$$- V \left. \frac{\partial C}{\partial z} \right)_T = \epsilon_B \left. \frac{\partial C}{\partial T} \right)_z + \hat{R} \tag{6.15}$$

$$\hat{R} = \rho_B \frac{\partial W}{\partial T} \tag{6.16}$$

$$\hat{R} = K_g \, A_c \, \rho_B \; (C - C_S) \tag{6.17}$$

80

Also, since it is assumed in this model that the pore diffusion and surface adsorption resistances are negligible and therefore, that equilibrium surface loading is equal to instantaneous surface loading, it can be written that:

$$C_S = \frac{W}{A_A - B_B W} = \frac{W_E}{A_A - B_B W_E} \tag{6.18}$$

An inspection of these equations shows that they do not have a simple analytic solution. However, the equations do lend themselves readily to machine computation. Numerical work of this sort requires discrete sized increments in time and bed distance and, therefore, double subscripts are required for the concentration variables.

Equation 6.15 can be written in backwards difference form as:

$$-\frac{V}{\Delta z}(C_{i,j} - C_{i-1,j}) = \frac{\varepsilon_B}{\Delta T}(C_{i,j} - C_{i,j-1}) + \overset{\scriptstyle\curvearrowright}{R}_{i,j} \tag{6.19}$$

Solving for $C_{i,j}$ gives:

$$C_{i,j} = \frac{C_{i-1,j}\frac{V}{\Delta z} + \frac{\varepsilon_B}{\Delta T}C_{i,j-1} - \overset{\scriptstyle\curvearrowright}{R}}{\frac{V}{\Delta z} + \frac{\varepsilon_B}{\Delta T}} \tag{6.20}$$

The defining expression for the adsorption rate can also be written in difference form:

$$\overset{\scriptstyle\curvearrowright}{R}_{i,j} = \frac{\rho_B}{\Delta T}(W_{i,j} - W_{i,j-1}) \tag{6.21}$$

For this mass transfer limiting case, the rate of adsorption can also be expressed as:

$$\overset{\scriptstyle\curvearrowright}{R}_{i,j} = K_g A_c \rho_B (C_{i,j} - C_{S_{i,j}}) \tag{6.22}$$

But using the (Equation 6.18) isotherm equation:

$$C_{S_{i,j}} = \frac{W_{i,j}}{A_A - B_B W_{i,j}} \tag{6.23}$$

gives

$$\frac{W_{i,j} - W_{i,j-1}}{\Delta T} = K_g \, A_c \, (C_{i,j} - \frac{W_{i,j}}{A_A - B_B W_{i,j}}) \qquad (6.24)$$

solving for $C_{i,j}$ gives

$$C_{i,j} = \frac{\dfrac{W_{i,j} - W_{i,j-1}}{\Delta T} + K_g \, A_c \, \dfrac{W_{i,j}}{A_A - B_B W_{i,j}}}{K_g \, A_c} \qquad (6.25)$$

Since

$$R_{i,j} = \frac{\rho_B}{\Delta T} (W_{i,j} - W_{i,j-1}) \qquad (6.26)$$

equation 6.20 can be written as:

$$C_{i,j} = \frac{C_{i-1,j} \dfrac{V}{\Delta z} + C_{i,j-1} \dfrac{\varepsilon_B}{\Delta T} - \dfrac{\rho_B}{\Delta T} (W_{i,j} - W_{i,j-1})}{\dfrac{V}{\Delta z} + \dfrac{\varepsilon_B}{\Delta T}} \qquad (6.27)$$

If the assumption can be made, that $C_{i,j-1}$, $C_{i-1,j}$, and $W_{i,j-1}$ are known at some initial z and T then equations 6.25 and 6.27 can be solved for $C_{i,j}$ and $W_{i,j}$.

A gridwork can be constructed with ordinate of time and abscissa of bed length (Figure 6.1). One can also imagine a bulk gas concentration axis perpendicular to the plane of the paper. That is, each point on the time-distance grid has associated with it a bulk gas concentration (and an adsorbent surface concentration). An examination of this grid shows that at any time, the bulk gas concentration at the front of the bed is the inlet concentration or:

$$C_{1,j} = C_{inlet} \quad \text{for all } T > 0 \qquad (6.28)$$
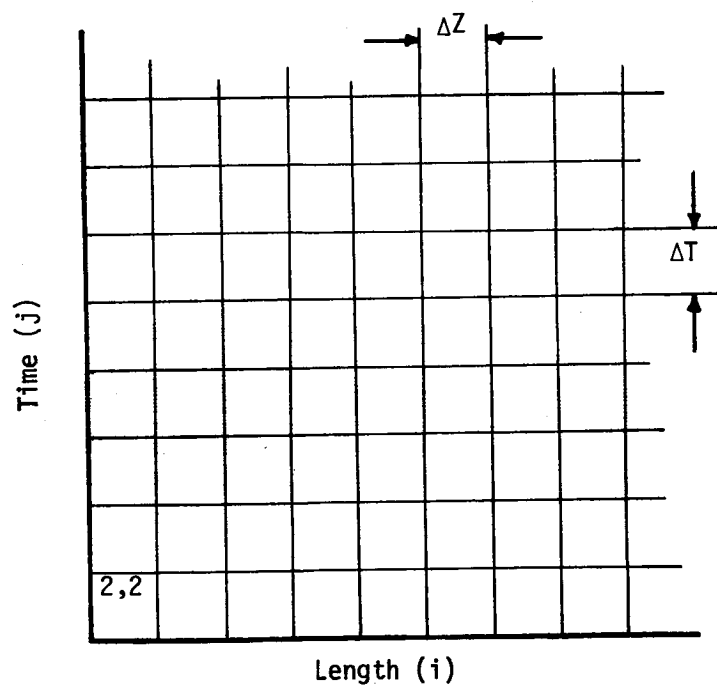
82

Figure 6.1 - Computational Grid

Also, initially, for any position in the bed, the bulk gas concentration and the surface concentration (loading) are zero or:

$$C_{i,1} = W_{i,1} = 0 \quad \text{for } T = 0, \ 0 \leq z \leq \text{ Total bed length} \qquad (6.29)$$

Therefore, all values of $C_{i,j}$ and $W_{i,j}$ on the ordinate and abscissa of the computational grid are defined. Taking the grid position 2 - 2 (Figure 6.1), $W_{i,j-1}$, $C_{i,j-1}$, and $C_{i-1,j}$ are all known and for this 2 - 2 position, $C_{i,j}$ and $W_{i,j}$ can be calculated using equations 6.25 and 6.27. Obviously if the 2 - 2 position is known, the 2 - 3 position can be solved for $W_{i,j}$ and $C_{i,j}$. Thus a march down the bed at constant time is clearly defined. Once the end of the bed is reached, $C_{i,2}$ and $W_{i,2}$ are known and $C_{i,3}$ and $W_{i,3}$ can be calculated. This process can be continued until the entire time-length grid has been covered.

A Fortran IV computer program was written based on the above technique. Inputs to the program are the experimental parameters such as inlet ammonia concentration, gas flow rate, bed height, and run duration. Also required as input are such constants as adsorbent particle size, apparent bulk density, surface area per gram of adsorbent and the experimentally determined Langmuir isotherm constants. The mass transfer coefficient is calculated within the program based on a correlation by Satterfield (ref. 9). Other important variables such as gas superficial velocity are also calculated within the program. Program outputs include the calculated mass transfer coefficient and bulk phase gas concentrations, adsorbent surface concentration and adsorption rate, all as functions of time and distance down the bed. Another program output is a machine plot of bulk phase gas concentration versus bed length at constant time for several fractions of the total run time.

Of special interest is the portion of the program in which equations 6.25 and 6.27 are solved by trial and error. The Langmuir isotherm equation is part of the solution and special care must be exercised so that one always operates in the first quadrant of the Langmuir equation. $C_{i,j}$ and $W_{i,j}$ must always be positive in a real system. Due to the asympotic nature of the equation, it is easy for the solutions to equations 6.25 and 6.27 to be outside the first quadrant, particularly, since these equations are solved by trial and error. Solutions to equations 6.25 and 6.27 outside the first quadrant can be convergent but physically meaningless.

6.2.2 Surface Adsorption Limiting Model.- Several other expressions relative to the adsorption rate have been proposed (ref. 15). However, the one most applicable to this study is the one introduced previously and rewritten

here for convenience:

$$\hat{R} = YK \ (W_E - W) \tag{6.30}$$

Equation 6.30 is similar to equation 6.17 in that both contain a driving force in terms of a concentration difference and a coefficient which is inversely proportional to the resistance encountered in that particular step. However, the term $(W_E - W)$ is proportional to the number of available adsorption sites on the surface and, therefore, the adsorption rate expression for this model assumes that surface adsorption offers the only significant resistance to adsorption. This rate expression can be used as was equation 6.22 above.

One other step is necessary when using equation 6.30 because W_E is a function of the local bulk ammonia concentration. Since in this model the surface adsorption resistance is assumed to be much greater than the bulk diffusion or pore diffusion resistances, it can be written that:

$$C = C_S \tag{6.31}$$

It has been previously stated that C_S is functionally related to the surface concentration by the Langmuir equation. Therefore, it follows that:

$$W_E = \frac{CA_A}{1 + CB_B} \tag{6.32}$$

where A_A and B_B are Langmuir constants.

New expressions for $C_{i,j}$ and $W_{i,j}$ can now be developed based on the above discussion but using the same computational sequence as before. The new expressions are (in computational order):

$$W_{E_{i,j}} = \frac{C_{i-1,j} \ A_A}{1 + C_{i-1,j} \ B_B} \tag{6.33}$$

$$W_{i,j} = \frac{YK \ W_{E_{i,j}} + \frac{\rho_B}{\Delta T} W_{i,j-1}}{\frac{\rho_B}{\Delta T} + YK} \tag{6.34}$$

85

$$C_{i,j} = \frac{C_{i-1,j} \frac{V}{\Delta z} + C_{i,j-1} \frac{\varepsilon_B}{\Delta T} - \frac{\rho_B}{\Delta T}(W_{i,j} - W_{i,j-1})}{\frac{V}{\Delta z} + \frac{\varepsilon_B}{\Delta T}} \qquad (6.35)$$

As presented, equations 6.33, 6.34, and 6.35 can be solved in a straight-forward manner without the trial and error that was necessary with the bulk diffusion model.

6.3 Experimental Data

In order to use the numerical algorithms it is necessary to have numerical values for the parameters contained within these models. Since the equilibrium relationship plays a key role in both of these algorithms, the experimental method used to evaluate the two constants contained in the Langmuir form of this expression will be discussed first.

6.3.1 Bed Capacity Calculations. - A graphical integration technique was used to calculate adsorbent capacities. If the plot of exit ammonia concentration versus time is graphically integrated and the resulting number divided by total run time, the time averaged exit ammonia concentration is obtained. Since the inlet ammonia concentration is held constant, the difference between the inlet and average exit concentrations is the average ammonia concentration adsorbed. This concentration in mols per ft^3 can be multiplied by the total run time and the flow rate to give the moles of ammonia removed during a run. Since the amount of material in the bed is known, the bed capacity in grams of ammonia per gram of bed may be calculated.

Bed saturation runs were made at temperatures of 72°F and 100°F. Air flow rates ranged from 0.164 cfm to 0.202 cfm while ammonia inlet concentrations went from 90 ppm to 520 ppm and bed length ran from two to eight cm. Fresh adsorbent was used in all runs except Run 24R.

The sorbent for Run 24R was the same sorbent used in Run 24. The material from Run 24 was regenerated in an oven at 383 ± 5°F for five days. A plot of exit ammonia concentration against time for Run 24 and 24R is shown in Figure 6.2.

The gravimetric capacity listed in Table 6.1 is the difference of the bed weight after and before a run divided by bed weight before a run. From Table 6.1, it can be seen that calculated bed capacities are uniformly higher than the gravimetric capacities. This, coupled with an observed color interface which passed through the bed during the run and the fact that no compounds other than air and ammonia were detected (no attempt was made to analyze for water) in the bed effluent, leads one to consider that some chemisorption was taking place in the bed. A specific chemical reaction which
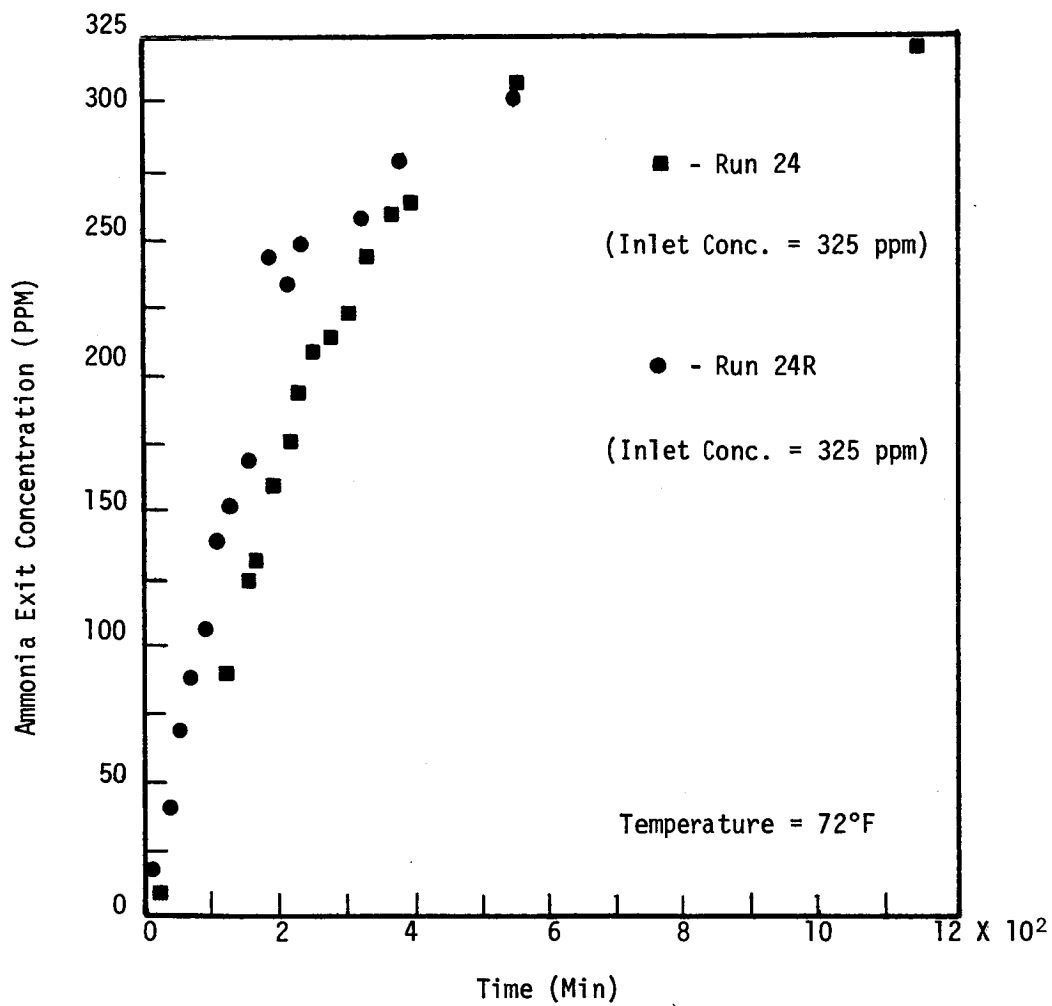
Figure 6.2 - Experimental Points

for Runs 24 and 24R

TABLE 6.1

VARIABLES IN AMMONIA ADSORPTION RUNS

Run No.	Material	Air Flow cfm	Inlet NH$_3$ Conc., ppm	Bed Gravimetric Capacity g NH$_3$/g bed	Calculated Capacity g NH$_3$/g bed	Temp. °F ± 2°F
21	CSTS	0.18	290	0.0250	0.029	72
22	CSTS	0.176	150	0.0184	0.021	72
24	CSTS	0.187	325	0.0249	0.027	72
24R	CSTS	0.18	325	0.0150	0.022	72
25	CSTS	0.202	520	0.0254	0.030	72
26	CSTS	0.176	90	0.0135	0.016	72
27	CSTS	0.177	215	0.0193	0.022	72
28	CSTS	0.17	235	0.0110	0.009	72
29	DHMB	0.164	290	0.0056	0.016	100
30	CSTS	0.186	440	0.0100	0.012	100
31	DHMD	0.18	505	0.0072	0.017	100
32	CSTS	0.164	210	-	0.008	100
34	WHMB	0.169	303	0.015	0.020	72
35	DHMB	0.193	160	0.003	0.011	72
36R	CSTS	0.187	325	0.015	0.022	72
37	WHMB	0.18	80	0.004	0.008	72
39	WHMB	0.20	175	-	0.005	72

Pressure drop across bed   0.2 in Hg guage.
Run 23 scrapped because of experimental error.
CSTS - Copper Sulfate Treated Sorbeads
DHMB - Dry Hambeads
WHMB - Wet Hambeads

would give such results is the replacement

$$CuSO_4 \cdot 5H_2O + 4NH_3 \rightleftarrows CuSO_4 \cdot 4NH_3 + 5H_2O$$
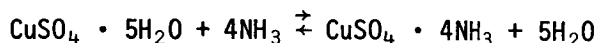
The color change could be accounted for by the fact that the characteristic color of $CuSO_4 \cdot 4NH_3$ is dark blue which was the color that the bed turned.

Adsorbent from Run 24 was regenerated at 385°F and resaturated as Run 24R. At these rather mild conditions the adsorbent was regenerated to approximately 80 percent of the fresh adsorbent's capacity based on calculated bed capacities. At more severe conditions, perhaps 500°F, the adsorbent would likely be regenerated to an even higher fraction of the original capacity. The regeneration, color change, and gravimetric results leads one to suspect that both chemical and physical adsorption were taking place in the bed.
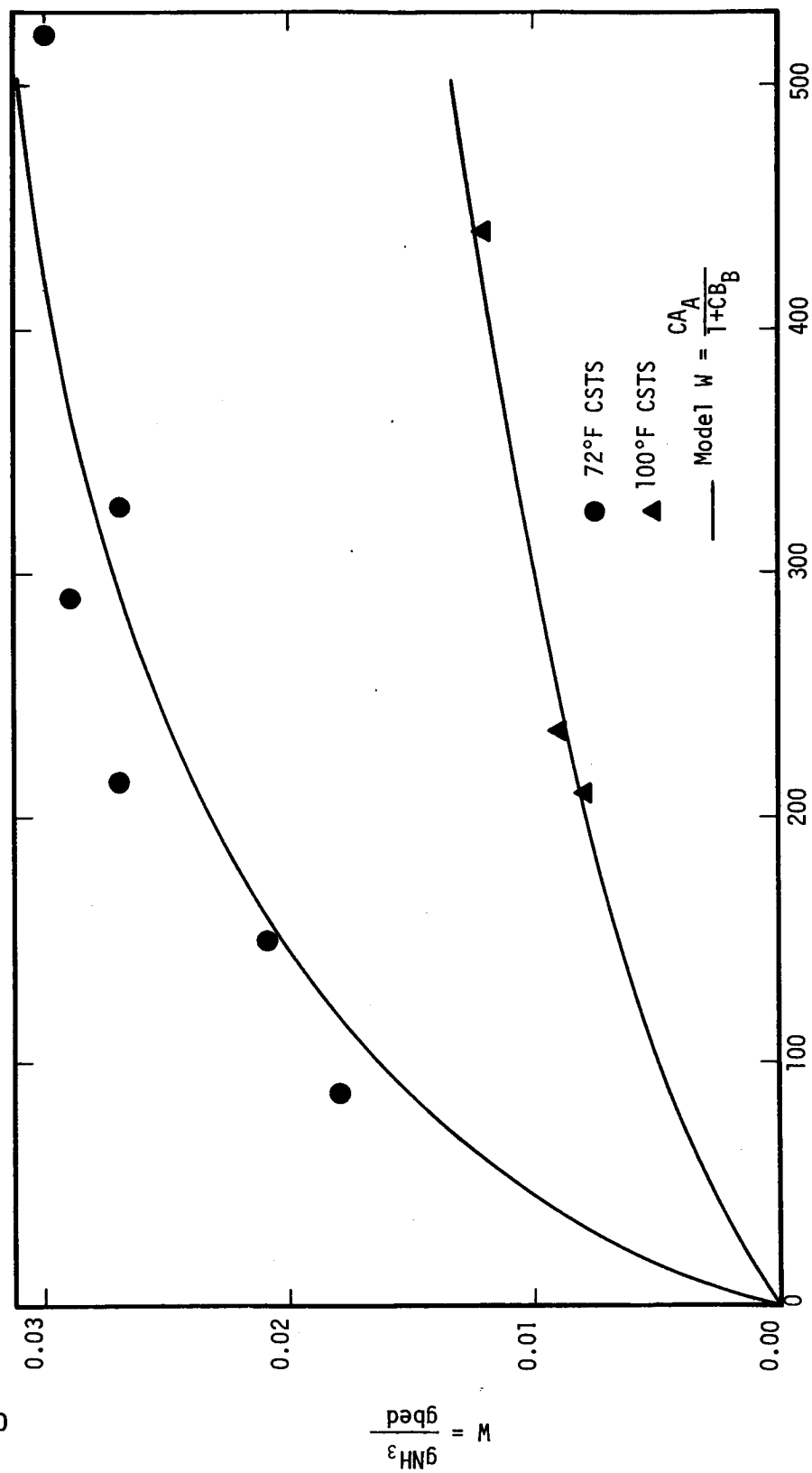
6.3.2 Determination of the Languir Constants. - When there is no change in concentration of the ammonia stream as it passes through the bed then the adsorbent within the bed is in equilibrium with that stream. Therefore, the calculated values for the bed capacities can be used in conjunction with a least squares analysis to find the best fit of the data to an equilibrium relationship of the Langmuir form.

Figures 6.3 through 6.5 illustrate the agreement between the fitted adsorption isotherms and the experimental results. As can be seen this two parameter model is adequate to describe the data over the entire experimental range. The form of the Langmuir isotherm equation is such that curves drawn from it pass through the origin (as would be expected on theoretical grounds for all isotherms).

6.3.3 Isostere Analysis. - Isosteres were plotted (Figure 6.6) using the copper sulfate treated sorbeads at three adsorbent loadings. The data for the plots were obtained from the fitted isotherm equations and not from the experimental points. (The loadings used were, however, within the range of the experimental sorbent loadings). The data for the plots were generated using equation 6.7. This equation is valid for both 72°F and 100°F (with the proper temperature dependent constants). Therefore a given sorbent loading and the appropriate constants can be substituted into the equation and the free stream concentration at both temperatures can be calculated.

In Figure 6.7, ammonia vapor pressure is plotted against inverse absolute temperature on semi-log coordinates at vapor pressure of from five to 60 mm Hg. The data for this plot is taken from thermodynamic charts for ammonia.

Since the latent heat of adsorption is directly proportional to the negative slope of the isosteric plot, this latent heat of adsorption can easily be calculated from Figure 6.6. Also, since the latent heat of condensation is directly proportional to the negative slope of the vapor pressure plot, this latent heat can be calculated from Figure 6.7. These

Inlet Gas Concentration, (PPM NH_3)

Figure 6.3 - Least Squares Fit of Copper

Sulfate Treated Sorbeads

$W = \dfrac{gNH_3}{gbed}$

90

● 72°F CSTS

▲ 100°F CSTS

—— Model $W = \dfrac{CA_A}{1+CB_B}$

Temperature 72°F
$A_A = 2.81 \times 10^{-4}$ $B_B = 7.09 \times 10^{-3}$

Temperature 100°F
$A_A = 6.19 \times 10^{-5}$ $B_B = 2.83 \times 10^{-3}$
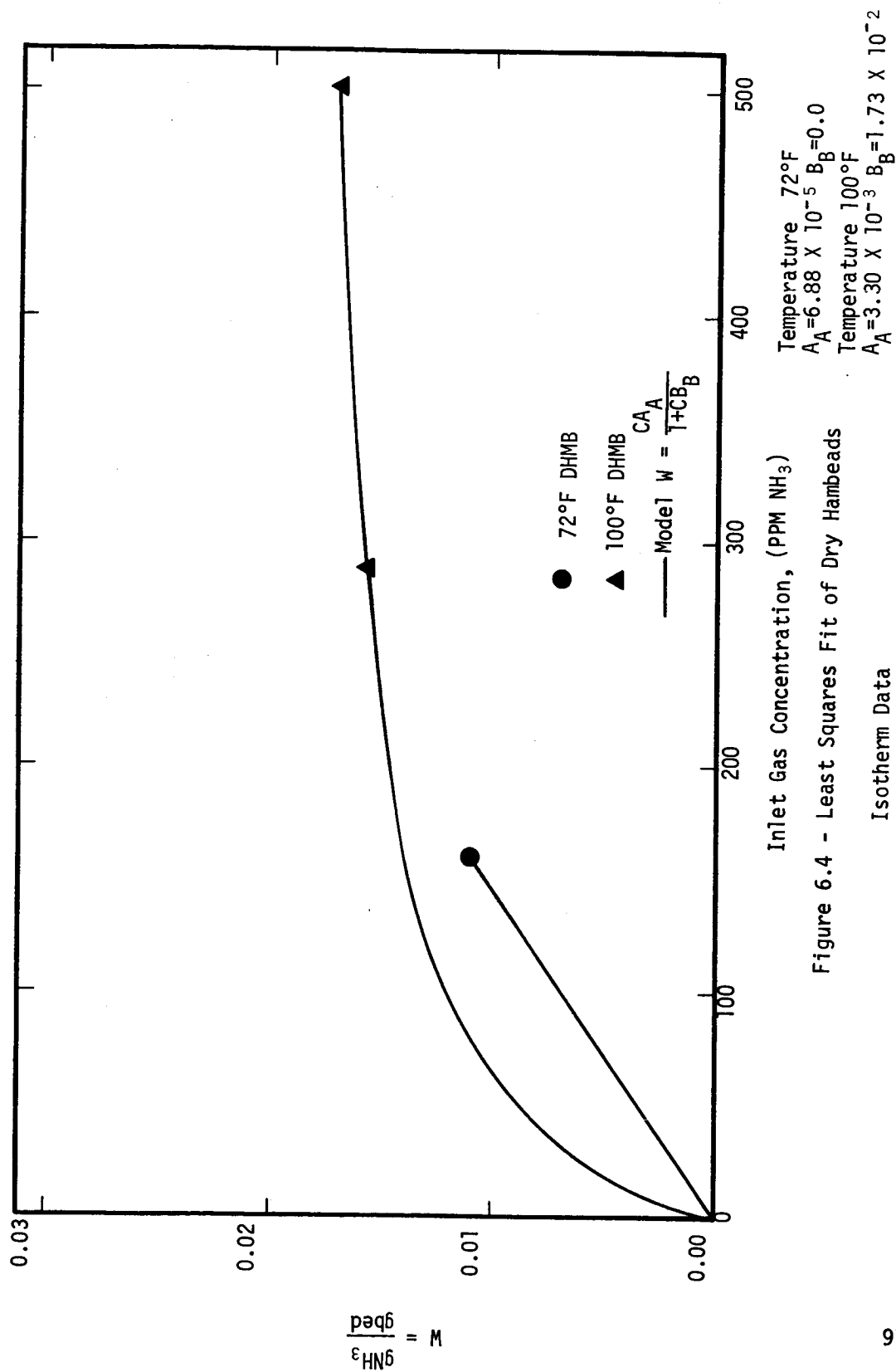
Figure 6.4 - Least Squares Fit of Dry Hambeads

Isotherm Data

Temperature 72°F
$A_A = 6.88 \times 10^{-5}$ $B_B = 0.0$
Temperature 100°F
$A_A = 3.30 \times 10^{-3}$ $B_B = 1.73 \times 10^{-2}$

● 72°F DHMB

▲ 100°F DHMB

—— Model $W = \dfrac{CA_A}{1+CB_B}$

Inlet Gas Concentration, (PPM NH_3)

$W = \dfrac{gNH_3}{gbed}$
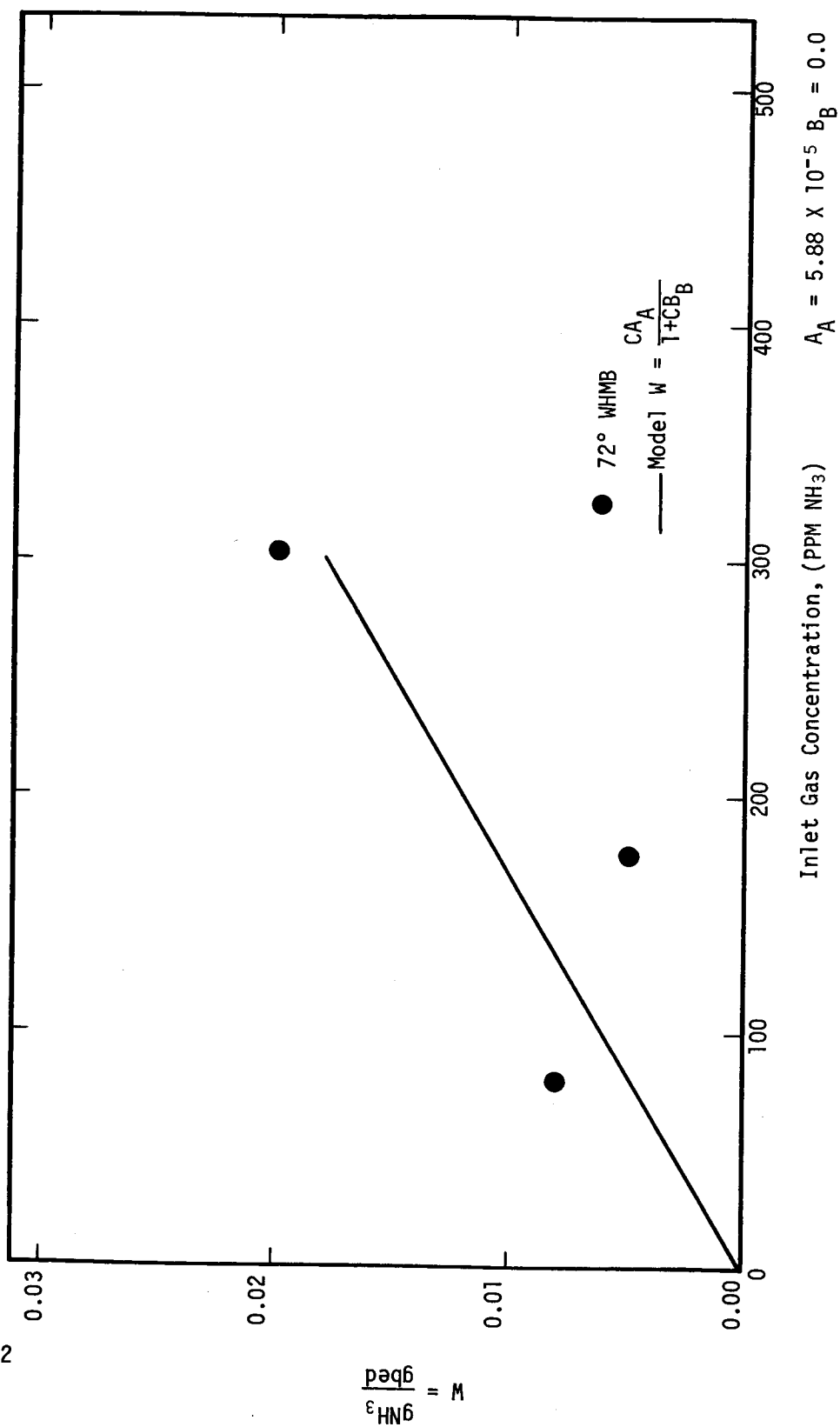
Figure 6.5 - Least Squares Fit of Wet Hambeads
Isotherm Data

$A_A = 5.88 \times 10^{-5}$ $B_B = 0.0$

● 72° WHMB

—— Model $W = \dfrac{CA_A}{1 + CB_B}$

Inlet Gas Concentration, (PPM NH_3)

$W = \dfrac{gNH_3}{gbed}$

92

Figure 6.6 - Isosteres for Copper Sulfate

Treated Sorbeads

Figure 6.7 - Plot of Ammonia Vapor Pressure

vs Inverse Temperature

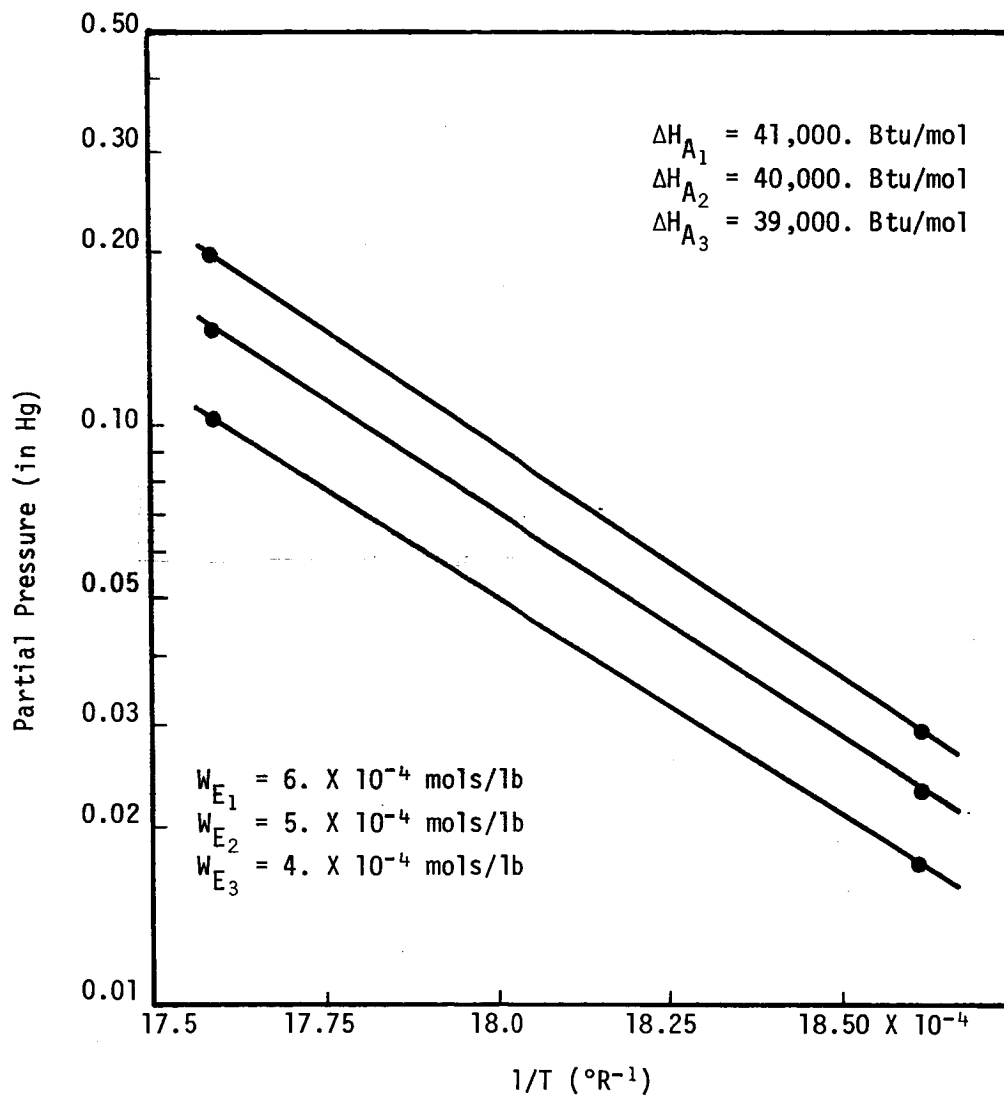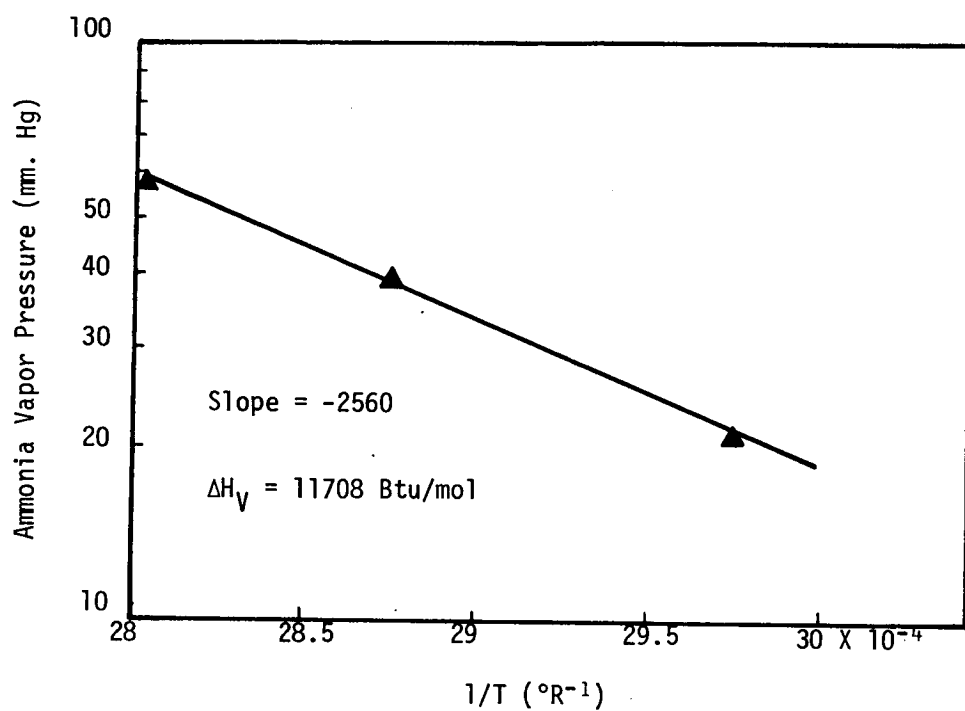calculations indicate an average latent heat of adsorption of about 40,000 Btu/mol and a latent heat of condensation of about 11,000 Btu/mol. This means that, because of the higher heat of adsorption, chemical reaction is probably taking place during the adsorption and is, therefore, contributing to the adsorption. This supports the conclusion that the sorption capacity of the bed may not be determined gravimetrically.

6.3.4 Physical Properties of the Adsorbents. - In addition to the equilibrium relationship, the density and the void fraction of the sorbent in the bed must be known before the algorithms can be used. When the mass transfer rate in the gas phase is assumed to be limiting, the external area of the adsorbent must also be measured experimentally for substitution into the algorithm.

The void fraction of the bed was determined using benzene as the displacing liquid. A sample of adsorbent was placed in a graduated cylinder and the level volume recorded. The benzene was added (Benzene was used because it does not adsorb on silica gel strongly enough to cause thermal cracking of the gel.) to some level in the cylinder (above the adsorbent). The difference in volume between the adsorbent and benzene was then subtracted from the total amount of benzene added. This adjusted volume of benzene added, divided by the volume of adsorbent in the cylinder, represented the total void fraction of the adsorbent. The experiment was repeated before the benzene in the adsorbent's internal pores has evaporated, and, therefore, the void fraction calculated for the second experiment was the external void fraction. This procedure was repeated several times and an average void fraction was used in subsequent calculations.

Some physical data concerning the surface area of the adsorbent was measured for copper sulfate treated silica gal (CSTS) but not for Hambeads. The Hambeads were received at a later point in the study when preliminary testing of the algorithms had indicated that these parameters did not need to be measured. Table 6.2 contains a summary of this data.

6.4 Testing of the Numerical Algorithms

One of the most important components of a model for the system was developed when the adsorption isotherms were adequately described using an equation of the Langmuir form. Once this relationship had been modelled, it could be used in a testing program of the nuemrical algorithms.

6.4.1 Bulk Phase Mass Transfer Model. - The first model tested was the bulk phase mass transfer controlling model. In this model it was assumed that pore diffusion and surface adsorption resistances to adsorption are insignificant relative to the overall adsorption rate. This model can be reduced to two equations and two unknows as shown by equations 6.25 and 6.27. Therefore, this model has a straightforward solution.

A plot of exit ammonia concentration versus time as predicted by the mass transfer model is given in Figure 6.8. Superimposed on this plot is a set of typical experimental data from Run 21. From this figure, it is seen

TABLE 6.2

ADSORBENT PROPERTIES

	CSTS	Hambeads
Total void fraction (measured)	0.61 ± 0.03	0.52 ± 0.06
External void fraction (measured	0.325 ± 0.02	0.38 ± 0.01
Density (measured)	51. ± 0.2 lbs_m/ft^3	52. ± 1.0 lbs_m/ft^3
Particles per gram (measured)	313. ± 10	-
External area per gram (calculated)	0.0717 ± 0.0002 ft^2/g	-
Particle "diameter" (measured)	0.0724 ± 0.004 in	-

that the mass transfer model predicts a much faster saturation of the adsorbent than actually occurs. This is not surprising when one considers the computed magnitude of the mass transfer coefficient. A mass transfer coefficient of 1000 - 1200 ft/hr is considered quite large by most sources and would lead to an early saturation of the bed.

Since the computed mass transfer coefficient is subject to some error, the model was also run for values of 120 percent and 80 percent of the computed mass transfer coefficient. Differences in the three computer runs were insignificantly small and therefore the breakthrough curves predicted by the runs with high and low mass transfer coefficients were not shown in the figure.

Useful information can, however, be gleaned from this model. First, both the size of the mass transfer coefficient and the shape of the predicted breakthrough curve indicate that the resistance to bulk phase mass transfer is small and is probably not a significant factor in the overall adsorption process. Also, the basic modelling procedure is sound and convergent. This was determined by running the program several times until the results indicated that the model gave consistent answers which are neither time nor length dependent. Time and length increments were varied over a range of one half to twice the basic time and length increments with negligible change in the final results.

The trial and error nature of the solution to the mass transfer equations (Equations 6.25 and 6.27) necessitates using computer search techniques not generally needed in adsorption calculations. Since this procedure was required in only the mass transfer model, it was incorporated in a subprogram in the general computer program.

6.4.2 Surface Adsorption Model. - Experimental runs were made with two different types of adsorbent in the bed, Hambeads and copper sulfate treated sorbeads (CSTS). The humidity level in the feed was zero for all of the CSTS runs, but three of the Hambead runs were made with the relative humidity of the feed at approximately 50%.

Figures 6.9 through 6.12 are plots of the calculated ammonia exit concentration for the surface adsorption controlling case versus time for all of the runs made with copper sulfate treated sorbeads except Runs 24R and 36R. Superimposed on the plots are the experimental data for those runs. The agreement is quite good on all runs[1] except Run 25. This agreement between calculated and experimental points suggests that, over the range studied, surface adsorption, by the proposed mechanism, is the controlling resistance to adsorption.   •

---

[1]The constant YK of equation 6.30 was determined by trial and error. In this trial and error, the sum of differences between calculated and experimental points (at constant time) squared was minimized. The YK shown in the figures was selected when YK's 25 percent higher and 25 percent lower gave higher sums of squares. A five percent change in YK produced a negligible change in the shape of the breakthrough curve.
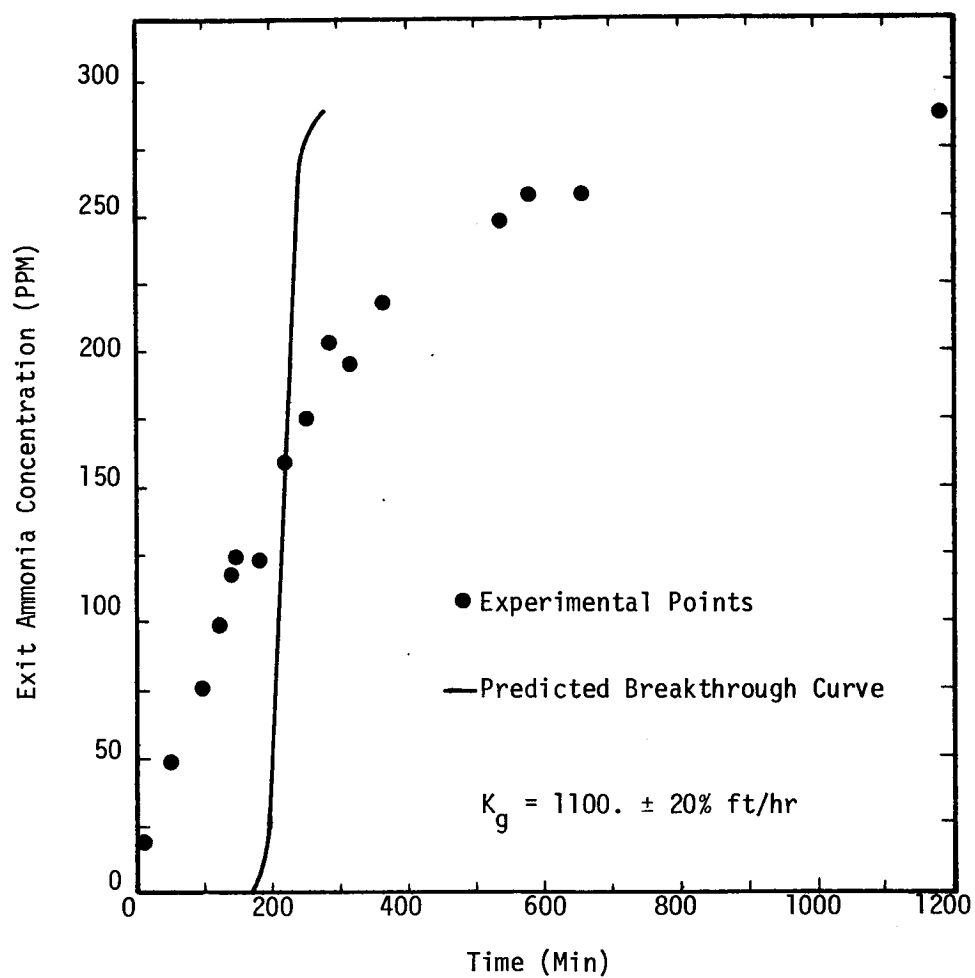
Figure 6.8 - Predicted Breakthrough Curve for
Run 21 with Bulk Phase Mass Transfer
as the Controlling Resistance with
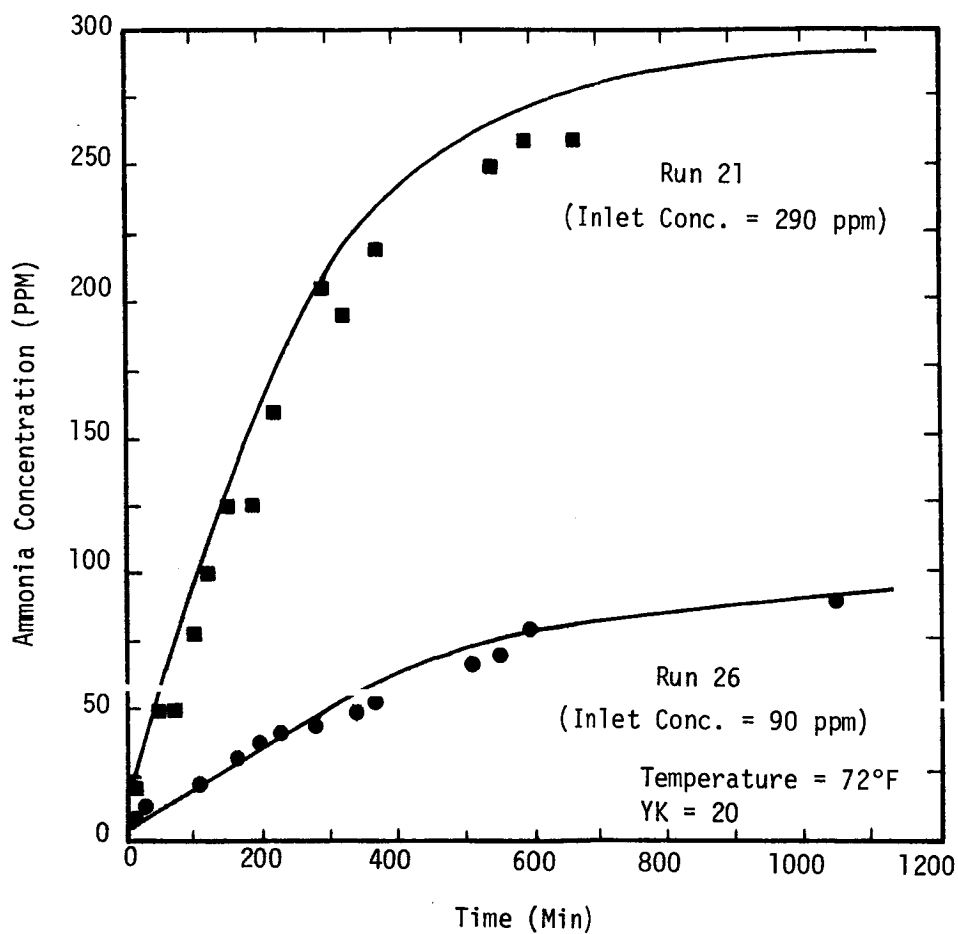Experimental Points

Figure 6.9 - Plot of Ammonia Exit
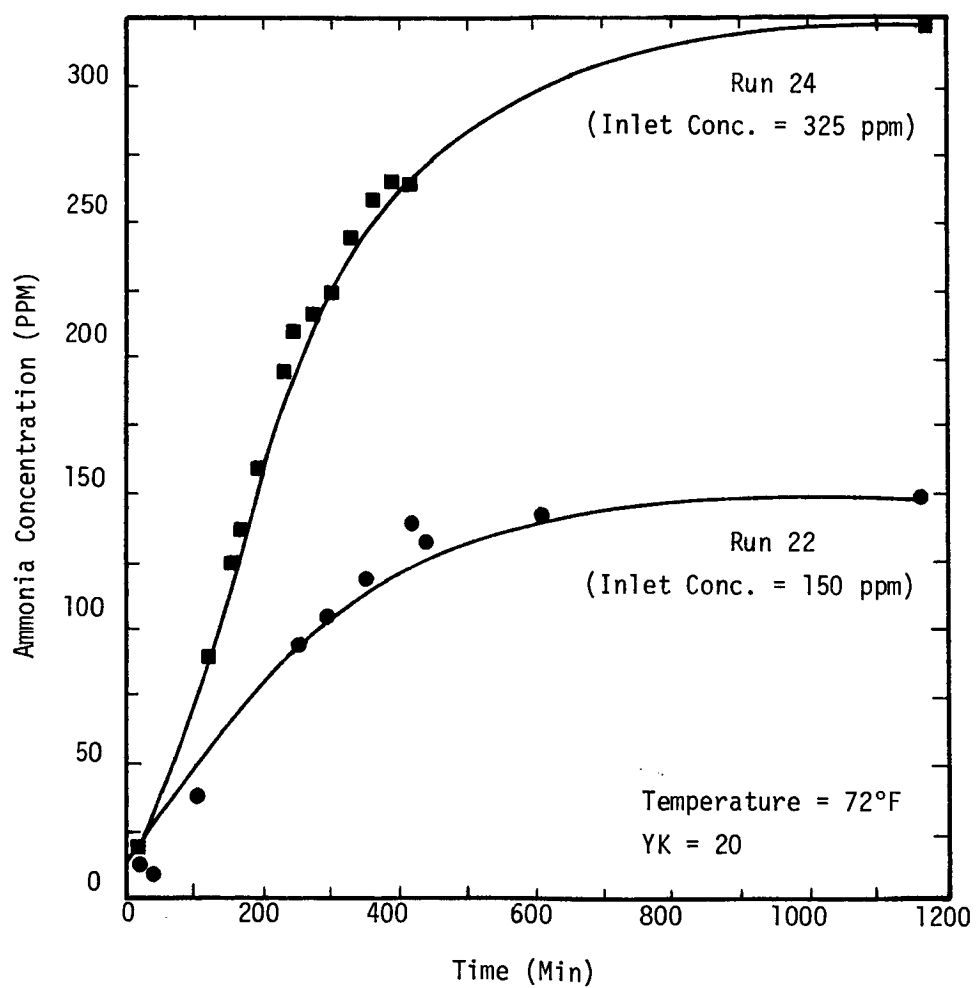
Concentration vs Time

Runs 21 and 26

Figure 6.10 - Plot of Ammonia Exit

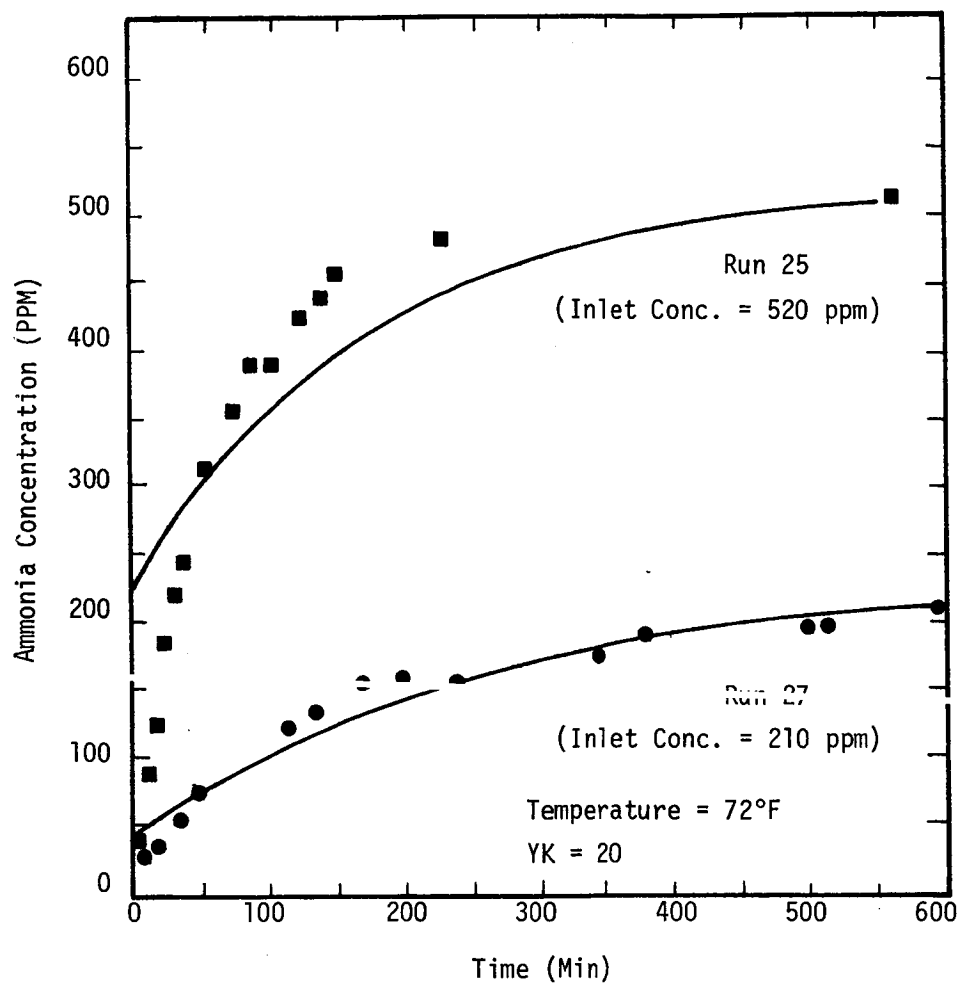Concentration vs Time

Runs 22 and 24

Figure 6.11 - Plot of Ammonia Exit
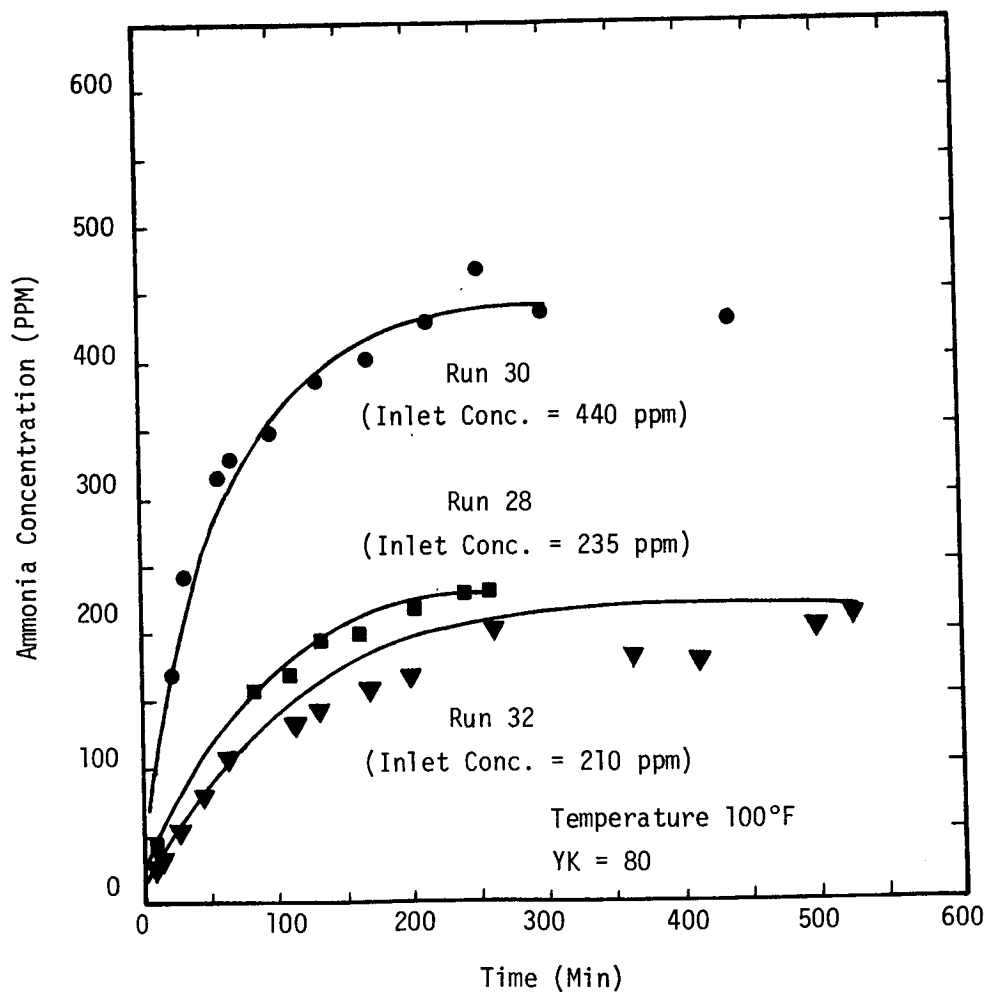
Concentration vs Time

Runs 25 and 27

Figure 6.12 - Plot of Ammonia Exit

Concentration vs Time

Runs 28, 30 and 32

From Figure 6.11, it can be seen that the observed adsorption rate for Run 25 is higher than the predicted rate. Aside from this, the predicted breakthrough curves have the same basis shape as those observed experimentally.

For all of the runs conducted at 72°F, a value of 20 lb/ft^3 hr for the constant YK produced an acceptable correspondence between the predicted and observed bed effluent concentration. At 100°F, the preferred value of YK changed to 80 lb/ft^3 hr.

Runs 29 and 31 were made at 100°F with Hambeads in the adsorber and no moisture in the gas stream fed to the bed. The best least squares value for YK in these two cases was 20 and 29, respectively, with 25 being a reasonable value to use in both cases. A comparison between the predicted and observed concentrations at the bed exit are given in Figure 6.13.

Only one run, number 35, was made at 72°F with a dry ammonia feed and Hambeads in the bed. There is considerable scatter in the experimental data which leads to an unusually high least squares value of 54 for YK. However, as Figure 6.14 indicates a YK value of 25 still provides a reasonable fit of the data.

Three runs were made at 72°F when the relative humidity of the feed to the bed of Hambeads was approximately 50%. These data and fitted curves are shown in Figures 6.13, 6.14, and 6.15. In one of these runs, number 37, there is a considerable amount of scatter in the experimental data which leads to an unusually high least squares value of 81. However, for the other two runs, the least squares value of YK is the same at 25. Even for Run 37, a YK value of 25 does a creditable job of describing the data. This is shown in Figure 6.15 where the experimental and computed profiles are compared.

All of this data suggests that a YK value of 20 to 25 would be a good design value when considering adsorbent beds of Hambeads or copper sulfate treated silica gel at a temperature of 72°F. This value is probably conservative when a moisture level of approximately 50% relative humidity is added to the stream.

6.5 Estimated Performance of an Adsorption System

The performance of any adsorption system will be strongly influenced by the nature of the adsorption isotherm for the material in the bed. In Figure 6.17 a comparison is made between the fitted euqations for all of the isotherms used in this study. As the data in the figure indicates, the copper sulfate treated sorbeads had the highest capacity at inlet gas concentrations greater than 30 parts per million. No speculations are made concerning the reason for this difference in capacity since no information concerning the preparation of Hambeads was available. The preparation of CSTS is discussed in section 7.0.

Figure 6.13 - Comparison of Computed and Observed
Ammonia Exit Concentrations for Dry
Hambeads at 100°F

104
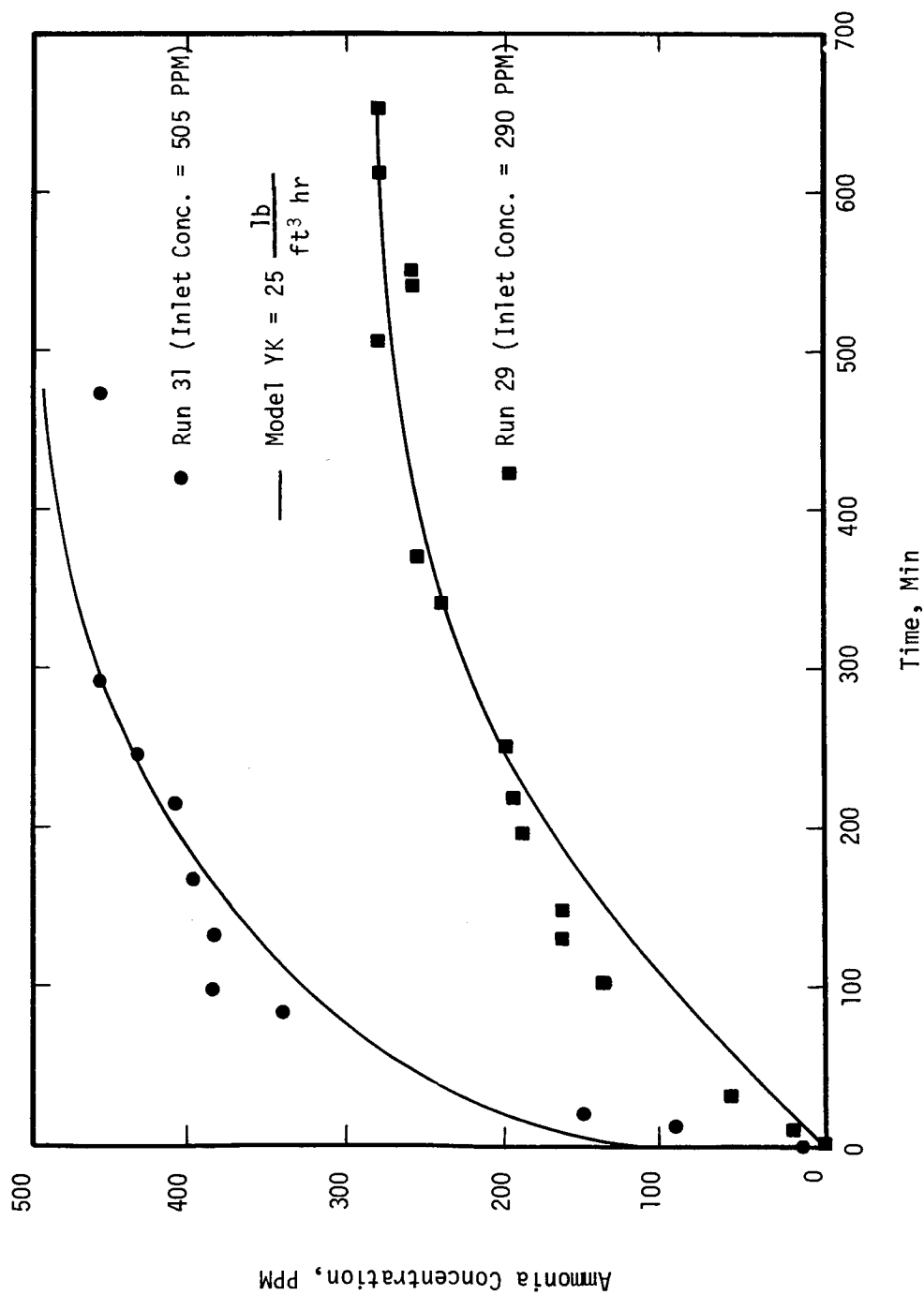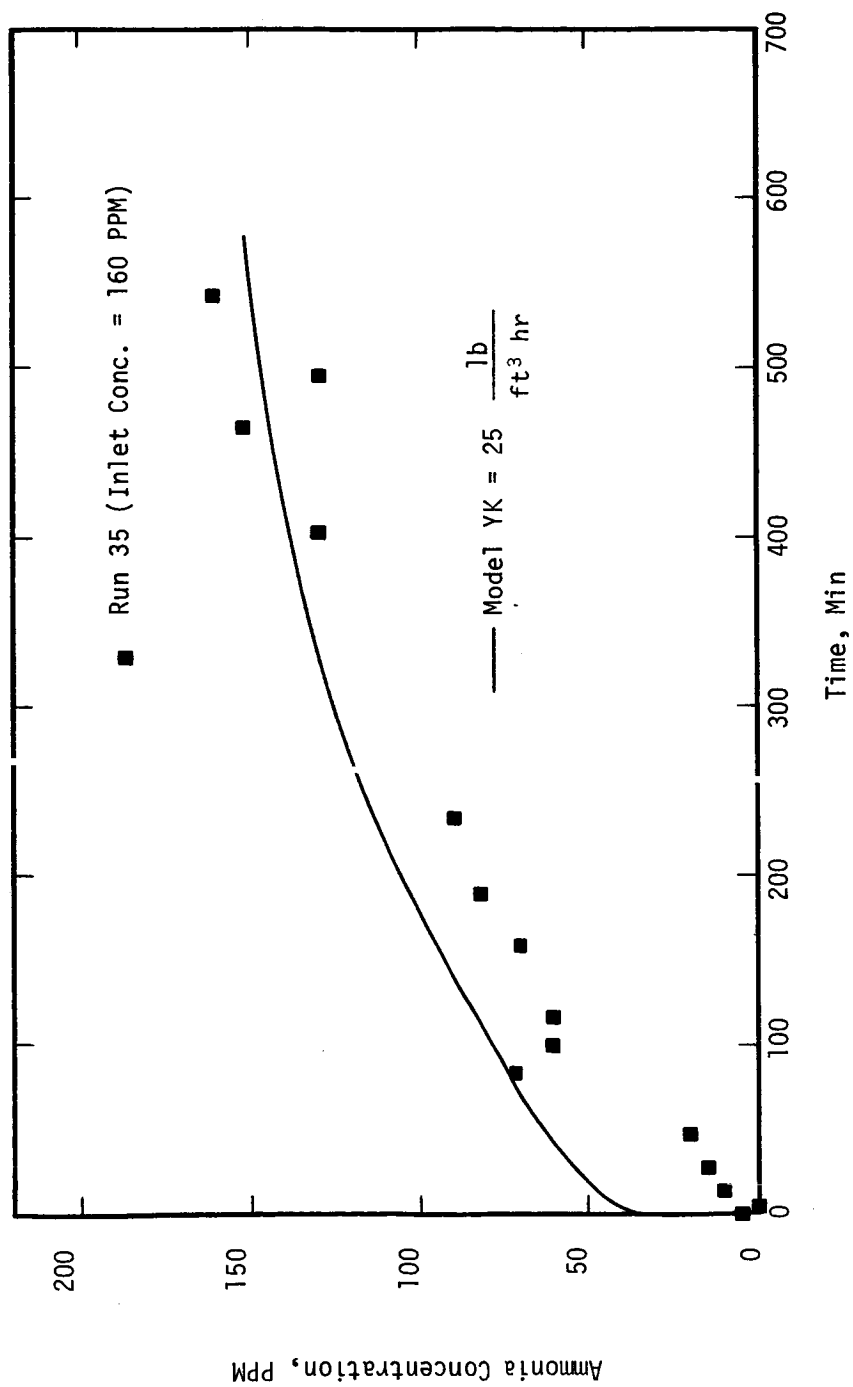
Figure 6.14 - Comparison of Computed and Observed
Effluent Concentrations for Dry
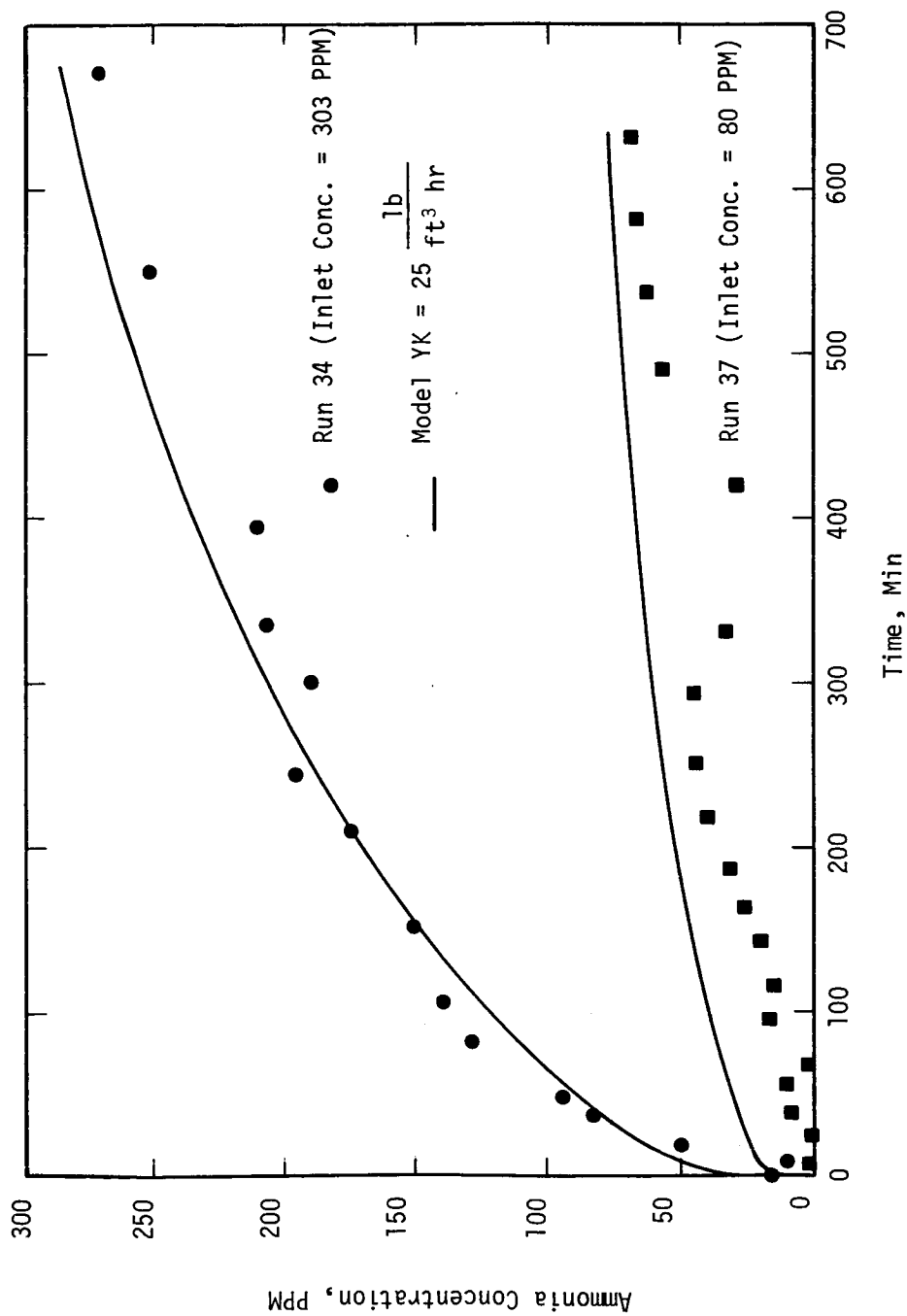Hambeads at 72°F

Figure 6.15 - Comparison of Computed and Observed
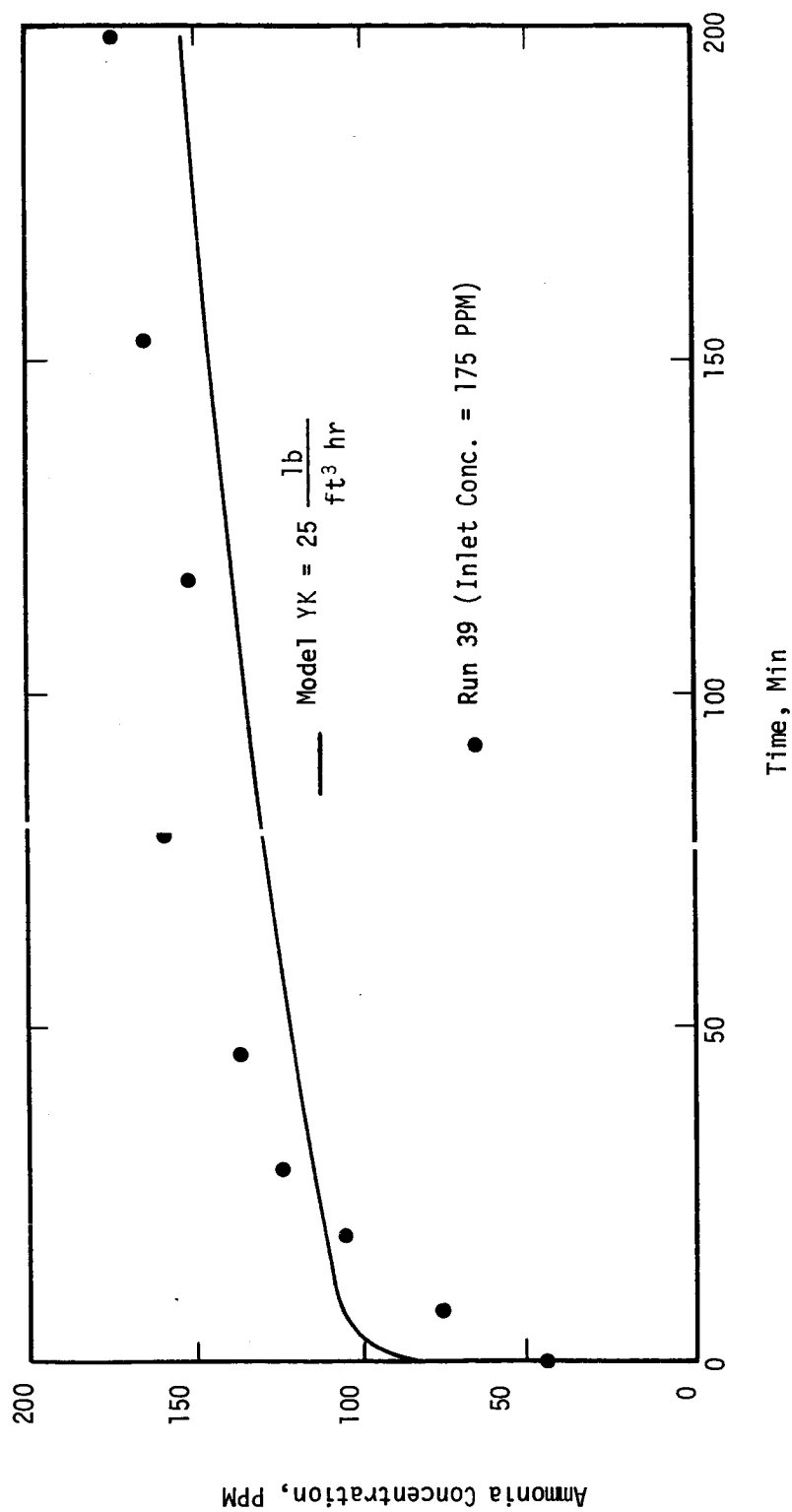Effluent Concentrations for Wet
Hambeads at 72°F

106

Figure 6.16 - Comparison of Computed and Observed
Effluent Concentrations for Wet
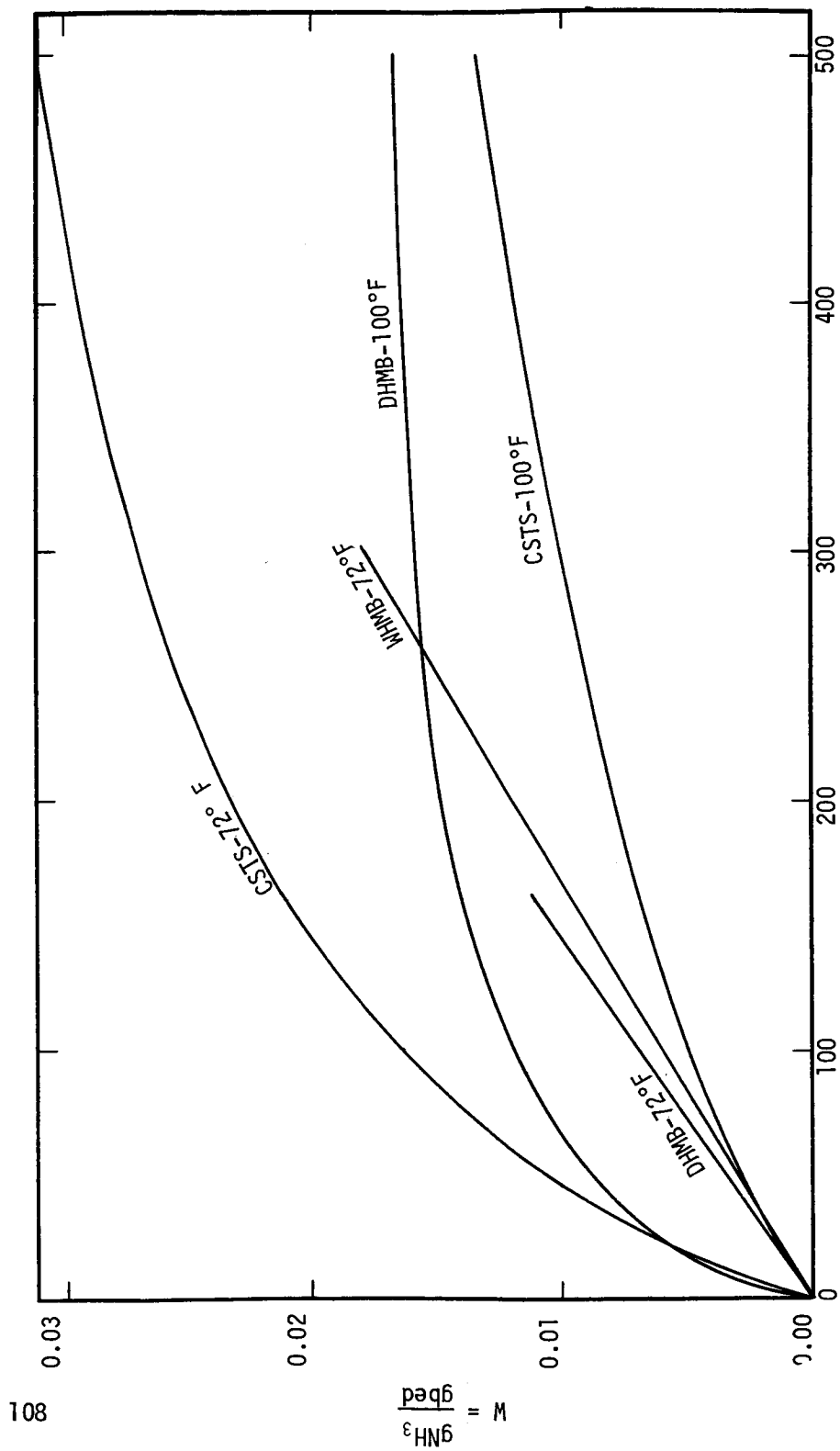llambeads at 72°F - Run 39

Figure .6.17 - Comparison Between the Fitted Isotherms

108

An estimate of the minimum amount of adsorbent that would be required to adsorb a particular load can be obtained using these curves. As an example, assume that a one pound per hour stream which contains 100 parts per million ammonia is to be passed through a bed of CSTS at 72°F. For one days operation:

$$\frac{1 \text{ lb}}{\text{hr}} \cdot \frac{24 \text{ hr}}{\text{day}} \cdot \frac{100 \times 10^{-6} \text{ lb NH}_3}{\text{lb air}} = \frac{2400 \times 10^{-6} \text{ lb NH}_3}{\text{day}}$$

The capacity of CSTS at 100 ppm and 72°F is 0.0161 lb NH_3/lb adsorbent. Multiplying these two numbers indicates that:

$$\frac{2400 \times 10^{-6} \text{ lb NH}_3}{\text{day}} \cdot \frac{\text{lb adsorbent}}{0.0161 \text{ lb NH}_3} = \frac{0.15 \text{ lb adsorbent}}{\text{day}}$$

At 100°F, the capacity of CSTS drops to 0.005 lb NH_3/lb adsorbent and therefore 0.48 pounds of adsorbent would be required as a minimum. Using a density of 51 lbs_m/ft^3 would allow the volume of these beds to be estimated.

The data concerned with the regeneration of CSTS indicate that, for one run at least, 80 percent of the fresh adsorbents capacity was regained upon regeneration at 383°F. This suggests the possibility of having two beds with a swing cycle or of having one large bed which is removed from service occasionally and regenerated. No attempt has been made to optimize the regeneration time or temperature. However exposure to the environment in outer space would probably result in drastic reductions in both time and temperature.

None of the adsorbents have the ideal shape for their breakthrough curves. If a perfect adsorbent could be ordered for this service, one would undoubtedly specify that the ammonia concentration in the effluent remain near zero until the entire bed was saturated. A review of the breakthrough curves for CSTS and Hambeads reveals that for the small beds used in this study, the effluent attains 50% of the influent concentration when approximately 20-25% of the time required to reach steady-state has passed. Neither sorbent appears to possess any significant advantage over the other relative to this desirable feature.

The shape of the breakthrough curve can be estimated using the surface adsorption limiting algorithm once an estimate for YK is available. As stated previously, a value of 20-25 would be a good design value when using Hambeads.

More data is available for copper sulfate treated sorbeads and so the variation of YK with temperature can be estimated. If this rate constant is assumed to follow an Arrhenius form in a manner similar to kinetic constants, an equation of the form:

$$YK = H' \, e^{-(E'/R_g T')}$$

would be in order. The values of YK = 20 at 72°F and YK = 80 at 100°F can be used to obtain the two constant H' and E':

$$H' = 2.2 \times 10^{13} \; lb/ft^3 \; hr$$

$$E' = 29,000 \; Btu/lb \; mole$$

Since data were collected at only two temperatures, the validity of these constants cannot be checked. However Daniels and Alberty (ref. 16) have considered similar reactions and obtained values of H' and E' of the same order of magnitude.

Due to the reduced capacity of the bed at the higher temperatures there is little incentive to raise the temperature above 72°F. This equation would be useful however in making estimates of minor changes around 72°F.

In summary, the isotherms provide a lower limit on the amount of material required while the small amount of regeneration data suggests the possibility of a significant retention of capacity upon regeneration.

110

7.0 EXPERIMENTAL SYSTEM FOR AMMONIA ADSORPTION

In order to measure the capacities of the adsorbents it was necessary to construct an experimental apparatus with which the concentration, flow rate, and temperature of the feed stream to the bed could be held constant. The effluent concentration was measured using the techniques discussed in section 8.0.

7.1 Description of the Adsorption Apparatus

The apparatus used in this study was simple in concept and design. The essential elements were a metered air supply, an air-ammonia mixing section, a fixed support for the adsorption bed and a thermostatic bath surrounding the adsorber.

Specifically (Figure 7.1), compressed air at 80 psig from the university air system was cleaned by passing it over a four to six mesh silica gel bed contained in a carbon steel holder. This holder had an inside diameter of approximately two inches and was about four inches long. Air saturated with water vapor at 80 psig is relatively dry (2200 ppm water) at the atmospheric pressure of the study so the main function of the silica gel was to remove dust, rust, and entrained oil. (Bimonthly changes of silica gel were made. At no time was more than the upstream half of the bed soiled). Air flow was maintained via a small air regulator upstream of the silica gel bed.

Air flow (0.16 - 0.20 ± 0.05 cfm) was measured by a calibrated mass flowmeter (Hastings Mass Flowmeter and Mass Flow Transducer by Hastings Raydist, Inc., Hampton, Virginia). This meter could be checked and adjusted for a zero flow easily, and the meter never required more than a ten percent adjustment due to instrument drift.

Air and ammonia were mixed in a tee (all tubing and fittings were 1/4 inch 316 stainless steel by Swagelok unless otherwise specified) approximately 13 linear feet from the adsorber. Prior to mixing, the ammonia was stored under pressure in an aluminum tank about two feet high with an inside diameter of nine inches. The transfer lines from this tank to the mixing tee were of glass, Teflon, and stainless steel. A 1/4 inch three way valve was provided just downstream of the mixing tee.

The fixed support for the adsorber was made of 21.5 - 22.0 mm inside diameter glass tubing, an aluminum adsorber support plate and Teflon packing under the support plate. An excellent glass on steel seal was provided by nominal one inch Teflon Swagelok ferrules at each end of the glass tube. Given a few minutes to "set", the seal showed no leaks at the pressure encountered in this study.

Thermostatic conditions were maintained in the adsorber by a constant temperature bath (Sargent Thermonitor Model ST by E. H. Sargent and Company
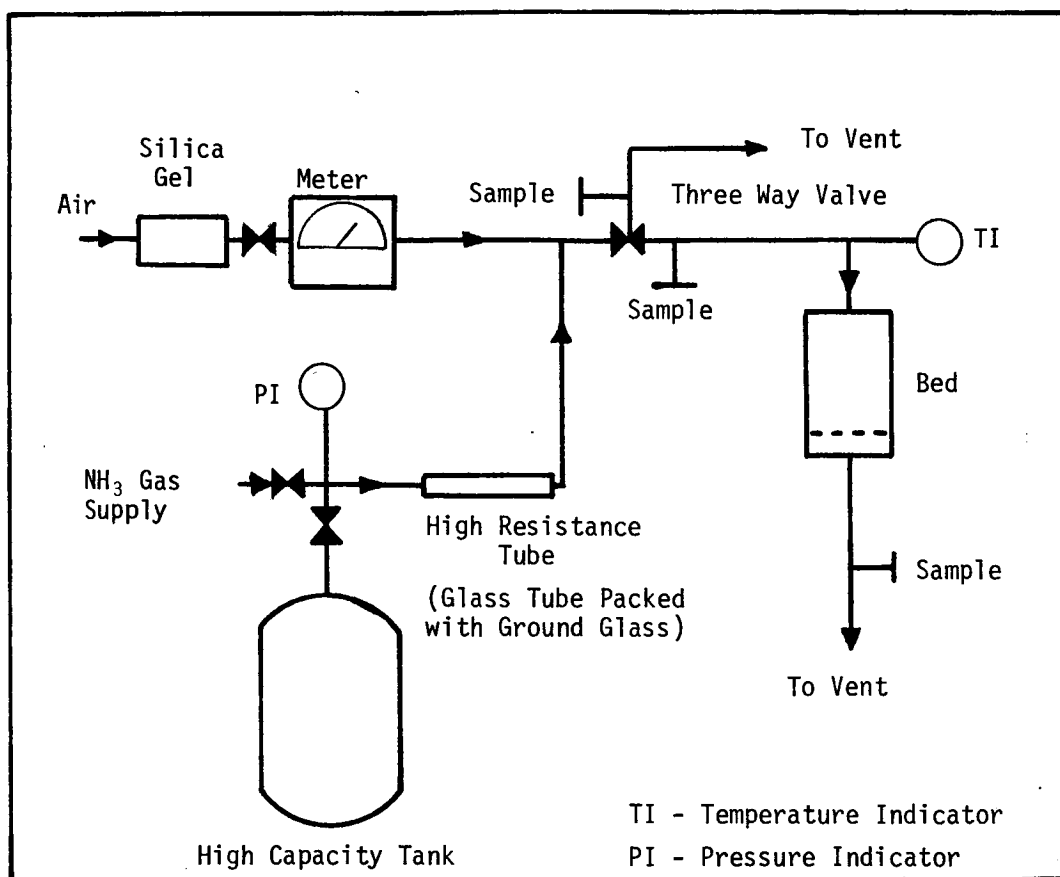
Figure 7.1 - Ammonia Adsorption Apparatus

and Heater and Circulator for Thermostatic Baths by Sargent-Welch Scientific Company). The bath was used only for the 100°F adsorption runs and the temperature control here was excellent with no noticeable variations. A coil of tubing was placed in the bath and upstream of the adsorber to insure that the bath temperature was the same as the air-ammonia temperature entering the adsorber.

Valves, pressure indicators (PI), thermometers (TI), and sample ports were located strategically throughout the process in order to maintain steady flows, and to monitor the temperature and ammonia concentrations into and out of the adsorber.

All materials used in this study were tested and found to be chemically inert to parts per million concentrations of ammonia. This was determined by passing a known parts per million concentration of ammonia through the empty system and ascertaining that the inlet and exit ammonia concentrations were the same.

7.2 System Flows

Compressed air from the air header flowed first through the regulator, through the silica gel bed, (Figure 7.1), then through the mass flowmeter, and finally to the air-ammonia mixing tee. From there the air-ammonia mixture went either to vent or through the adsorber bed depending on the position of the three way valve. This procedure allowed the concentration of the air-ammonia mixtures to be adjusted before starting an adsorption run.

7.3 Experimental Procedure

For at least 48 hours prior to making a run, the copper sulfate impregnated silica gel was preconditioned by putting it in the adsorber and flowing process air over it. This was done so that the silica gel was properly acclimated to the air and so that any observed changes during an adsorption run were solely due to the presence of the ammonia. Weight changes in the silica gel were under 0.02 grams for this preconditioning step.

Just prior to starting a run (after preconditioning) the air flow was diverted to the vent and the ammonia holding tank was pressurized using a lecture bottle of liquid ammonia. After the concentration of ammonia in the air-ammonia mixture had reached steady state in the vent line, this vent was sampled to determine the particular concentration. If the ammonia concentration was not acceptable for the particular run, ammonia vapor was bled from or added to the holding tank (thereby lowering or raising the holding tank's pressure). If the ammonia concentration was acceptable, the flow was directed into the adsorber, the timer was started, and a sample of the effluent from the adsorber was taken.

Samples of adsorber exit and inlet gas flows were taken (in the ratio of four or five to one) on a rapid basis at the start of a run. As the bed

became saturated with ammonia, the rate of change of exit concentration with time decreased and samples were taken less frequently.

System variables, such as air flow and bath temperature, were monitored and recorded approximately every 60 minutes. A given run was considered over when the exit concentration approached within ten parts per million of the inlet as this was considered to be within the accuracy of the analysis.

After a run was completed, the adsorbent bed was removed, weighed, and stored. The empty system was then flushed with pure air for at least one hour to desorb ammonia from the system and thereby to start the next run with an ammonia free system.

Samples at the bed entrance and at the exit from the adsorber were analyzed for ammonia using Nessler's Reagent. Samples were removed by gas syringe through silicone rubber septa. The details of this test are given in section 8.0.

A periodic check of the entire gas stream was made using a Varian Aerograph gas chromatograph equipped with a column packed with approximately nine feet of Porapak Q packing. This chromatographic check was made to determine if any oxides of nitrogen were being formed in the adsorber bed.

7.4 Preparation of Copper Sulfate Treated Silica Gel

Silica gel in the form of Mobil Oil Company's Sorbead R was treated with an aqueous solution of copper sulfate, allowed to come to equilibrium with the solution, and then dried in an oven. Specifically, the procedure was as follows:

> 100 grams of $CuSO_4 \cdot 5H_2O$ (from batch 34385 of J. T. Baker Company) were dissolved in 200 milliliters of distilled water to give an unsaturated solution of copper sulfate in water (some heating required). About 200 milliliters of Mobil Sorbead R was added to the solution. About four hours, with stirring, was allowed for the system to come to equilibrium. The Sorbeads-copper sulfate solution was then vacuum filtered and dried in an oven at 350-450°F. Finally the beads were crushed to the 14 to 16 mesh size used in the study.

Untreated Mobil Sorbead R is the characteristic off-white of silica gel. The treated beads took on a light green hue.

114

8.0   CHEMICAL ANALYSIS METHODS

This study of the removal of ammonia required chemical analysis techniques for the quantitative measurement of ammonia, nitrogen dioxide, and nitrous oxide in the range from about 5 ppm to 500 ppm in a background of humidifed air. In order to be most useful the methods needed to be accurate, simple, rapid, harmless, and inexpensive. The gas sample size available for analysis was generally not more than about 100 cc at ambient temperature and pressure. After considerable investigation, the analysis methods chosen were colorimetric in the cases of ammonia and nitrogen dioxide, and chromatographic for nitrous oxide.

8.1   Ammonia Analysis

A relatively extensive effort was made in the early stages in this investigation to develop a reliable analysis for ammonia using a helium ionization gas chromatograph (Varian model 1532-B). This work is summarized in the following section. The ammonia analysis method finally chosen was a colorimetric technique using Nessler's reagent. A description of the method is given in Section 8.1.2.

8.1.1 Chromatographic Ammonia Analysis. - Many different schemes for the chromatographic analysis of ammonia were tried during the course of the project. Ammonia peaks under all conditions had extremely long retention times and tailed very badly. Summarized below are the columns and conditions that were investigated.

Support	Dimensions	Temp. Range	Column Const.
Porapak Q	1/8" x 20'	Ambient to 150°	SS
Porapak Q	1/8" x 10'	Ambient to 150°	SS
Porapak R	1/8" x 15'	Ambient to 150°	SS
Chromo 104	1/8" x 15'	Ambient to 150°	Teflon Lined Aluminum
Porapak Q	1/8" x 12'	Ambient to 150°	Teflon Tubing Encased in SS Shield

The shape of the ammonia peak is indicative of physical adsorption of ammonia on the column and chromatographic hardware. This is further strengthened by the fact that a five foot length of unpacked tubing for a column gave identically shaped peaks. In order to minimize the adsorption of ammonia on the chromatograph hardware approximately 50% of the tubing and fittings which are outside the oven were wound with electrical resistance wire and heated to 120°C. This also had little effect on the ammonia peak shape.

Effort was also directed toward using a very short column. This would allow everything but ammonia to pass through the column quickly as well as minimize the column surface area. This effort did not significantly improve the ammonia peak shape. Further attempts to improve the ammonia peak shape were to inject directly into the column and to use Teflon coated tubing. Neither of these methods have proved satisfactory.

8.1.2 Colorimetric Ammonia Analysis and Calibration. - Gas samples in this investigation were analyzed for ammonia colorimetrically using Nessler's reagent in a technique similar to that described in Standard Methods (ref. 17). The method consists of contacting water containing absorbed ammonia with Nessler's reagent and reading the transmittance of the resulting yellow-brown solution against an appropriate blank on a colorimeter. The intensity of the color change which occurs is proportional to the ammonia concentration.

The step by step analytical procedure is as follows:

1. 50 cc polypropylene syringe is loaded with 2 cc of distilled and deionized water.

2. The water is contacted with sample gas by drawing 48 cc of gas into the syringe, being careful to let the gas bubble through the water. The syringe is shaken for approximately one minute to promote ammonia absorption.

3. The contents of the syringe are transferred to a cuvette and 1 cc of Betz Nessler reagent No. 246 which has been diluted 5 to 1 with distilled water is added.

4. After allowing approximately ten minutes for color development, the sample is read on a Bausch and Lomb Spectronic 20 colorimeter at 420 mμ against a blank containing 2 cc of distilled water and 1 cc of diluted Nessler reagent. The sample cuvette and the blank cuvette are chosen such that they yield the same transmittance values when filled with distilled water.

Approximately midway through the experimentation it was found advantageous to modify the syringe sampling technique by loading the syringe with 3 cc of water instead of two and drawing two 47 cc gas volumes instead of one

116

48 cc volume. For this case the blank consisted of 1 cc of diluted Nessler reagent and 2 cc of distilled water. The new procedure had the effect of decreasing the deviation in percent transmittance readings between samples. With modified sampling procedure a standard deviation of 3.4 ppm was calculated at 121 ppm versus 5.1 ppm at 135 ppm for the original procedure. Since there was no interaction between precision and concentration, these numbers seem to indicate an increased precision for the modified procedure. Three determinations were made of each gas stream sampled.

In order to have a quantitative analysis it was necessary to obtain a calibration curve which relates ammonia concentration to percent transmittance. This was done by preparing known concentrations of ammonia in air and establishing the percent transmittance associated with each concentration. Known ammonia concentrations were prepared by passing measured amounts of air over a liquid ammonia filled Teflon permeation tube in the apparatus diagrammed in Figure 8.1. The permeation tube, when held at constant temperature, lost weight linearly with time and thus allowed one to know the exact concentration of ammonia when the air flow rate was known. The permeation tube weight loss was determined by periodic removal from the apparatus and weighing.

The apparatus in Figure 8.1 was operated by passing air from a compressed air cylinder through a coil in a constant temperature bath, over the ammonia filled permeation tube and through a calibrated wet test meter. The permeation tube was held at constant temperature in a jacketed glass housing. Water from a constant temperature bath was circulated through the housing via a positive displacement pump.

From the above calibration procedure it was possible to prepare the calibration curves of Figure 8.2. The upper line of Figure 8.2 was obtained using 2 cc of water in the syringe and one 48 cc gas draw, while the lower line was obtained with 3 cc of water in the syringe and two 47 cc gas draws. The linearity of both lines shows that Beer's law is obeyed in the concentration range investigated.

The only interference problem encountered with the Nessler reagent was that aldehydes cause the solution to be clouded and give false reading. Careful attention to the purity of the water used in preparing reagents and avoidance of aldehydes around the analysis area prevented interference.

8.2 Nitrogen Dioxide Analysis

The analysis of NO_2 was performed in a manner similar to the ammonia analysis. Sample analysis was performed colorimetrically using the modified Saltzman reagent (ref. 18) and the syringe method of Meador and Bethea (ref. 19).

The analysis is performed by loading 5 cc of Saltzman reagent into a 50 cc polypropylene syringe and withdrawing 45 cc of gas sample. The syringe is shaken vigorously for approximately three minutes after which
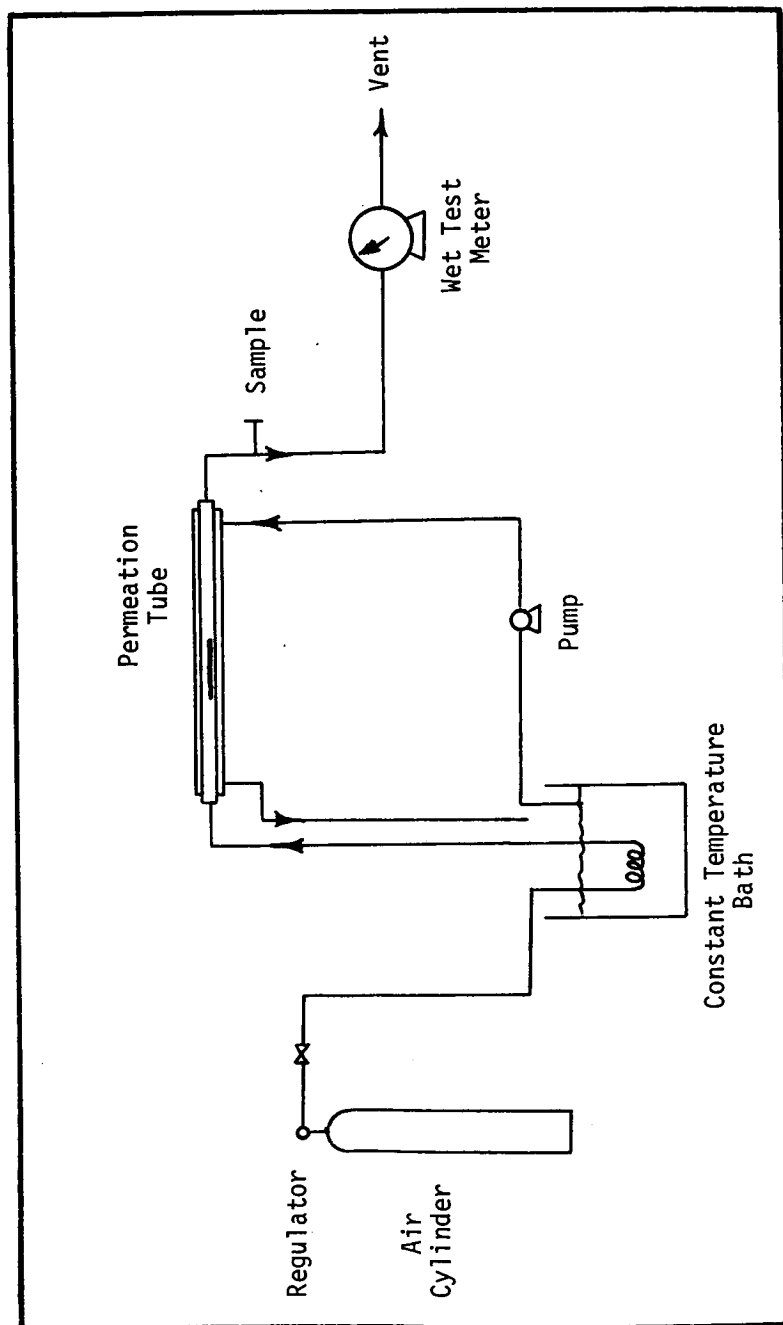
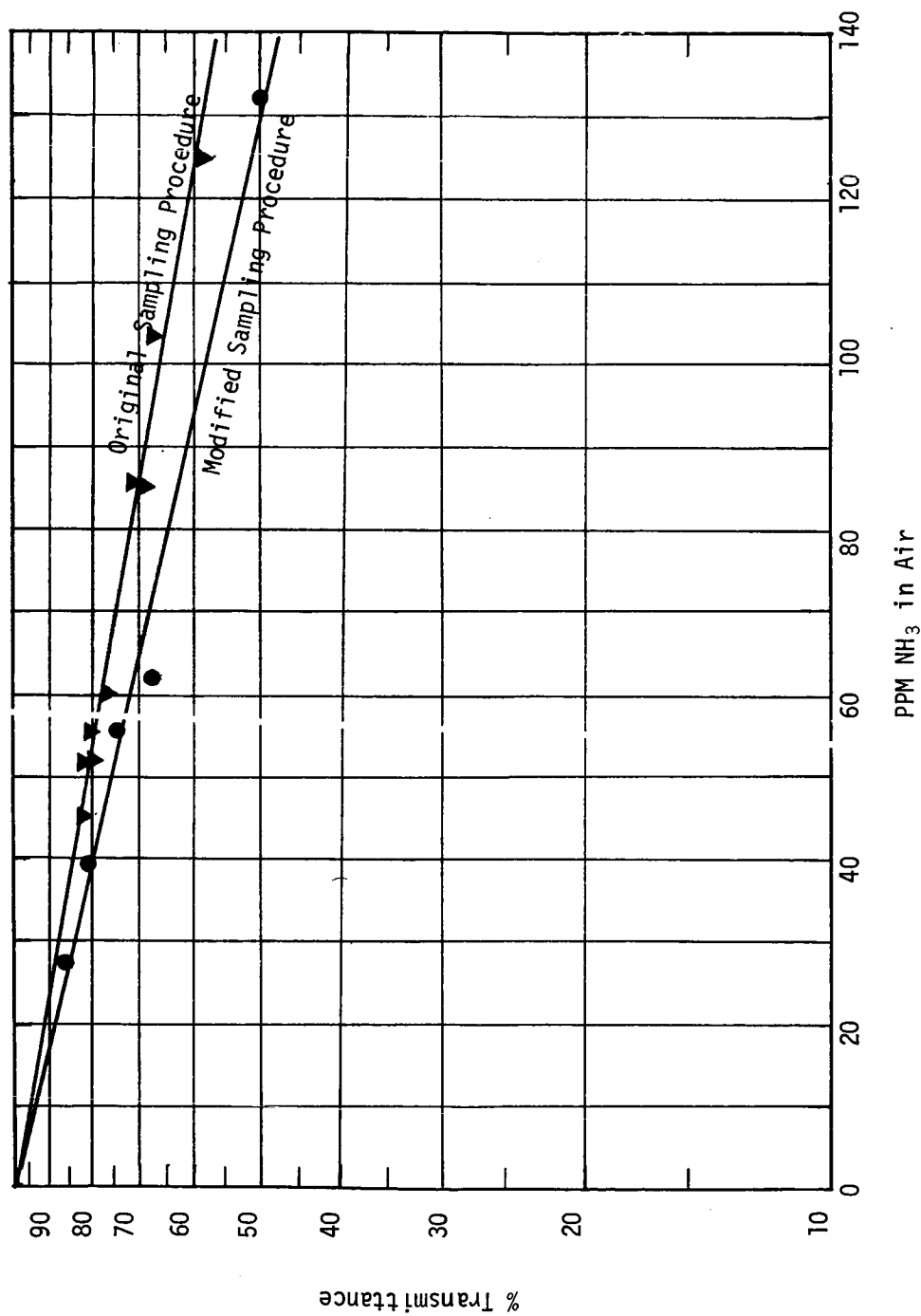Figure 8.1 - Calibration Apparatus
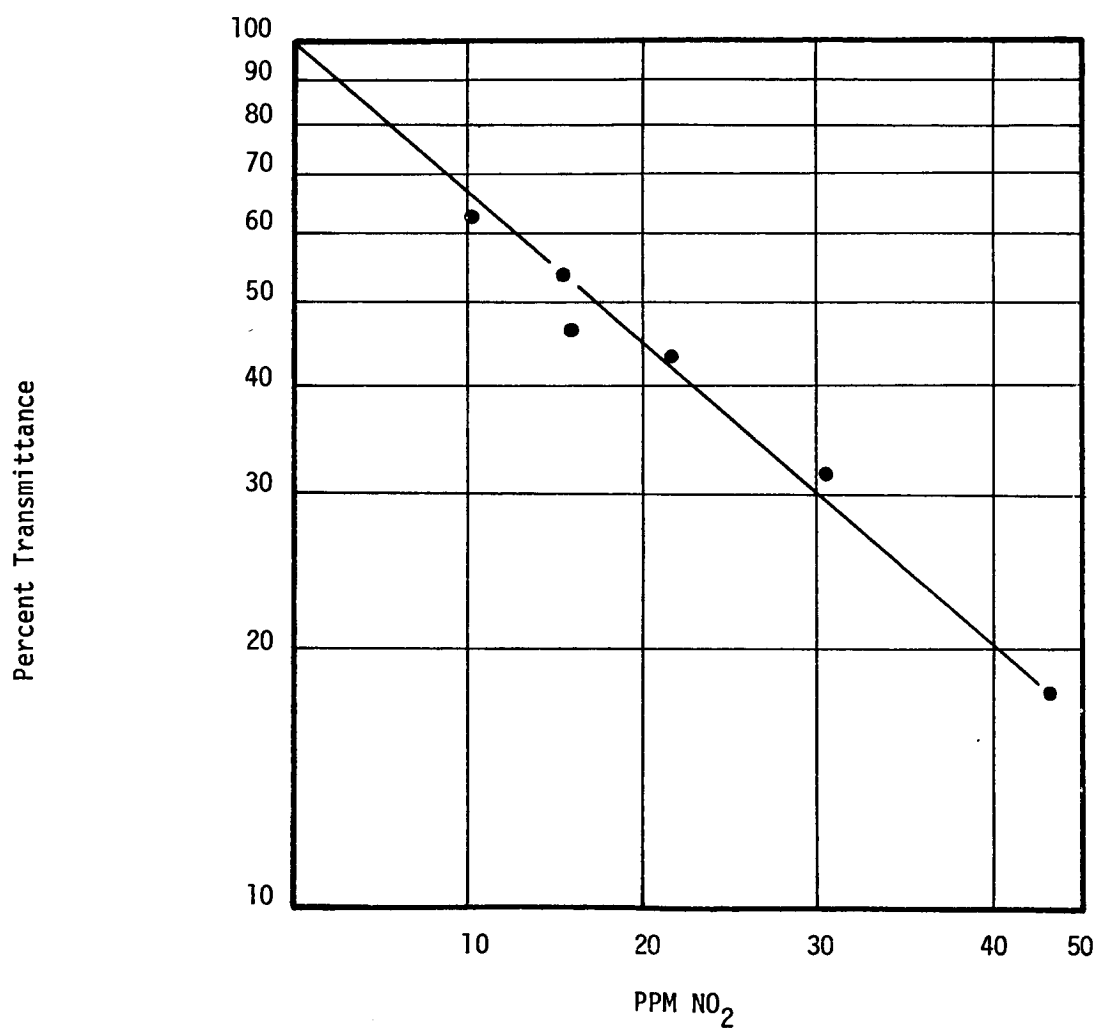
Figure 8.2 - Nessler Method Ammonia Calibration Curve

Figure 8.3 - Saltzman Calibration Curve

time a magenta color completely developed. The contents of the syringe
are emptied into a cuvette and read on the Bausch and Lomb Spectronic
20 colorimeter at 550 mμ against a blank consisting of 5 cc of undeveloped
Saltzman reagent. Using this technique Meador and Bethea (ref.19) report a
relative error of 0.43% at 41.3 ppm, 1.03% at 26.3 ppm, 2.83% at 9.8 ppm,
1.77% at 5.7 ppm, and 2.29% at 2.6 ppm.

Calibration of the Saltzman reagent for NO_2 analysis was done in the
same manner as for the ammonia analysis. Known concentrations of NO_2 in
air were prepared by passing air from a compressed air cylinder over a
Teflon permeation tube filled with liquid NO_2. The apparatus diagrammed
in Figure 8.1 was used for this purpose, as it was in the ammonia cali-
bration work. A typical NO_2 calibration curve is shown in Figure 8.3.

The Saltzman reagent was prepared by mixing the following chemicals
with enough distilled and deionized water to make a one liter solution:

    0.050 g N (1-napthyl) ethylene-diamine dihydrochloride
    0.050 g 2-napthol 3,6 disulfonic acid disodium salt
    1.500 g sulfanilamide
    15.0 g tartaric acid.

8.3   Nitrous Oxide Calibration and Analysis

Nitrous oxide was analyzed chromatographically using a Varian model
1532-B trace gas analyzer employing helium ionization detector. The
following is a listing of the pertinent chromatograph operating condi-
tions which were used:

                 packing material........Porapak Q
                 column length...........20 ft
                 column temperature......35°C
                 detector temperature....100°C
                 detector voltage........360 V
                 helium flow rate........1 cc/sec

Because the sensitivity of the helium ionization detectors decayed
with time, it was necessary to calibrate the chromatograph daily. This
was easily done with two prepared sample cylinders purchased from the
Matheson Company containing 33 ppm and 103 ppm N_2O in air. Approximate-
ly four each of these samples were injected daily to provide calibration
peak heights. Nitrous oxide peak heights from reactor gas samples were
then referred to these standard peak heights in order to determine N_2O
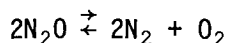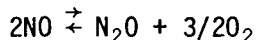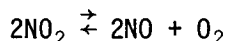concentration.

A standard deviation of 0.59 ppm at 33 ppm was calculated from
typical calibration data.

9.0 NITROGEN OXIDES REDUCTION

The reduction of nitrogen oxides in the presence of excess oxygen has been studied to a considerable extent. Wikstrom and Nobe (ref. 20) studied the decomposition of NO_2 over CuO-alumina and a CeO_2-alumina catalyst and found that even in the presence of oxygen a 45% conversion of 968°F (520°C) could be obtained using the CuO-alumina catalyst. Bachman and Taylor (ref. 21) and Sakaida, et al. (ref. 22) investigated the high temperature (above 1000°C) decomposition of NO on platinum, nickel oxide, and platinum oxide catalysts. Both invesgigators found the reaction to be retarded by the presence of oxygen. Fraser and Daniels (ref. 23) investigated the decomposition of NO over various oxide catalyst at temperatures from 740°C to 1040°C. They found the reaction was zero order on all catalysts studied and was very slow at temperatures below 800°C. Tamaka and Ozaki (ref. 24) along with Winter (ref. 25) have investigated the decomposition of pure N_2O over oxide catalysts in the temperature range of 400°C to 650°C. Both investigations found the reaction to be first order with respect to N_2O and to be retarded by the presence of oxygen. Amphlett (ref. 26) studied the decomposition of N_2O in an excess of oxygen and obtained a conversion of 81% at 500°C using a supported copper oxide catalyst. Sterbis (ref. 27) studied the decomposition of pure N_2O on nickel oxide over the temperature range of 300°C to 400°C and found the rate was severely reduced by the presence of oxygen.

All of the work in the literature indicates that for the catalytic materials known, the reduction of the oxides of nitrogen (N_2O, NO, and NO_2) in the presence of oxygen is extremely slow at temperatures below about 500°C-600°C (932°F-1112°F). At these high temperatures the energy requirements for a spacecabin application would be very high.

The set or reactions by which the removal of the nitrogen oxides might proceed is as follows:

$$2NO_2 \overset{\rightarrow}{\leftarrow} 2NO + O_2$$

$$2NO \overset{\rightarrow}{\leftarrow} N_2O + 3/2O_2$$

$$2N_2O \overset{\rightarrow}{\leftarrow} 2N_2 + O_2$$

From a theoretical viewpoint, the oxides could be reduced to the thermodynamic equilibrium concentration which, since all of the reactions are endothermic, decreases with decreasing temperature. Using calculated equilibrium constants and an atmosphere with an oxygen partial pressure of 0.2 atm and a nitrogen partial pressure of 0.48 atm, equilibrium concentrations of the oxides were calculated. In order to reduce the NO_2 concentration to 0.2 ppm, the catalyst would have to be active at a temperature of 370°C (700°F) or less. The equilibrium concentration of NO is less than that of NO_2 for temperatures below 430°C (800°F). The equilibrium concentration of N_2O is

extremely low, being less than 10^{-5} ppm at 400°C. From the thermodynamic calculations it becomes clear that the catalytic removal of nitrogen dioxide down to fractional ppm levels without a reducing reactant puts rather severe activity requirements on the catalyst since it must promote the reduction reaction at a relatively low temperature. Unfortunately no catalysts are known or were found which are active at temperatures below about 500°C.

In order to clarify the behavior of nitrous oxide in the presence of the ruthenium catalyst at the temperatures expected in a catalytic oxidizer, N_2O was substituted for ammonia at approximately 100 ppm in the reactor inlet. At temperatures below 650°F no reaction was detected. Taking into account the accuracy of the chromatographic analysis, the N_2O disappearance rate could not have been higher than 2.6×10^{-6} gmole $N_2O/hr/g$ cat. This rate is not high enough to account for either the NO_2 or N_2 which was produced in the ammonia oxidation, indicating that N_2O is not a precursor for NO_2 or N_2. This finding is in agreement with Schriber's (ref. 5) conclusion that N_2O is not reduced to nitrogen at the temperatures investigated. Thus the N_2O which is formed at these temperatures can be expected to be inert with respect to the ruthenium catalyst.

From the investigations made it appears that the best policy to follow for nitrogen oxides control is:

1. Carefully avoid the formation of these oxides from ammonia oxidation by passing all ammonia containing streams through an ammonia oxidizer filled with supported ruthenium catalyst. This oxidizer should be operated at the minimum acceptable temperature which will probably be about 250°F but definitely should not be operated above 350°F.

2. Nitrogen dioxide can be adsorbed on activated carbon with some success.

3. Nitric oxide is rather rapidly oxidized to nitrogen dioxide at room temperature and thus should not itself be a problem.

4. If nitrous oxide formation cannot be avoided, then the only known method for its removal in the presence of oxygen is reduction at a temperature of about 500°C using either supported copper oxide or nickel oxide.

10.0 OXIDATION OF AMMONIA IN A STEAM BACKGROUND

A preliminary investigation was made into the feasibility of carrying out the oxidation of small concentrations of ammonia in a stream consisting mostly of steam. The reactor assembly shown in Figure 10.1 was used in this investigation. An ammonia water solution was prepared which contained 12 to 20 ppm by weight of ammonia. This stream was passed through a vaporizer coil and then mixed with air or oxygen, both were used in different phases of the investigation. The steam-air-ammonia stream then passed through a second preheater coil and through the fixed bed reactor. After passing through the reactor, the steam was condensed and cooled to ambient temperature. During the condensation any ammonia present is absorbed back into the water stream. Several analysis of the gas stream from the condenser failed to show any ammonia in the gas stream. (Detection limit about 1 ppm of gas by volume). The reactor was always operated at atmospheric pressure.

The catalysts shown in Table 10.1 were investigated for their ammonia oxidation efficiency at temperatures up to 200°C. By far the best catalyst of those investigated was the 0.5% platinum on alumina. At the temperatures used (140°C to 200°C) the platinum exhibited approximately twice the activity of the next best catalyst which was a 0.5% palladium on alumina. Both of these catalysts showed a tendency to lose activity with use. It is not clear what the mechanism for the catalyst deactivation was. The water used in feed preparation was distilled and deionized and thus should contain no halogens, heavy metals, or sulfur compounds. There is a strong possibility that the water caused a phase change in the alumina support thus altering the surface area. Drying the catalyst at 200°C did not appear to restore any of the lost activity.

The oxygen partial pressure did not appear to influence the reaction rate in the range from 0.5 atm down to 0.05 atm.

An extended run was made using a 25 gm charge of 0.5% platinum on alumina (Engelhard Industries). The feed to the reactor was a 14 ppm solution of ammonia in distilled water and a oxygen flow of 500 standard cc/min. The temperature was 146°C (295°F). Under this condition with a ammonia-water flow rate of 5.8 ml/min. approximately 97% of the ammonia was oxidized to nitrogen and water with no significant formation of nitrate.

After having processed 13 liters (520 ml solution/gm cat.) of ammonia-water solution, the catalyst was oxidizing approximately 94% of the ammonia. Therefore the catalyst was losing its activity at a very low rate. The effect of impurities in the feed was not determined. The activity at higher temperatures was not determined since when the temperature was increased above 150°C the ammonia was essentially 100% oxidized.

Although the investigation was preliminary it does indicate that ammonia removal from a steam background is feasible. Catalysts supported on non-alumina

124
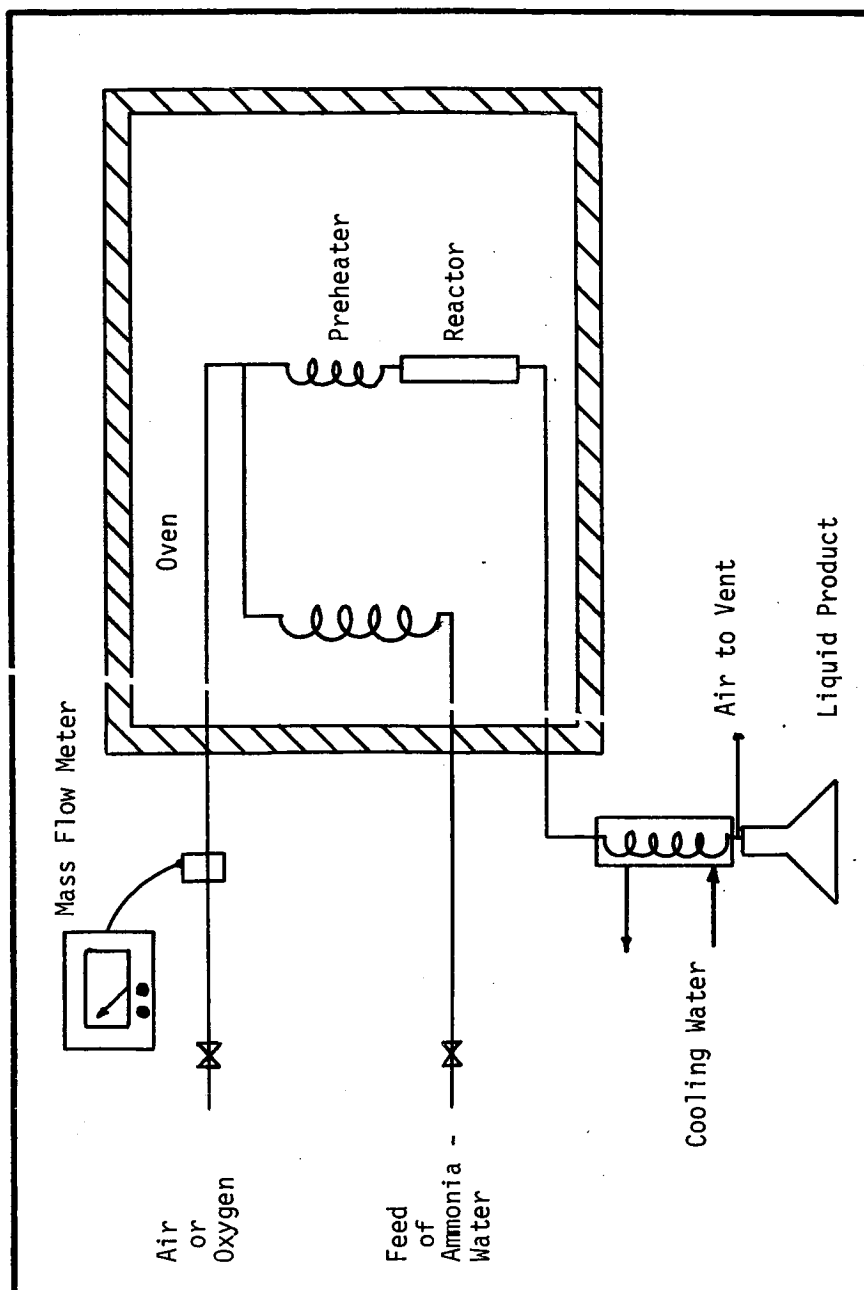
Figure 10.1 - Appara:tus for Investigation of Ammonia Oxida:ion in a Steam Background

125

TABLE 10.1

LIST OF CATALYSTS TESTED FOR ACTIVITY IN THE OXIDATION

OF AMMONIA IN A HIGH WATER BACKGROUND

CATALYST	MANUFACTURER	SURFACE AREA m^2/g
1. 0.5% ruthenium on alumina	Engelhard Industries	74
2. 0.5% platinum on alumina	Engelhard Industries	93
3. 0.5% palladium on alumina	Engelhard Industries	unknown
4. 4% nickel oxide, 4% iron oxide, 4% cobalt oxide supported on alumina	Harshaw Chemical	78
5. 10% vanadium pentaoxide on alumina	Harshaw Chemical	115
6. 4% manganese dioxide on silica	Harshaw Chemical	258

126

materials should be invesitgated since it is probable that the deactivation experienced may have been due to the support. The deactivation was not so severe as to make the process unusable however. Higher temperatures could be investigated to determine if undesirable products are produced. Also the effect of impurities in the feed water should be determined.

11.0 CONCLUSIONS

1. Ammonia in small concentrations (less than 300 ppm) can be oxidized to nitrogen and water with essentially no nitrogen oxide formation by using a supported ruthenium catalyst and carefully limiting the reactor temperature to 250°F or less. At reaction temperatures from 300°F to 400°F nitrous oxide is a product and at temperatures above 400°F nitrogen dioxide is also produced.

2. Other good catalysts for the reaction are platinum on alumina and Hopcalite. Both of these materials, however, tend to produce more oxides of nitrogen as products of the ammonia oxidation than does ruthenium.

3. Quantitative relationships for the ammonia oxidation rate as a function of temperature and ammonia concentration are presented.

4. Ruthenium catalyst does not tend to be deactivated with use as one charge operated for over 1400 hours without a loss of activity. The reaction rate using ruthenium is not greatly affected by changes in humidity level and oxygen concentration. Exposure to hydrogen sulfide caused a loss of activity of about 50%.

5. No catalyst is known which will promote the reduction of nitrogen oxides in the presence of oxygen at temperatures below 800°F. Thus nitrogen oxide formation must be carefully avoided.

6. Ammonia in a background of mostly steam can be oxidized to nitrogen and water using supported platinum and temperatures of 250°F to 400°F. The reaction needs further investigation to determine the effect of impurities on reaction rate and catalyst stability.

7. At 72°F the equilibrium sorption capacity of copper sulfate treated sorbeads was significantly greater than that of Hambeads over the range of 0-500 parts per million ammonia in the bulk gas phase.

8. The equilibrium adsorption isotherms can be adequately modelled using an expression of the form proposed by Langmuir. These isotherms may also be used to estimate the minimum amount of material required to adsorb a given load.

9. The combination of an expression that assumed the surface adsorption was controlling with an overall material balance resulted in a mathematical model which adequately described the observed breakthrough curves. A least squares analysis was used to determine recommended design values of the rate constant.

10. One experimental run suggested the possibility of regeneration of copper sulfate treated sorbeads. Further work is needed to determine the performance of this material under extended cycling.

APPENDIX A

CATALYSTS DATA

A.1 Ruthenium Catalyst Data

Catalyst Manufacturer .... Engelhard Industries

Lot Number 16-988

Ruthenium Content 0.5%

Support Material .... Alumina

Catalyst Dimensions .... 1/8 in. X 1/8 in.

Surface Area .... 74 m^2/g

Catalyst External Area .... 10.7 cm^2/g

Apparent Bulk Density .... 60 lb/ft^3

Total Pore Volume .... 0.4 cm^3/g

A.2 Hopcalite Catalyst Data

Catalyst Manufacturer .... Mine Safety Appliances

Content .... Mixed Oxides of Copper and Maganese

Catalyst Dimension .... Irregularly Shaped Particles

Surface Area .... 156 m^2/g

External Area .... 12 cm^2/g (Approximate)

A.3 Platinum Catalyst Data

Catalyst Manufacturer .... Engelhard Industries

Lot Number 18,381

Platinum Content 0.5%

Support Material .... Alumina

Catalyst Dimensions .... 1/8 in. X 1/8 in.

Surface Area .... 97 m^2/g

Catalyst External Area .... 10.7 cm^2/g

Apparent Bulk Density .... 60 lb/ft^3

Pore Radius .... 25-35 angstroms

REFERENCES

1. Lockheed Missiles and Space Co.: "Design and Fabrication of a Trace Contaminant Removal System for Apollo," Prepared for NASA under Contract No. NAS 9-3415, (1966).

2. Zawadzki, J.: "The Mechanism of Ammonia Oxidation and Certain Analogous Reactions," Trans. Faraday Soc., $\underline{8}$: 140 (1950).

3. Griffiths, D. W. L., Hallam, H. E., Thomas, W. J.: "Infra-Red Study of Adsorption and Oxidation of Ammonia on Silica-Supported Platinum and Silica," Trans. Faraday Soc., $\underline{64}$: 3361-3369 (1968).

4. Amano, A. and Taylor H.: "The Decomposition of Ammonia on Ruthenium, Rhodium and Palladium Catalysts Supported on Alumina," J. Am. Chem. Soc., $\underline{76}$: 4201 (1954).

5. Schriber, T. J. and Parravano, G.: "The Low Temperature Oxidation of Ammonia Over a Supported Ruthenium Catalyst," Chem. Eng. Sci., $\underline{22}$: 1067-1078 (1967).

6. Giordano, N., et al: Journal of Catalysis, $\underline{5}$: 325-331 (1966).

7. Hougen, O.A. and Wilkie, C.: Trans. Am. Inst. Chem. Engrs., $\underline{45}$: 445 (1945).

8. Smith, J. M.: Chemical Engineering Kinetics, McGraw-Hill, New York (1956).

9. Satterfield, Charles N.: Mass Transfer in Heterogeneous Catalysis, M.I.T. Press, Cambridge (1970).

10. Thiele, E. W.: "Relationa Between Catalytic Activity and Size of Particle," Ind. Eng. Chem., $\underline{31}$: 916 (1939).

11. Johns, R. H.: "Kinetics and Catalyst Selection in the Combustion of Atmospheric Trace Contaminants," Chem. Engr. Prog. Symp., $\underline{62}$: 81-88 (1966).

12. Brunauer, S., Emmett, P. H., and Teller, E.: J. Am. Chem. Soc., $\underline{60}$: 309 (1938).

13. Antson and Dranoff: Chem. Eng. Prog. Symposium Series, $\underline{65}$: 96 (1969).

14. Dubinin, Jr.: Colloid and Interface Science, $\underline{23}$: 4 (1967).

15. Drew, T. B. and Hoopes, J. W., ed.: Advances in Chemical Engineering, Vol. II, Academic Press, New York (1958).

16. Daniels, F. and Alberty, R. A.: Physical Chemistry, John Wiley and Sons, New York (1962).

17. Standard Methods for The Examination of Water and Wastewater, 12 ed., p. 186, American Public Health Assoc., New York (1966).

18. Lyshkow, N. A.: "A Rapid and Sensitive Colorimetric Reagent for Nitrogen Dioxide in Air," J. Air Poll. Control Assoc., 15: 481 (1965).

19. Meador, M. C. and Bethea, R. M.: "Syringe Sampling Technique for Individual Colorimetric Analysis of Reactive Gases," Environ. Sci. Tech., 4: 853-855 (1970).

20. Wikstrom, L. T. and Kobe, K.: I&EC Process Design and Development, 4: 191 (1965).

21. Bachman, P. W. and Taylor, G. B.: J. Phys. Chem. 33: 447 (1929).

22. Sakaida, R. R., et al.: AIChE Journal, 7: 659 (1961).

23. Fraser, J. M. and Daniels, F.: J. Phys. Chem., 62: 212 (1958).

24. Tamaka, ken-Ichi and Ozaki, Atsumu: Journal of Catalysis, 8: 370-311 (1967).

25. Winter, E.: Journal of Catalysis, 15: 144 (1969).

26. Amphlett, C. B.: Trans. Faraday Soc., 50: 273 (1965).

27. Sterbis, E. E.: Unpublished M.S. Thesis, University of Colorado, Boulder (1966).

ADDENDUM

TO THE FINAL REPORT

THE CATALYTIC REMOVAL OF AMMONIA AND NITROGEN

OXIDES FROM SPACECABIN ATMOSPHERES

By A. J. Gully, R. R. Graham, J. E. Halligan,
and P. C. Bentsen

ABSTRACT

The adsorption of 100 to 500 ppm ammonia from dry air is investigated experimentally and mathematically. The adsorbent discussed is a copper sulfate treated commercial silica gel. The isotherm data is well represented by a Langmuir type equation. Using unsteady state material balances, a lumped type rate equation, and the Langmuir isotherm, the breakthrough curves are well fitted by adjusting the value of the one parameter in the model. A replacement reaction involving ammonia substitution for the water of hydration in copper sulfate is indicated.

Introduction

The removal of ammonia at concentrations of 500 ppm or lower from air is of interest for maintaining life supporting systems such as manned space vehicles as well as for the treatment of certain industrial vent streams. Several solid sorbents have been investigated for the removal of ammonia. These range from silica gel (1), to acid impregnated charcoal (2), to chemically treated glass (3). In our laboratory we investigated the removal of ammonia from essentially dry air at concentrations of 100 ppm to 520 ppm using a copper sulfate impregnated silica gel as the sorbent. Our objective in the investigation was to sufficiently correlate the experimental data for the system such that usable predictions of adsorber performance could be made. Since adsorbers are inherently operated as unsteady state devices, the describing equations for the system are partial differential equations in time and position.

Describing Equations

For a fixed bed adsorber, operating essentially isothermally, assuming plug flow through the adsorber, negligible pressure drop, constant velocity, and no radial gradients a material balance for the adsorbed component of interest yields equation (1).

$$-v \, \frac{\partial C}{\partial Z} = R + \epsilon_B \, \frac{\partial C}{\partial T} \tag{1}$$

where   C   =   gas phase adsorbate concentration mole/cm^3

      Z   =   bed position, cm

,T   =   time, min

v   =   superficial bed velocity cm/min

R   =   rate of adsorption, mole/cm^3/min

ε_B =   bed external void fraction.

A material balance for the adsorbate loading on the solid yields the defining equation for the rate of adsorption.

$$\rho_B \frac{\partial W}{\partial t} = R \qquad (2)$$

where ρ_B =   bulk density of the packed bed, g/cm^3

W   =   adsorbent loading, mole/g.

In a detailed, mechanistic analysis the rate of adsorption on the surface of the solid is no doubt an involved function of the fraction of the surface covered. At a given temperature and gas phase composition there is a fixed amount of adsorbate that can be held on the solid surface. It is reasonable, then, to say that one measure of the driving force for surface adsorption is the local displacement from equilibrium. The rate of adsorption can often vary with position within an individual adsorbent particle due to the existence of concentration gradients within a particle. However in this study the intent was to use as manageable a describing model as possible. The first attempt thus was to use a lumped type equation to describe the rate of adsorption. The rate equation used was

$$R = k (W_E - W) \qquad (3)$$

where   k   =   adsorption rate constant g/cm^3/min

W_E =   equilibrium loading, based on local gas phase adsorbate concentration, mole/g .

A4

Several models have been proposed to relate the equilibrium solid loading to the gas phase adsorbate concentration at constant temperature. Freundlich and Langmuir isotherm forms were considered for use in this work. The Langmuir form was found to yield a superior fit of the data and was used in the further analysis of the adsorber. Thus the equilibrium equation used was

$$W_E = \frac{aC}{1 + bC} \tag{4}$$

where a and b are temperature dependent constants.

For the work reported here the inlet concentration to the adsorber bed was stepped at time equal zero from a zero ammonia in air concentration to some preset constant concentration value. The adsorbent bed was in all cases but one an unexposed sample of copper sulfate treated silica gel. Thus the system initial and boundary conditions were

$$C(0,t) = C_{in} \tag{5}$$

$$C(Z,0) = 0 \tag{6}$$

$$W(Z,0) = 0 \quad . \tag{7}$$

The approach in this work was then to simulate the transient behavior of the adsorber using these seven equations which contain seven system constants. Values for all seven constants must be chosen a priori to a numeric solution of the equation set. A preferred approach might be to reformulate the problem such that the variables are dimensionless and such that a minimum number of parameters are involved in the problem solution.

The following changes of variables accomplish these objectives:

$$\hat{t} = tk/\rho_B \tag{8}$$

$$\hat{Z} = ZW_Fk/v/C_{in} \tag{9}$$

$$\hat{C} = C/C_{in} \tag{10}$$

$$\hat{W} = W/W_F \tag{11}$$

$$\hat{W}_E = W_E/W_F \quad . \tag{12}$$

After making the above substitutions the following two parameter equation set results:

$$- \frac{\partial \hat{C}}{\partial \hat{Z}} = \frac{\partial \hat{W}}{\partial \hat{t}} + \left(\frac{\varepsilon_B \, C_{in}}{\rho_B \, W_F}\right) \frac{\partial \hat{C}}{\partial \hat{t}} \tag{13}$$

$$\frac{\partial \hat{W}}{\partial \hat{t}} = \left[\frac{\hat{C}}{1 + bC_{in} \, \hat{C}}\right] - \hat{W} \tag{14}$$

$$\hat{C}(0,t) = 1 \tag{15}$$

$$\hat{C}(Z,0) = 0 \tag{16}$$

$$\hat{W}(Z,0) = 0 \quad . \tag{17}$$

For the physical system under consideration the last term in the gas phase material balance was found to be insignificant since

$$\beta = \frac{\epsilon_B \; C_{in}}{\rho_B \; W_F} = 10^{-6} \quad . \tag{18}$$

If the gas phase accumulation term is dropped the remaining equation set contains only one parameter, bC_{in}. For the special case where bC_{in} equal zero (a linear isotherm), the linear equation set can be Laplace transformed with respect to $\hat{t}$ and integrated with respect to $\hat{Z}$ to give the following equation in the Laplace domain:

$$L\hat{C} = \exp \left[-Z \left(\frac{s}{s+1}\right)\right]/s \quad . \tag{19}$$

By using the series expansion for the exponential

$$e^X = 1 + X + \frac{X^2}{2!} + \frac{X^3}{3!} + \text{etc.} \tag{20}$$

the following time domain solution for the linear case can be found

$$\hat{C} = 1 - \sum_{m=0}^{\infty} \sum_{n=1}^{\infty} \frac{(-1)^{n+1} \; Z^{n+m} \; t^m \; e^{-t}}{(m!)^2 \; (n-1)! \; (n+m)} \quad . \tag{21}$$

This analytic solution was utilized to help check the stability of the numerical solution program.

Adsorber Loading at Bed Inlet

The inlet of the adsorber is exposed to a constant gas phase ammonia concentration. Thus the loading as a function of time can be obtained analytically. At the inlet $\hat{W}_E$ equal one (note that this result is independent of isotherm form) thus

$$\frac{d\hat{W}}{dt} = 1 - \hat{W} \tag{22}$$

$$\hat{W}(\text{at } \hat{Z} = 0) = 1 - e^{-\hat{t}} \quad . \tag{23}$$

For an adsorber operated as described here, the bed loading is most rapid at the inlet, therefore any external mass transfer resistances would be most significant at the beginning of the cycle.

Numerical Solution Technique

Because of the non-linear nature of the problem, numerical solution techniques were used to solve the dimensionless equation set for various values of the parameters β and C_{in}. The approach used was to apply a Euler type finite difference equation to start the solution and then switch to second order finite difference formulae for the remainder of the calculations. For the relatively short beds and low concentrations used in this study, the gas phase accumulation term was found to be totally insignificant and was dropped.

Comparison with Experimental Data

The experimental data collected was in the form of concentration history (or breakthrough) curves. These curves are a plot of the bed exit

ammonia concentration as a function of run time. Calculated bed capacities were determined from the integrated average exit ammonia concentration. The isotherm data thus generated are shown in Figure 1 for the two temperatures investigated. The data are plotted a C vs C/W which for the Langmuir form should result in a linear relationship of intercept -1/b. In order to compare the experimental data to the numerical solution, the unknown system constant k had to be determined. Since for the particular dimensionless variables chosen both $\hat{t}$ and $\hat{Z}$ contain k, the numerical solution was utilized as a plot of $\hat{C}$ versus $\hat{t}/\hat{Z}$ with lines of constant $\hat{Z}$. Typical numerical solution results are shown in Figure 2. As may be seen from this figure, the solution is not greatly sensitive to changes in the parameter bC_{in} in the range from bC_{in} equal about 2 to bC_{in} equal about 4.

The central problem was to determine the value of k which would best represent the entire data set at each temperature. A crude estimate of k can be made using the initial breakthrough ammonia concentration. For the early minutes of the run, the bed loading is essentially zero for all lengths. Thus the material balance can be integrated assuming W = 0.

$$- \frac{\partial \hat{C}}{\partial \hat{Z}} = \hat{C} \left[\frac{1 + bC_{in}}{1 + bC_{in}\hat{C}} \right] \tag{24}$$

$$\hat{Z} = \frac{Z W_F k}{v C_{in}} = \frac{1}{1 + bC_{in}} [bC_{in}(1 - \hat{C}) - \ln \hat{C}] \tag{25}$$
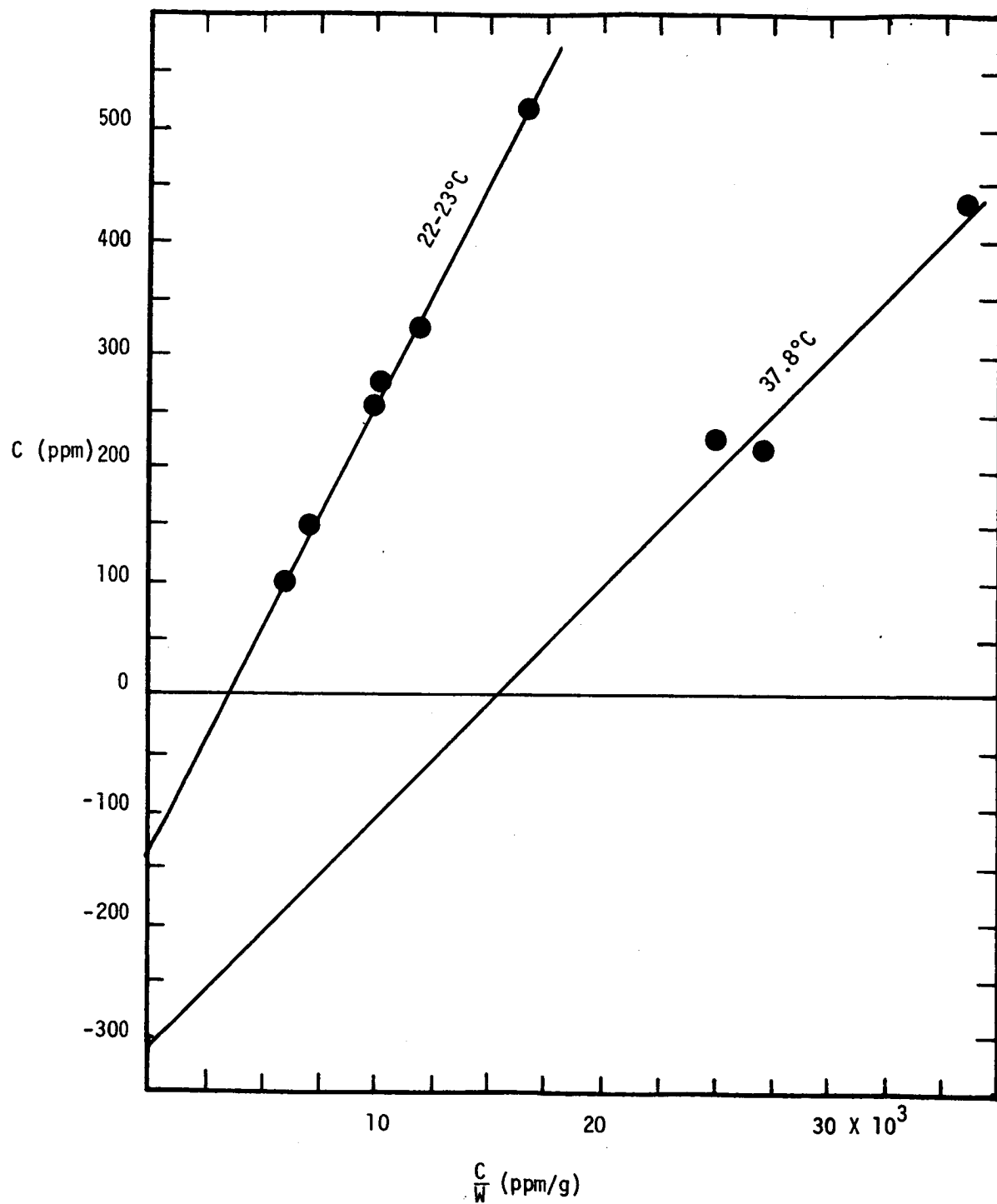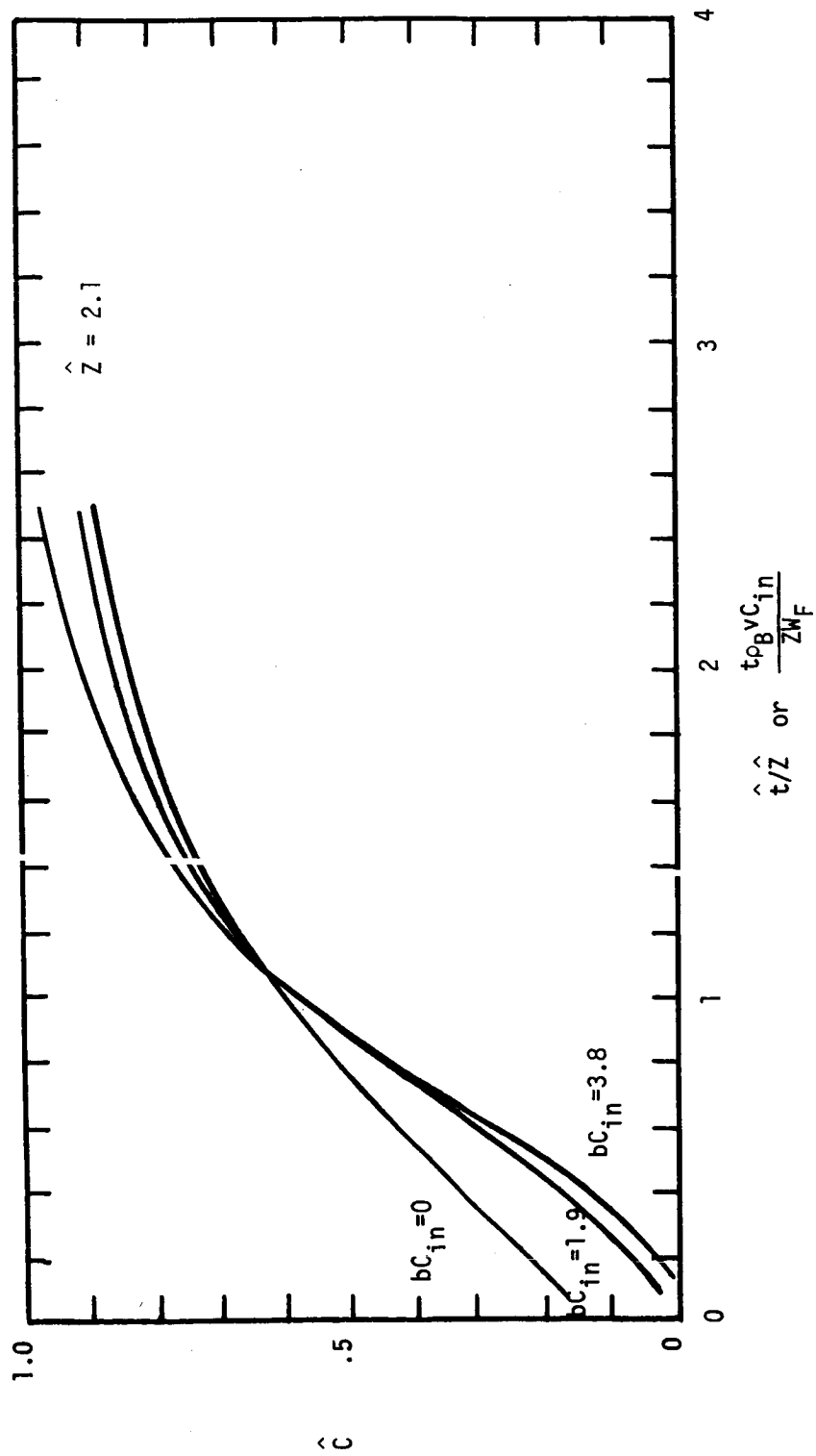
FIG. 1 - LANGMUIR ISOTHERM FIT

A10

FIG. 2 – EFFECT OF ISOTHERM PARAMETER

The algorithm used to obtain the best value of k is outlined below:

(1) The value of k was crudely estimated from the initial break-through ammonia concentration by the use of equation (25).

(2) The equation set was numerically solved for each value of the parameter bC_{in} and the results retained for values of k from one-half the smallest estimate to twice the largest estimate.

(3) A trial and error least squares fitting program was used in which a value of k was selected, the value of $\hat{Z}$ calculated for each run, and the summation of deviation squared determined.

(4) Step (3) was repeated until the minimum sum of squares was determined.

Using this least squares procedure the values of k determined were

$$k = 0.0053 \; \frac{g}{cm^3 min} \; \text{at } 72°F$$

$$k = 0.0214 \; g/cm^3/min \; \text{at } 100°F \quad .$$

The major experimental conditions for the adsorption runs considered are shown in Table 1. In addition the equilibrium loading and value for the parameter bC_{in} are shown. Figures 3 through 8 show the calculated break-through curves with data points superimposed. Since the solution is only weakly dependent on the value of the parameter bC_{in}, the calculated break-through curves for several of the runs are essentially the same, and these are shown on a common plot. The agreement between predicted and experimental

A12

TABLE 1 - EXPERIMENTAL CONDITIONS

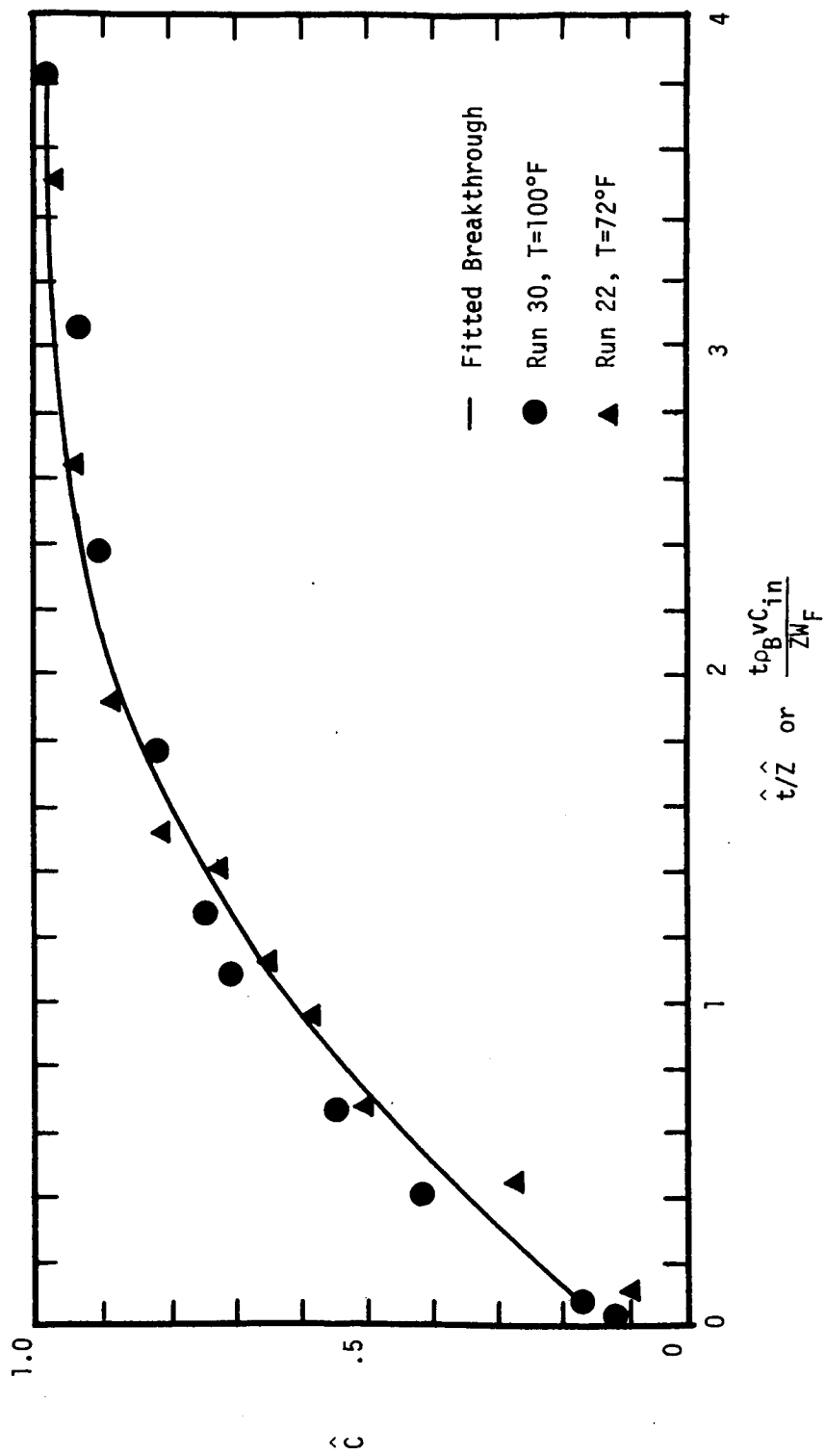| Run Number	V cm/min	Z cm	W_F g/g	C_{in} ppm	$P = BC_{in}$
21	1340	3.15	0.029	290	2.13
22	1365	1.92	0.021	150	1.10
24	1395	3.91	0.027	325	2.39
25	1509	1.98	0.030	520	3.82
26	1314	2.19	0.016	90	0.66
27	1320	1.91	0.022	215	1.58
28	1269	2.04	0.009	235	.74
30	1388	2.46	0.012	440	1.39
32	1223	2.37	0.008	210	.66

FIG. 3 - COMPARISON OF EXPERIMENTAL DATA AND
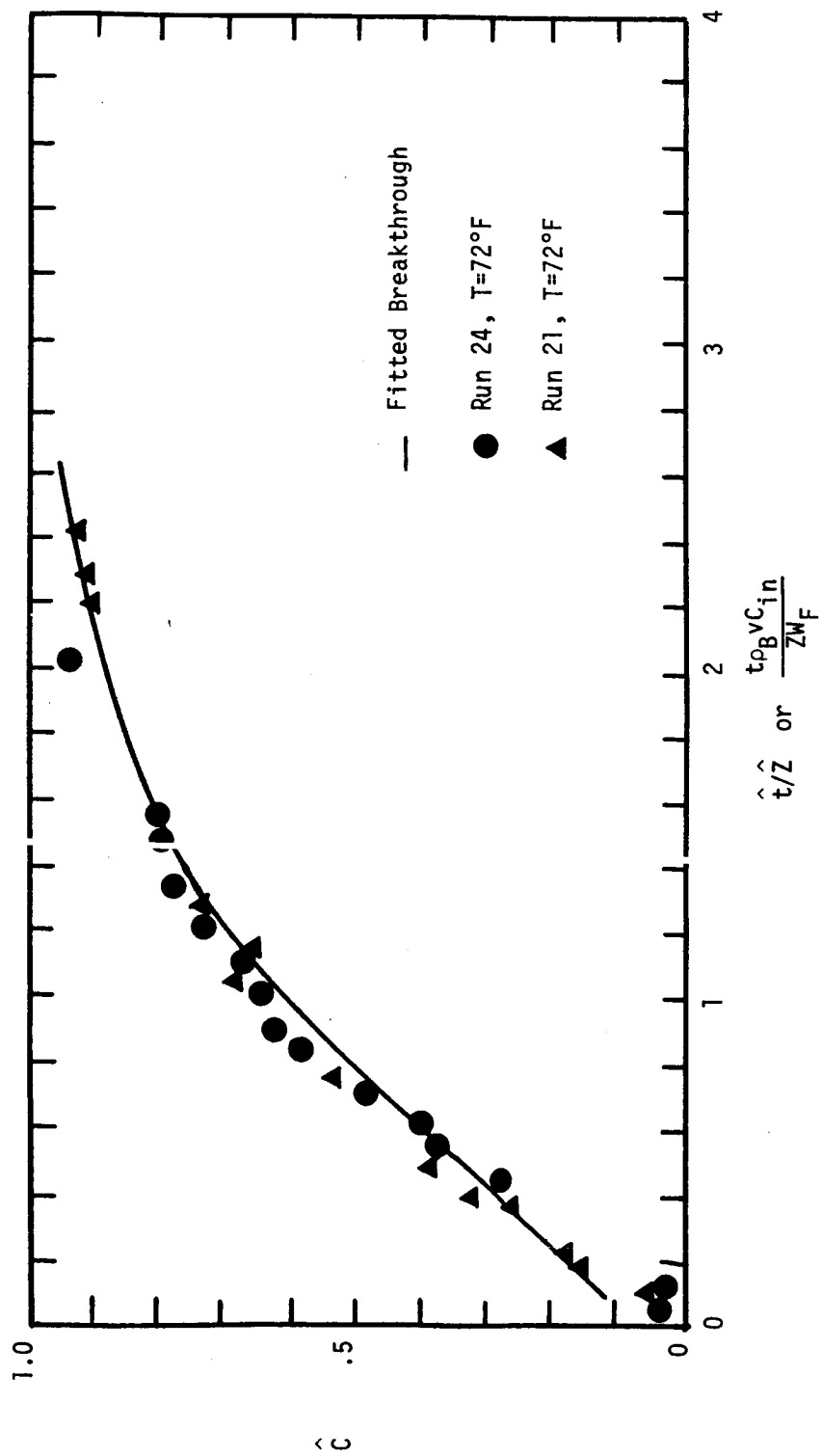CALCULATED BREAKTHROUGH

A14

FIG. 4 - COMPARISON OF EXPERIMENTAL DATA AND
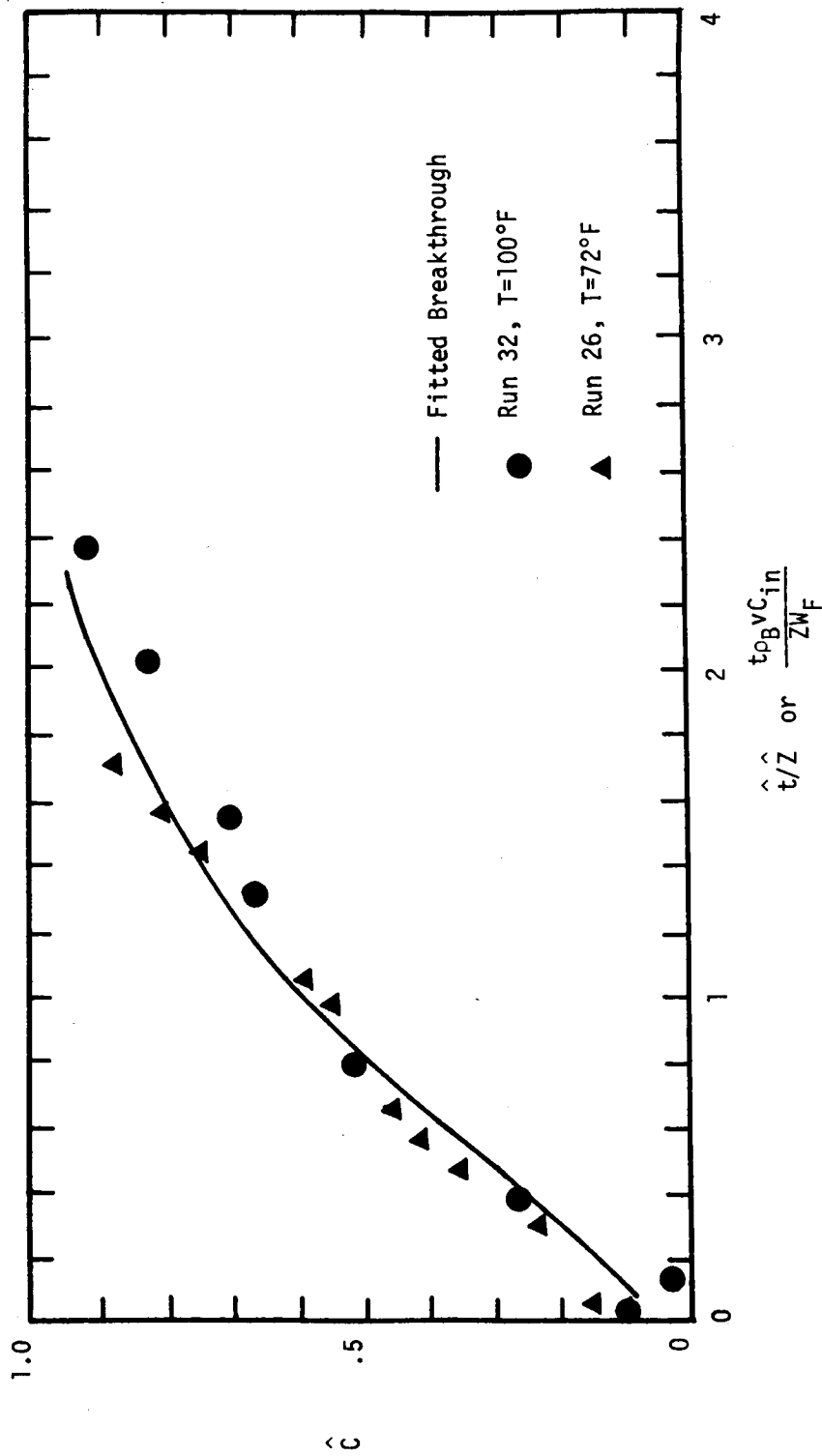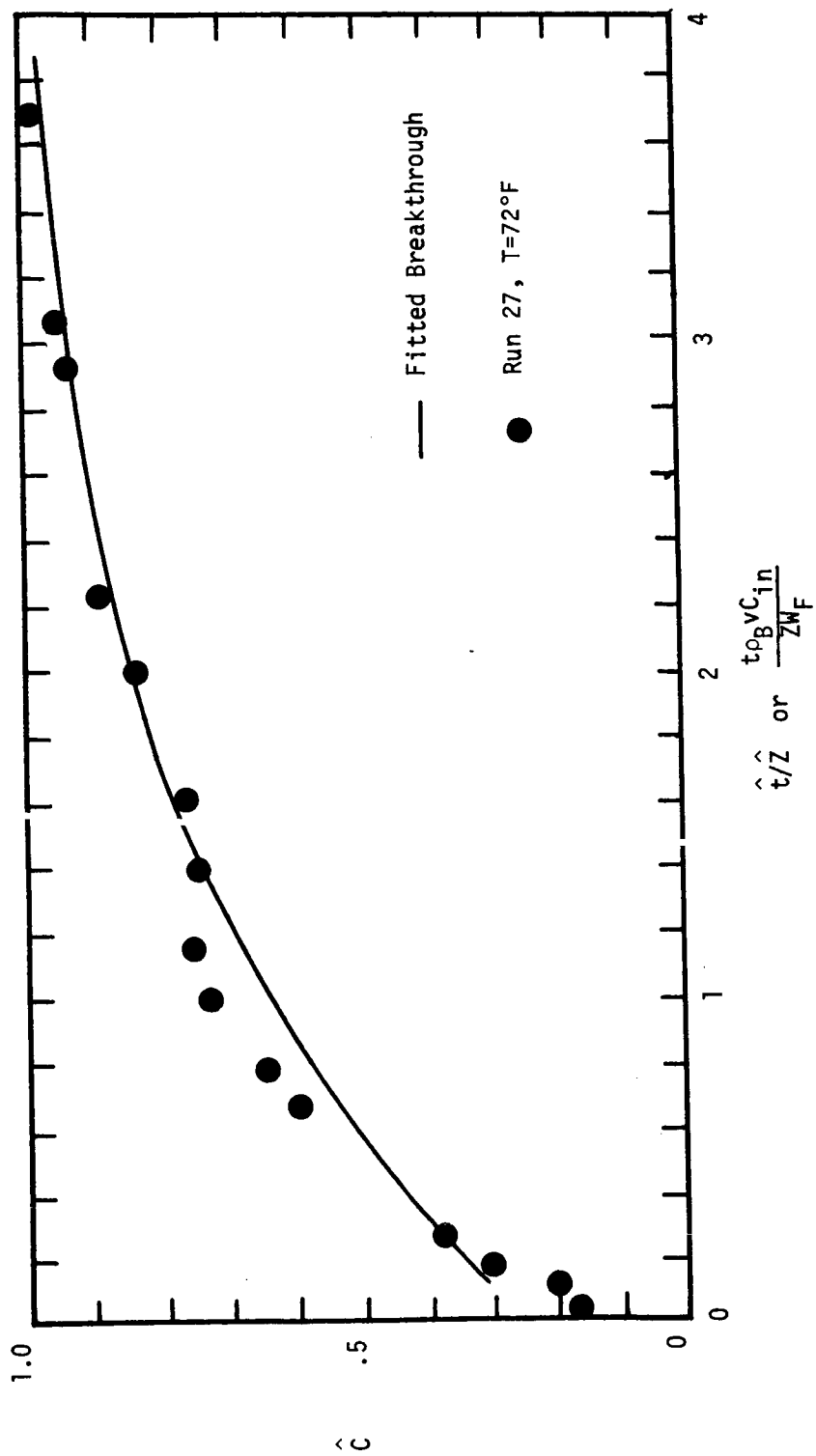CALCULATED BREAKTHROUGH

A15

FIG. 5 – COMPARISON OF EXPERIMENTAL DATA AND CALCULATED BREAKTHROUGH

A16

FIG. 6 – COMPARISON OF EXPERIMENTAL DATA AND

CALCULATED BREAKTHROUGH

— Fitted Breakthrough

● Run 27, T=72°F

$\hat{t}/\hat{Z}$ or $\dfrac{t\rho_B v C_{in}}{Z W_F}$

$\hat{C}$

A17

$\hat{C}$

1.0

.5

0

0   1   2   3   4

$$\frac{\hat{t}}{\hat{Z}} \text{ or } \frac{t\rho_B v C_{in}}{ZW_F}$$

—— Fitted Breakthrough
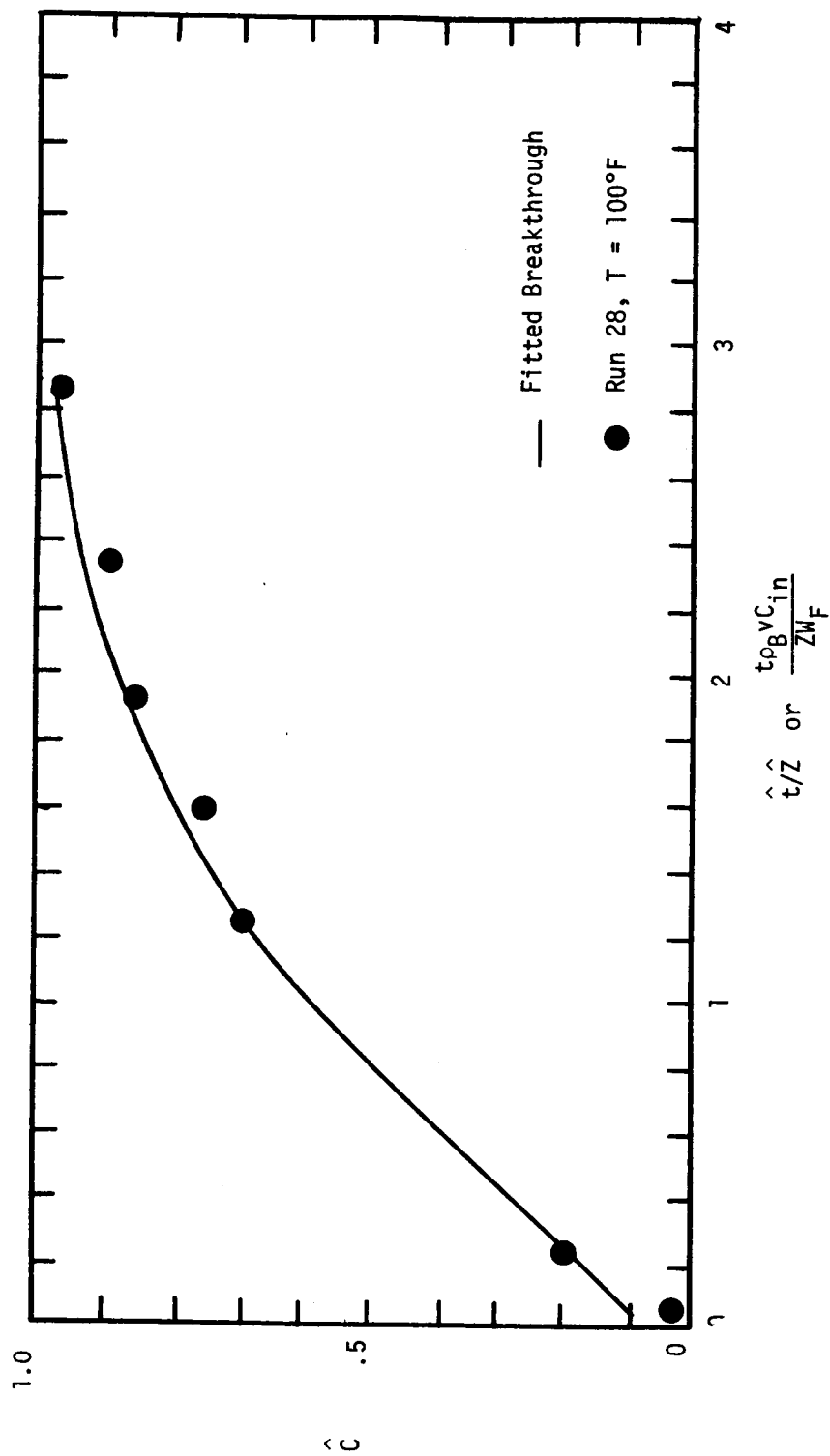
● Run 28, T = 100°F

FIG. 7 – COMPARISON OF EXPERIMENTAL DATA AND
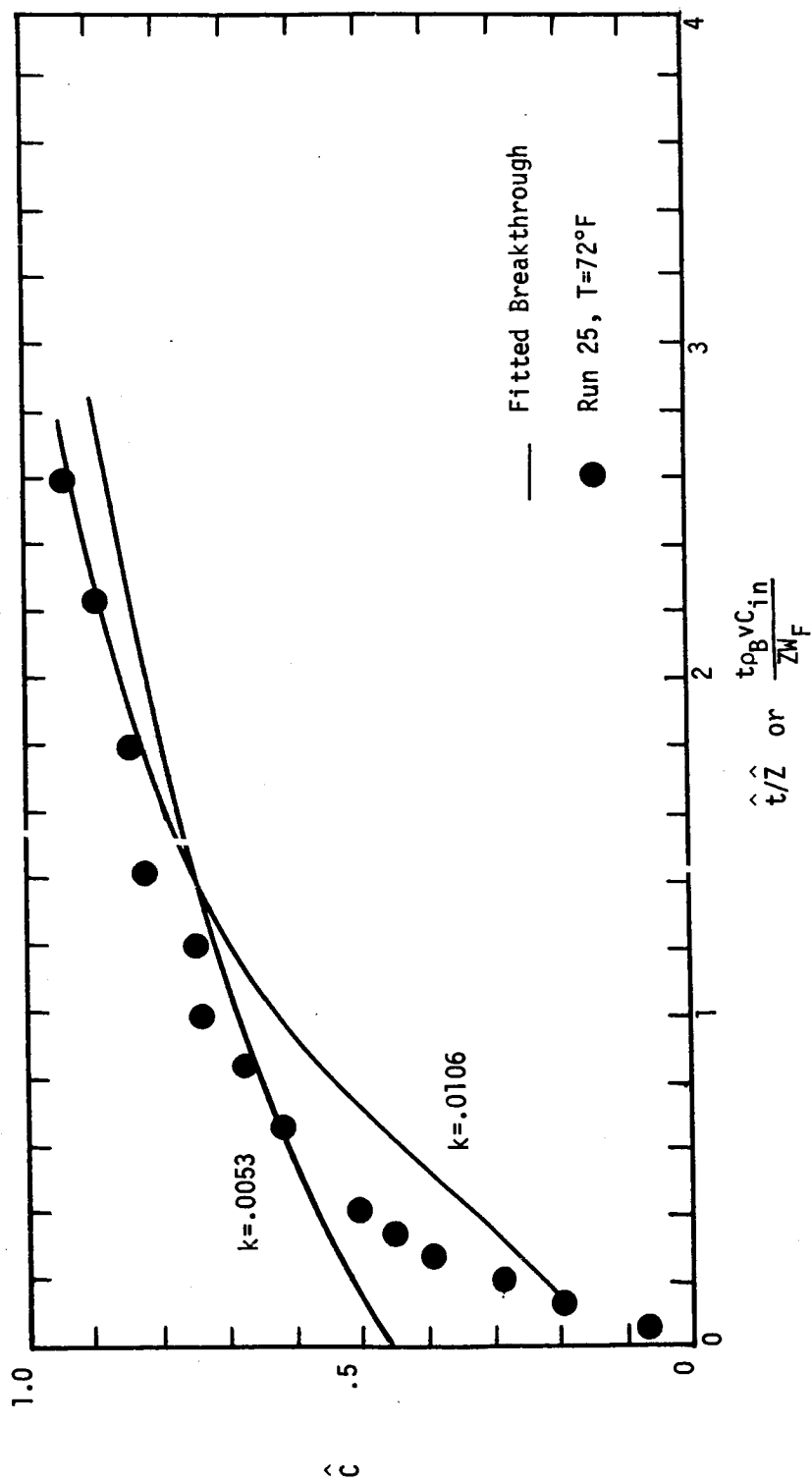
CALCULATED BREAKTHROUGH

A18

FIG. 8 – COMPARISON OF EXPERIMENTAL DATA AND

CALCULATED BREAKTHROUGH

curves is reasonably good for all runs except number 25. The cause for the poor fit for run 25 is not clear. This run had the highest inlet ammonia concentration. The point for run number 25 is well fitted by the isotherm equation which tends to rule out experimental error in the flow measurement, solid charge weight, and average exit concentration. For reference the breakthrough curve is given for a rate of adsorption twice the least squares value. For the 72°F data as a whole, a five per cent variation in k had an insignificant effect on the least squares calculation.

A color interface (aqua to dark blue) traversed the bed early in each run. Bed exit ammonia concentrations were less than 20 per cent of the inlet concentration during the traverse. There was, however, no detectable discontinuity in the breakthrough curves as the color interface exited the bed. The color change was thought to be due to the replacement reaction (4)

$$CuSO_4 \cdot 5H_2O + 4NH_3 \rightleftarrows CuSO_4 \cdot 4NH_3 + 5H_2O \ .$$
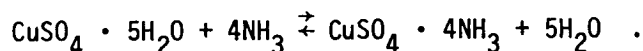
The characteristic color of $CuSO_4 \cdot 4NH_3$ is dark blue. Another indication that some type replacement occurred during a run was that the bed typically gained only 86% to 93% of the weight of ammonia adsorbed.

The latent heat of adsorption was determined using the two isotherms to be approximately 22 kcal/mole. Since the latent heat of condensation of ammonia is only about 6.5 kcal/mole, an activated adsorption is again indicated.

Regeneration Study

Only a very limited investigation was made on the regeneration of saturated sorbent. Adsorbent from run 24 was regenerated by heating in a cross flow oven for several hours at a temperature of 385°F. The sorbent was then resaturated at identical conditions to run 24. The adsorbent capacity after one regeneration was 80% of the fresh adsorbent's capacity. The characteristics of the breakthrough curve for the regenerated sorbent were similar to the fresh sorbent except with a slightly lower rate.

Conclusions

Copper sulfate impregnated silica gel compares favorably with other ammonia adsorbents. Acid impregnated charcoal is reported to have an ammonia capacity of 2.5% (mass) at a bulk ammonia concentration of 1000 ppm. The treated silica gel used in this study had a capacity of 3% (mass) at 520 ppm ammonia.

The isothermal breakthrough curves for the relatively short beds used can be well represented using a single parameter equation set. The model used assumes surface adsorption is the rate controlling step and that mass transfer resistances are minor. By putting the equation set in dimensionless terms only a single parameter remains, thus making the numerical solution more general.

The copper sulfate impregnated silica gel can be regenerated to 80% of its original capacity by heating at 385°F.

A21

References

1. Kvlividze, Brants, Kisselev, and Bliznakov, J. of Catalysis, 13: No. 3, 1969.

2. Robell, et. al., Design and Fabrication of a Trace Contaminant Removal System for Apollo, NASA Cr., NAS 9:3415.

3. Gant and Little, J. of Catalysis, 12:2, 1968.

4. Standen, E., ed., Kirk-Othmer Encyclopedia of Chemical Technology, Ed. 2, Interscience Publishers, New York, 1963.